SYNTHESIS AND PROPERTIES OF ALKALI METAL 18-CROWN-6 ALKALIDES AND ELECTRIDES

By

Dheeb Issa

A DISSERTATION

Submitted to
Michigan State University
in partial fulfillment of the requirements
for the degree of

DOCTOR OF PHILOSOPHY

Department of Chemistry

1982

ABSTRACT

SYNTHESIS AND PROPERTIES OF ALKALI METAL
18-CROWN-6 ALKALIDES AND ELECTRIDES

By

Dheeb Issa

Alkalides and electrides of alkali metals with 18-crown-6 as a complexing agent were synthesized by various procedures and the properties of these salts were studied by a number of different techniques. Two crystalline sodide salts, $Cs^{+}18C6 \cdot Na^{-}$ and $K^{+}18C \cdot Na^{-}$, were prepared. Analyses of these salts verified the stoichiometry, Cs18C6Na with no solvent present and K18C6Na (with, however, about 16% of amine solvent in the one sample analyzed). These are the first alkalide salts which utilize 18-crown-6.

Optical spectra of Cs18C6Na films showed one sharp peak at 16,500 cm^{-1} attributed to the Na^{-} anion. Films of K18C6Na showed a broad peak at 13,000 cm^{-1} and a shoulder at 10,000 cm^{-1}. Whether the peak at 13,000 cm^{-1} is caused by overlap of Na^{-} and K^{-} peaks or a red-shifted Na^{-}

peak is not known at this time. Powder d.c. conductivity measurements showed that these salts are semiconductors with average band gaps of 0.93 eV and 1.70 eV for $K^+18C6 \cdot Na^-$ and $Cs^+18C6 \cdot Na^-$, respectively.

Films and powders of electrides were prepared from methylamine solutions of cesium and 18-crown-6 in various proportions. The properties of the electrides were dependent on the ratio of the metal to crown used. Optical spectra of films with R=1 showed a localized peak due to e_t^- while the films with R=2 showed a "plasma type" absorption. EPR and magnetic susceptibility studies showed that the behavior of electrides with R=1 can be explained by the presence of two trapping sites, while for electrides with R=2 the results indicated a metallic behavior.

Films of electrides and alkalides were also prepared by direct reaction of the alkali metals and 18C6 deposited from the vapor phase. Optical spectra of these films showed the trapped electron and/or alkali metal anions can be obtained depending on the ratio of the metal to crown ether used.

A crystalline electride, $Cs^+18C6 \cdot e^-$ was prepared from equimolar solutions of cesium metal, lithium metal and 18-crown-6 in a mixed isopropylamine-diethylether solvent. The presence of lithium greatly stabilizes the solution but the crystals are essentially free of lithium metal. The lithium probably acts as a scavanger

for radicals produced by solvent and/or crown ether decomposition. Analyses of these crystals confirmed the stoichiometry Cs18C6. Optical spectra of annealed films showed a peak at 7,500 cm^{-1} attributed to trapped electrons. Powder d.c. conductivities of a polycrystalline sample showed a semiconductor behavior with an average band gap of 0.60 eV in the temperature range -54°C to +10°C. The magnetic susceptibility of crystals of Cs18C6 measured from 1.7 K to 300 K showed that the compound is essentially diamagnetic, with only about 1% unpaired spins. Single crystal EPR spectra showed the presence of two overlapping lines. One has g = 2.0023 and a linewidth of ∿0.75 G, independent of temperature from -135°C to +51°C. The other line has a smaller g-value (∿2.0016) and shows g-anisotropy upon rotation. It has a linewidth which broadens from ∿1.25 G at -135°C to ∿3.5 G at +31°C. This represents the first synthesis of a crystalline electride.

To My Family

ACKNOWLEDGMENTS

I am grateful to Professor James Dye for his encouragement, enthusiasm and guidance during this work. I would like to thank other members of the Group for their help. In particular, thanks go to Dr. Long Dinh Le, Michael Yemen, Brad VanEck and John Papaioannou. The MSU glassblowers, Keki Mistry, Andrew Seer and Manfred Langer, have given excellent service and cheerful cooperation.

Special thanks go to the Yarmouk University in Irbid-Jordan for supporting financially this educational opportunity.

Research support from NSF under Grant Number DMR-79-21979 is gratefully acknowledged.

TABLE OF CONTENTS

Chapter Page

LIST OF TABLES

LIST OF FIGURES

CHAPTER I

INTRODUCTION

Solutions of the alkali and alkaline earth metals in ammonia, some other amines and ethers have been studied for well over a century, and an extensive literature exists in this field (1-6). The work described here is based on that research. In the early 1970's Dye and coworkers used crown ethers and cryptands as complexing agents to enhance the solubility of alkali metals in amines, which opened the door to a new field in alkali metal solution chemistry. In this section the background for the research will be presented, beginning with metal ammonia solutions (MAS). This includes the nature of the species present in metal solutions, the solution properties, the metal-nonmetal transition and solid metal ammonia and methylamine compounds. The role of the complexing agents in enhancing metal solubilities is also described.

I. A. Metal Ammonia Solutions

Alkali metals dissolve in ammonia to a considerable extent giving blue solutions when dilute and metallic bronze solutions when concentrated. Sodium, potassium

and rubidium form saturated solutions at about 16 mole percent metal (MPM). Lithium is soluble up to 20 MPM and cesium to about 65 MPM (7). The solution properties range from electrolytic in the dilute and intermediate concentration ranges (<0.5 MPM) to metallic in concentrated solutions (>8 MPM) with a nonmetal to metal transition occuring between 2 and 9 mole percent metal. Very dilute metal ammonia solutions ($<10^{-3}$ M), contain solvated cations and solvated electrons. Although the structure of the latter is open to question, the most commonly accepted structure for the solvated electron (based upon theoretical calculations) is that of an electron trapped in a cavity from which one or more ammonia molecules have been excluded (8-11). This model was proposed first by Ogg and developed semi-quantitatively by Jortner. The cavity radius is 3.2 - 3.4 Å, and the electron is stabilized by orientation of nearest neighbor dipoles and by long-range polarization. As the concentration increases cation-electron and electron-electron interactions become important. However, the changes in such properties of these solutions as optical spectra, magnetic susceptibility, conductivity, density and activity coefficient are nearly independent of the cation. This suggests that if any new species are formed, they retain the essential characteristics of the solvated cation and the solvated electron. An ionic aggregation model has been proposed which explains these properties (12,13).

Based on this model, ion-pairing occurs between M^+ and e^-_{solv} which forms a non-conducting ion-pair. The magnetic interaction between the electron spin and the metal nucleus in this ion-pair is weak as shown by the small paramagnetic shifts of the alkali metal cations in the nmr spectra (14,15). Static susceptibilities (16,17) and EPR spin susceptibilities (18-20) show that in addition to ion-pairing between M^+ and e^-_{solv}, spin-pairing occurs to give diamagnetic states which become more predominant as the concentration increases. This has been attributed to the ion-triple, $e^- \cdot M^+ \cdot e^-$, although higher aggregates of stoichiometry M_2 and M_2^- might also form. As the metal concentration is increased ($3 < MPM < 9$), the properties change from non-metallic to metallic. Many theories have been developed to explain the nature of this transition (1). The simple qualitative picture for this transition is that, although a second electron may be added to a cavity to form spin paired species e_2^{-2}, at higher concentrations eventually there is not enough ammonia to provide such sites. Therefore, the electrons are forced to enter the conduction band at high concentrations resulting in the non-metal to metal transition. Concentrated metal ammonia solutions exhibit metallic characteristics. The absorption spectra show plasma edges, predicted by the Drude model for conduction electrons in a metal (21). Figure 1 shows the reflectance spectra of $Na\text{-}NH_3$ solution

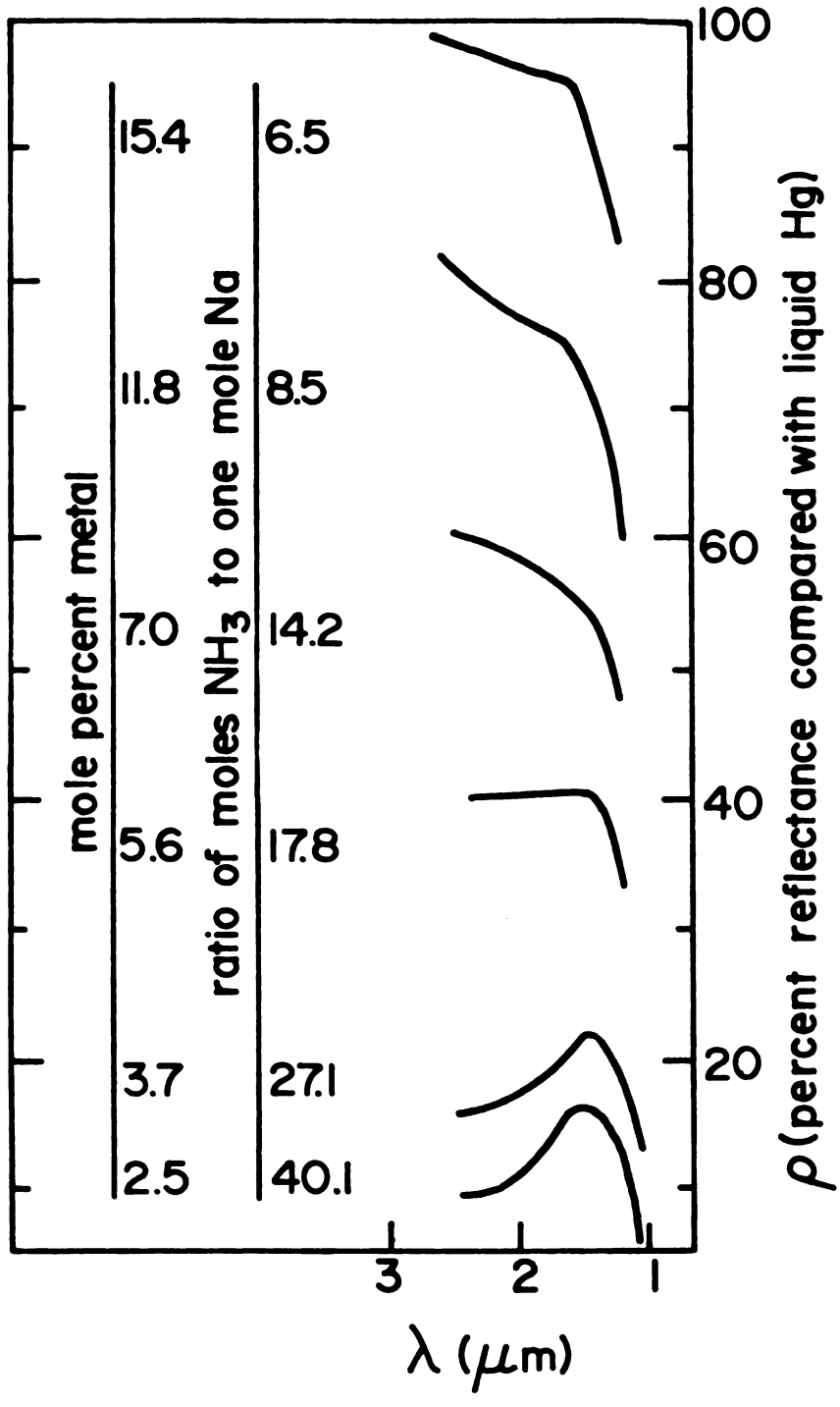

Figure 1. Reflectance spectra of Na-NH_3 solutions.

in the intermediate and concentrated regions (22). As the concentration of the metal increases above 5.6 MPM, the reflectance spectra show a very sharp drop at the plasma frequency which is a collective resonance of the conduction electrons. In contrast, the absorption spectrum of the solvated electron consists of a distinct peak in the infrared which drops to low absorbance as the wavelength is increased. The conductivity of concentrated metal ammonia solutions is high (comparable to that of liquid mercury) (23). The EPR spectra also show that concentrated metal ammonia solutions are metallic (24) as indicated by the asymmetric first derivative absorption curve predicted by Dyson for highly conducting materials (25).

I. B. Metal Ammonia Compounds

In contrast to the well-investigated metal ammonia solutions, relatively few studies have been made on metal ammonia compounds. Lithium is known to form the compound $Li(NH_3)_4$, calcium, barium and strontium form $M(NH_3)_6$ as do europium and ytterbium (1). The work that has been done to date suggests that these "expanded metals" have many novel and interesting structures as a result of their low conduction electron density. Recent re-examination of the crystal structure of $Li(NH_3)_4$ by Sienko and coworkers (26) shows the presence of three solid phases at different temperatures. All are indexed as body-centered

cubic, but with different space groups. Solid phase I is stable in the range 89-82 K, solid phase II in the range 82-25 K and the third phase below 25 K. Glaunsinger and Sienko (27) studied the EPR spectra of $Li(NH_3)_4$ in phase I. The experimental results were fitted to the theoretical lineshape equation derived by Dyson (25). In 1955 Dyson formulated a theory to account for the diffusion of conduction electrons into and out of the region penetrated by the EPR microwave-frequency field. For a metallic sample which is thick compared to the skin depth (δ) and with a relaxation time long compared to the diffusion time, the first derivative lineshape is asymmetric about its center with the low-field amplitude A greater than the high field amplitude B. This is now known as the Dysonian lineshape and results in $2.7 < \frac{A}{B} < 20$. The EPR spectra of $Li(CH_3NH_2)_4$ system have also been studied (28-30). The spectra indicate an asymmetrical lineshape with $1 < \frac{A}{B} < 2.7$. The magnetic susceptibility of $Li(NH_3)_4$ and $Li(CH_3NH_2)_4$ have been measured over the temperature range 4.2 - 300 K. The results for $Li(NH_3)_4$ (31) showed that the susceptibility is small and positive and that it is temperature independent above 89 K. In solid phase I (between 89 and 82 K) a smaller temperature independent paramagnetism was observed, while in solid phase II (from 82 to about 25 K), Curie-Weiss paramagnetism was found which changed to antiferromagnetism below 25 K. However, the magnetic behavior of $Li(CH_3NH_2)_4$ is quite different (25). The susceptibility was found to decrease

with decreasing temperature showing a large drop at 155 K which is believed to be the melting point of the compound $Li(CH_3NH_2)_4$. It then became constant and diamagnetic in the solid phase. The hexammine compounds $M(ND_3)_6$ where (M is Ca, Ba, Sr) show interesting structural features which are worth mentioning. Powder neutron diffraction and x-ray diffraction studies (32-34) show that within the complexes the six nitrogens are arranged in an exact octahedron with a rather long M-N distance. The neutron diffraction data indicate that the ND_3 molecules are nearly planar and have two inequivalent sets of deuterons. One N-D bond is short ($\sim$0.9 Å), while the other two are extremely long ($\sim$1.4 Å). A second feature of the $M-ND_3$ structure is its built-in disorder. Although each ammonia molecule is coordinated to the metal by its nitrogen, its "pseudo-trigonal" axis is not coincident with the M'-N bond but makes an angle of $\sim$13° with it. Based on the properties of these compounds such as electrical transport, magnetic susceptibility and magnetic resonance, these compounds constitute model examples of metals with low electron densities.

I. C. Electrons in Low Temperature Glasses

In 1962 the transient optical spectrum of the solvated electron in water was discovered by pulse radiolysis methods (35). Since that time transient solvated electrons have been observed in a variety of other polar and

nonpolar liquids (36). One offshoot of this work was the study of trapped electrons in glassy disordered media at liquid nitrogen temperatures, and recently in the liquid helium range on the picosecond and nanosecond time scales. Electrons are usually generated by ionizing radiation, and the formation of solvated electrons can be visualized kinetically as occurring in two stages (37,38). The first stage is localization which depends upon the relative energies of the conduction electron level of the medium and the energy of the localized electron state in the medium. The second stage, after localization occurs is solvation, in which the electron induces rearrangements in the surrounding solvent-shell molecules to create a geometry characterized by the forces between the electron and the solvent molecules. Electrons trapped in organic and alkaline ice glasses all give broad absorption spectra in the visible or near-infrared with long tails on the high energy side of λ_{max} and shorter tails on the low energy side (39). These spectra have linewidths at half-heights ranging from $\sim$ 0.5 eV for hydrocarbons to >1 eV for some alcohols, and trap depths which increase with increasing polarity of the matrix molecules. The initial spectrum of the trapped electron at $\leq$200 nsec in C_2H_5OD glass at 77 K has λ_{max} $\sim$1300 nm and shifts with time to a stable position near 540 nm. If 10-20 mol % of water is added to the ethanol, the absorption band remains structureless but its maximum

shifts slightly toward the red (40). These time-dependent spectral changes reflect the orientation of surrounding molecular or bond dipoles around the electron in the process of solvation. In 1975 Willard and co-workers (41) conducted a series of bleaching experiments (on the spectra of e^-_{trap}, produced in 2-methyltetrahydrofuran (MTHF) glass) in which the optical density in the near infrared is reduced at the bleaching wavelength and at longer wavelengths, but the remainder of the spectrum is unaffected. They found that the entire spectrum bleaches nearly uniformly when 1064-nm, rather than 1338-nm light is used. This indicates that all electrons apparently have high energy tails. Trapped electrons contribute differently to the optical density according to their λ_{max}. Consistent with the trapping model suggested by the optical spectra, the linewidths of the EPR singlet of the trapped electron in glasses at 77 K does not change indicating a symmetrical equilibrium environment, but as the polarity of the matrix molecules increases the linewidths increases indicating increasing hyperfine interaction with atoms along the walls of the trap as the traps become deeper (42). The structure of the solvated electron in different glassy media has been reported (43). Most of the information about the structure came from optical spectra and spin-echo studies. In aqueous systems, spin-echo studies of 10 M sodium hydroxide aqueous glasses showed that the electron has only water molecules in its

first solvation shell. The electrons are solvated by six water molecules, each with one of its OH bonds arranged approximately octahedrally around what is presumably the center of the odd electron density. The distance to the closest proton of the solvent water molecules is 0.21 nm while that to the more distant proton is 0.36 nm. These two distances, with an appropriate OH bond orientation are consistent with the known structure of the water molecule. The structure indicated that there are relatively strong interactions between the solvated electron and the first solvation shell. Another system that has been studied in great structural detail is electron solvation in MTHF (43). A quantitative model of the organization of molecules around trapped electrons at 77 K based on electron spin-echo studies indicates that three MTHF molecules are oriented around each electron with the plane of each molecule perpendicular to a line from the center of the ring to the electron at a distance of $\sim$3.7 Å, and that the CH_3 group is on the side away from the center of the electron spin density. The molecules of MTHF are oriented statistically causing multiple environments for the electron. In 1975 Willard (41) proposed that, because the spectrum of solvated electrons in MTHF showed three different peaks, the structures ascribed to different discrete preferred orientations of MTHF molecules would give different trap depths. The structure of the solvated electron in glassy ethanol

was also reported, which shows that the first solvation shell consists of four molecules with the CD_3 deutrons at 0.38 nm, the CD_2 deutrons at 0.33 nm and the OD deutron at 0.22 nm from the electron. In methanol glasses the solvation shell is 4 ± 2 molecules with an electron to hydroxyl proton distance of 0.23 ± 0.02 nm and the OH bond points towards the electron. In mixed matrix glasses, there is a single absorption peak due to the electron and λ_{max} shifts according to the composition of the matrix provided the glass is made from a mixture of similar types of molecules. By contrast when a glassy matrix is made from different molecules, two distinct absorption peaks characteristic of the two components are found. The electron is initially trapped in the less polar solvent and then moves to more polar regions as it anneals. This could also be due to solvent orientation effects. Electrons generated in single carbohydrate crystals show similar properties to those in glassy media (44,45). The electron g-value is nearly the same as that of the free electron. In both media the EPR absorption can be bleached by using visible light and electrons in single crystals show strong anisotropic hyperfine interactions with the hydroxyl groups. However, the traps in single crystals are shallower. It is of interest to note that in single crystals only a single trapping site is utilized even though many of the crystal structures offer more than one site. There are several theoretical models

to explain the structure of solvated and trapped electrons. They have been reviewed by Feng and Kevan (46) and only two of them will be mentioned here, since the others have failed to explain satisfactorily the properties of solvated electrons. Even the two models described here are controversial. The continuum model was first formulated mathematically by Jortner (47). In this model the medium is assumed to be a polarizable continuous dielectric, and the electron is assumed to be located physically in a spherical symmetric cavity. At distances outside the cavity, the electron interacts with the continuous dielectric through a $\frac{1}{r}$ Coulombic potential, while within and at the cavity boundary R, the potential remains constant. The semi-continuum (48,49) model considers the electron to be at the center of the cavity surrounded by a fixed number of solvent molecules which are arranged symmetrically. These solvent molecules interact with the electron to give short-range interactions which account for the values of electronic energy levels. Outside of the solvation shell is the dielectric continuum. However, there are still several arguments about these models. In 1980 T. Ichikaw and H. Yoshida (50) proposed a cavity model for localized electrons in nonpolar media. In this model, the depth of the potential well was derived from the Hartree-Fock molecular potential and the polarization potential. It was found deep enough to account for electron localization. They

found that the energy of quasifree electrons, the total energy for electron localization and the cavity radius (estimated from the simulation of the absorption spectra) were in reasonable agreement with the experimental data available for the 3-methylpentane glassy matrix used in the study as a typical example. Another theoretical formalism was developed by Banerjee and Simon (51). In their formula, the Hamiltonian was written as the sum of electronic and vibrational contribution of the system which includes a trapped electron plus solvent. The absorption band shape results from two major contributions, the localized (bound-bound) transition which makes the largest contribution and the nonlocalized (bound-free transitions). The latter, with the effect of rotational-translational contributions accounts for the asymmetry of the absorption band. The model was found to explain successfully the absorption spectra of excess electrons in ethanol and anthracene glasses, suggesting that this model might be a general model for excess electrons in condensed media.

I.D. F-Centers

F-centers are defined as anion vacancies in an ionic lattice occupied by electrons. Their characteristic color (from which they got the name "color centers") is due to an interaction, or series of interactions, between excess electrons and negative vacancies. F-centers have

been studied most completely in alkali halide crystals. The optical spectrum of an F-center consists of a broad absorption band, described as a bell-shaped curve. The wavelength at which the absorption peak occurs varies from 250 nm for LiF which has the shotest interionic distance to 785 nm for CsI with the longest interionic distance (52). Möllow first reported a relation between ν_m (the frequency of the absorption maximum) and the inverse square of the interionic distance a. ν_m (in eV) = 20.7 a^{-2} for the NaCl structure. Later this equation was modified to give a better fit. The new relation known as the Möllow-Ivey relation is ν_m (in eV) = 17.6 $a^{-1.84}$. The temperature effect was studied by Möllow and others. It was found that the absorption (A(ν)) drops off faster towards the red-end of the peak than towards the violet, and that the shape is more symmetric at higher temperatures. Pressure also affects the peak; as the pressure increases, the position of the peak shifts toward higher energy and the peak gets broader. Studies of the EPR spectra of F-centers show that the g-values vary slightly depending on the system, but that all the g-values are close to 2.0 (53). The linewidths are very broad because of hyperfine interactions of the electron with its nearest neighbors. In 1975 Schindewolf (54) studied the optical absorption spectra of excess electrons produced by electrolysis in melts of alkali halide salts in the temperature range 600-900°C. As expected,

the position of the peak varied with temperature. The relative half-width (half-width/peak position) of the spectra is almost 1, and a quadratic relation similar to that given by Möllow was obtained but with a wider spread of data and a steeper slope than for solids. This was explained by assuming that the cavity radius of the electrons in melts is larger than in the corresponding solids.

I.E. The Metal-Nonmetal Transition

A metal-nonmetal transition occurs in many crystalline and disordered systems. There are several theories which explain the transition and which will be reviewed here in a qualitative manner. Mott (55) first showed that a metal-nonmetal transition can occur if the lattice spacing is varied. When the electrostatic repulsion between electrons equals the band width a transition to the conduction state occurs. Using a screening constant, Mott calculated the criterion on the atomic density for the metal-nonmetal transition as

$$n^{1/3} a_H = 0.25$$

where n is the electron density and a_H is the Bohr radius of the isolated species. This relation was found to be empirically applicable to several systems (56) when an "effective" Bohr radius is used together with a critical

electron density n_c:

$$n_c^{1/3} \, a_H^* = 0.26$$

In his approach, Hubbard (57) viewed the problem in terms of band theory. In isolated atoms the bound energy levels of the electrons are discrete. When the energy levels overlap they smear out into bands with a bandwidth w. If u is the electrostatic repulsion energy at a particular site, then when $\frac{w}{u} \geq 1.15$ a transition from nonmetal to metal occurs. Later Mott found the condition for the transition is $\frac{w}{u} \sim 1$, hence the theory has been advanced as the Mott-Hubbard model. Anderson's approach (58) was based on the assumption that the lattice is composed of potential energy wells with variable depths with V_o being the spread in energy. Using w, the band width, as in the Hubbard model, a metal-nonmetal transition occurs at $\frac{w}{V_o} \sim 0.5$ for Z = 6, where Z is the number of nearest neighbors. A combination of the Mott-Hubbard and Anderson's models has been used to explain the metal-nonmetal transition in systems such as $Li(CH_3NH_2)_4$ solutions (30).

I.F. Alkali Metal Anions

It has been known for some time that the alkali metals dissolve in a number of amines and ethers, giving blue solutions with one or two broad absorption bands. One

of these, in the infrared region at 1200-2000 nm corresponds to the metal-independent band of the solvated electron. The position of the other band depends upon the metal, solvent and temperature and the absorption peak is strongly asymmetric on the high-energy side (59). These features are characteristic of the so called charge-transfer to solvent (CTTS) bands of other anions such as the halides. Figure 2 shows the spectra of Na^-, K^-, Rb^-, Cs^- and e^-_{solv} in ethylenediamine (60). The infrared shoulders observed for solutions of potassium, rubidium and cesium are attributed to the solvated electron and the ratio of this absorbance to that of the anion depends strongly on concentration as indicated by the following equation.

$$M^- \rightleftarrows M^+ + 2e^-_{solv}$$

Matalon, Golden and Ottolenghi showed that the wavenumber of maximum absorbance of the alkali metal anions varies inversely with the estimated anion radius, in accord with the predictions of CTTS theory (60). The observed temperature dependence of the peak position is also predicted by this theory. The oscillator strength (61), Faraday effect (62) and formation of Na^- in pulse-radiolysis studies (63)all supported the assignment of the metal-dependent band to M^-. The strongest evidence for "genuine" alkali metal anions in solution came from the ^{23}Na NMR spectrum

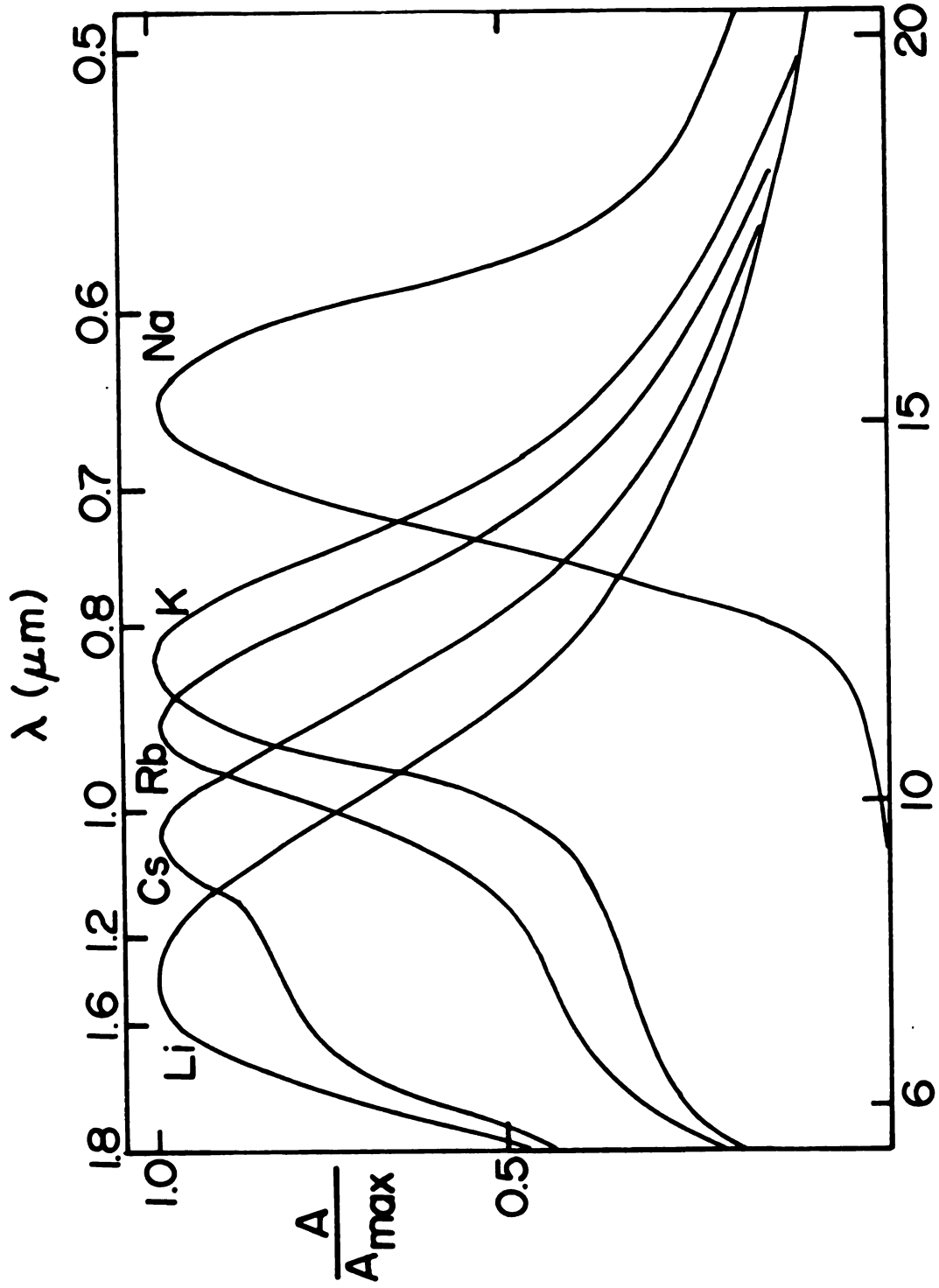

Figure 2. Optical spectra of alkali metal-EDA solutions.

of Na^- in three solvents (64,65). The absence of a solvent paramagnetic shift (compared with the gaseous anion) shows that the solvent cannot interact strongly with the p electrons of the alkali metal as it does in the case of solvated cations. In addition, the narrowness of the lines suggests that M^- is large and spherically symmetric. Later observations of the NMR spectra of Rb^- and Cs^- were also in accord with this picture (65). Finally, in 1974 the proof was completed when Dye and co-workers (66,67) isolated and characterized a crystalline salt of the sodium anion which was free of solvent. All of these observations provide proof of the existence of alkali metal anions both in solution and in ionic solids.

I.G. Nature of Alkalides and Electrides

After the synthesis of crown ethers by Pedersen (68) in 1967 and cryptands by Lehn (69) in 1969, Dye and co-workers used these macrocyclic compounds as cation complexing agents. They found that 18-crown-6 greatly enhanced the solubility of metals in amines and ethers, and that the cryptands were even better complexing agents. This work also expanded the range of solvents in which the alkali metals could be dissolved (70-72). The equilibria in metal solution can be described as

$$2M(s) \rightleftarrows M^+ + M^- \qquad (1)$$

$$M^- \rightleftarrows M + e^-_{solv} \qquad (2)$$

$$M \rightleftarrows M^+ + e^-_{solv} \qquad (3)$$

Depending on the metal and solvent used, the species e^-_{solv}, M^- and M can be detected. When a complexing agent is added to the solution, the complexation equilibrium (4) occurs

$$M^+ + C \rightleftarrows M^+C \qquad (4)$$

This will shift the equilibria in 1 and 3 to the right. Depending on the solvent used, either e^- of M^- or both can be produced. Another characteristic of the cryptand complexing agents is that M^+C consists of the bare cation trapped in the cryptand with no solvent included. Other important properties of these complexing agents are their high stability, high selectivity towards various cations and ability to shield the cation from the solvent environment. By controlling the ratio of the complexing agent to the metal it was possible to differentiate among various models for the solution structure of M^- in amines and ethers. This was done by Dye, Ceraso and Andrews by using alkali metal NMR (64,73). ^{23}Na NMR studies for solutions of sodium bromide and C222 cryptand at several mole ratios in various solvents showed separate peaks for Na^+ and Na^+C222

which merged into a single peak as the temperature was increased. Therefore, because of the slow release of Na^+ from the complex it was possible to obtain separate signals due to Na^+C and Na^- for solutions which contained C222 and sodium in a 1:2 mole ratio. The position and linewidth of the signal from Na^+C coincided with those obtained for solutions of simple sodium salts in the presence of the cryptand. The signal from Na^- is extremely narrow and is shifted diamagnetically from that of the cation in the same solvent. The absolute chemical shift of the Na^- resonance is practically the same as that of gaseous Na^- and is independent of the solvent. These results showed that the sodium p-electrons in Na^- are well-shielded from interactions with the solvent molecules. The narrowness of the line indicated that Na^- is highly symmetric, and the solvent-independence strengthened the overall conclusion that Na^- is a spherically symmetric anion with two electrons in the 3s-orbitals. It was also possible to obtain the NMR spectra of Rb^- and Cs^-. Solvent-free solids have been obtained from concentrated alkali metal amine and ether solutions which contain complexing agents. This has been done in two ways: first by slow cooling of relatively concentrated solutions to form crystals of $M^+C{\cdot}N^-$, ("alkalides"), and second, by evaporating the solvent to dryness leaving a precipitate with the composition $M^+C{\cdot}e^-$ ("electrides"). Early attempts to grow crystals

from solutions of sodium and C222 resulted in the crystallization of the compound $Na^+C222 \cdot Na^-$ (66,67,74). This compound has been fully characterized. The crystals are stable for long periods of time in vacuum or in an inert atmosphere at about 0°C (at least several years). The crystals are, however, sensitive to air, water, high temperatures and light. The stability of the crystals made it possible to determine the crystal structure. The x-ray structure showed that the two sodium moieties are in different environments in the crystal. One is inside of the cryptand and the other is outside of the cryptand. The sodium anions form parallel planes separated by the cryptated sodium cations. The cryptand has three-fold symmetry and an antiprismatic oxygen atom arrangement about Na^+. The Na^--N closest distance is 8.83 Å, the Na-N closest distance is 5.55 Å and the Na^--O distance is 5.76 Å. Although the compound appears metallic, conductivity measurements showed that it is a semiconductor. After the synthesis of $Na^+C222 \cdot Na^-$ a number of different kinds of crystals which used different cryptands and metals were prepared. However, the instability and/or poor quality of these crystals made them unsuitable for x-ray structural studies. At the beginning of the present research none of these crystals had been completely analyzed or characterized. The second type of compound, called "electrides", were studied by optical spectroscopy, electron paramagnetic

resonance, microwave conductivity and magnetic susceptibility, and the properties of these electrides will be reviewed here (75-78). Dry films made from ammonia solutions of potassium and C222 with a metal to cryptand ratio R = 1 yielded time-dependent spectra with two peaks; one at 11,000 cm^{-1} (900 nm) attributed to K^-, and the other at 6500 cm^{-1} (1800 nm) corresponding to the trapped electron. With time, the K^- peak decayed to a shoulder and the absorption of e_t^- increased. The final spectrum showed a "plasma-type" absorption spectrum similar to that of conduction electrons in concentrated metal ammonia solutions. The EPR spectra of solid K-C222 with R = 1 showed that the ratio of the low-field derivative peak to the high-field peak $\frac{A}{B}$, is larger than 1. This result is one characteristic of a metallic system as shown by Dyson. The spectra showed that multiple lines appeared below 77 K and that the system may be anisotropic. X-band microwave conductivity studies of a cryptand-rich $K^+C \cdot e^-$ sample indicated that the solid is highly conducting in the microwave region. Another type of electride which was investigated more thoroughly is that formed with lithium and cryptand C211 (79). The properties of LiC211 electride depend on the mole ratio of metal to cryptand, R. Films from solutions with $R < 1.15$ have an absorption spectrum with low far-infrared absorbance and peaks at 5000 cm^{-1} and 7000 cm^{-1}, and a high energy shoulder at $\sim$12000 cm^{-1} suggesting that the electrons are

trapped in several different non-equivalent environments. On the other hand, dry films with R = 2 showed a "plasma" edge presumably due to conduction electrons. A metal non-metal transition apparently occurs between R = 1.5 and R = 2. The EPR spectra of $Li^{+}C211 \cdot e^{-}$ showed that the g-values are at or near the free electron value, 2.0023, the linewidth ΔH_{p-p} is only about 0.5 - 0.6 Gauss, but below 60 K the linewidth increases gradually to 1.5 Gauss at 3 K. The $\frac{A}{B}$ ratios are less than 1.25 even for samples which showed metallic character. Except for a sample with R = 1.5, all samples showed at least one additional EPR peak at low temperatures. The EPR spectra showed that there is a tendency for the spins to pair as the temperature is decreased. There was apparently only a single spin-pairing process in the sample for which R = 1.57. This sample also showed only one peak in the optical spectrum. Systems which showed more than one peak in the optical spectra exhibited two spin-pairing processes. Static magnetic susceptibility measurements (80) verified the EPR results, which showed that the number of unpaired spins tends to decrease as the temperature is decreased. The temperature of maximum susceptibility ranged from 70 K for the system with R = 0.6 to 20 K for the system with R = 1.57. The susceptibility approached zero at low temperatures and the number of unpaired spin (based upon a Curie-Law approach) varied exponentially with $\frac{1}{T}$ down to 3 K. Except for the

most homogeneous sample (R = 1.57), it was difficult to describe the behavior below the temperature of maximum susceptibility. Above this temperature the susceptibility was described by the spin-pairing equation

$$\chi_m = \frac{f \cdot N_{avg}\, g^2 \mu_B^2}{k_B T[3 + \exp(-J/k_B T)]} \qquad (5)$$

in which f is the fraction of electrons which participate an J is the Heisenberg exchange integral. At high temperatures the above formula approaches the Curie-Weiss Law. The fit to a spin-pairing equation does not necessarily imply only pair-wise interaction of the electrons. However, the presence of several trapping sites and the lack of information about the structure made it impossible to interpret the data quantitatively.

I.H. Alkali Metal Crown Ether Systems

The macrocyclic polyethers first reported by Pedersen (68), the so-called crown ethers, are known to be effective in increasing the solubility of inorganic salts in non-polar media (81-87). The common factor governing all these processes is the ability of crown ethers to form stable complexes with cations. These complexes are mostly of 1:1 stoichiometry where the cations are held in the crown

ether ring by ion-dipole forces. The stability of crown-ether complexes depends on several factors; these include cavity size of the ligand, cation diameter, spatial distribution of ring binding sites and the type of solvent used. Very stable complexes can be formed when there is a good match between cation and crown ether with respect to size. However, the results of Izatt et al. (88) confirmed that correspondence of ligand ring cavity "size" to cation size is an important factor in determining the stability of complexes formed with cations small enough to enter the ligand cavity. Specifically, those cations which exactly fit the ligand cavity are bound more strongly than those which are too small. However, among cations which are too large to enter the ligand cavity, size correspondence is not predominant in determining cation selectivity, which is then governed by other factors. The cavity size of 18-crown-6 is large enough to allow entry of all alkali metal cations except Rb^+ and Cs^+. The selectivity of 18-crown-6 towards K^+ has been demonstrated. On the other hand, for cations whose radii are larger than the hole size, sandwich complexes can be formed in which the cation is located between two molecules of crown ether (68,89,90). The formation of such complexes was detected by alkali metal NMR techniques (91). Crown ethers were used in the early 1970's by Dye and co-workers (70) to enhance the solubility of alkali metals in amine and ether solvents. It was found that the crown ethers form stable complexes with

alkali metal cations. These complexes were detected by alkali metal NMR (93). Evaporation of alkali metal solutions in methylamine which also contain 18-crown-6 produces dark blue film or powders which apparently contain complexed alkali metal cations and either trapped electrons, "electrides", or alkali metal anions, "alkalides", depending on the ratio of the metal to crown ether. Previous studies on "electrides" and "alkalides" of alkali metal 18-crown-6 systems have concentrated on the optical spectra of thin films made from solutions containing Na, K, Rb and Cs with 18-crown-6 (75,76,78). The optical spectra of films made from sodium 18-crown-6 solutions with $R = \frac{[Na]}{[18C6]} = 2$, showed a strong band at 16,000 cm^{-1} characteristic of Na^-, as well as, a small broad peak at 25000 cm^{-1} and a shoulder at 19000 cm^{-1}. Potassium films with R = 2 have a strong absorption band at 12,200 cm^{-1} and a pronounced shoulder at 9000 cm^{-1}, while films made with R = 1 have bands at 12,000 cm^{-1} and 6500 cm^{-1}. The peak at 12000 cm^{-1} is probably that of K^-, while those at 9000 cm^{-1} and 6500 cm^{-1} may be caused by trapped electrons. Films of Rb with 18-crown-6 with R = 2, show absorptions at 12000 cm^{-1} and 9100 cm^{-1} which are assigned to Rb^- and e_t^-, respectively, with the band of e_t^- shifted to higher energies probably by interaction with Rb^-. However, the behavior of Cs 18-crown-6 films is different. Films formed from solutions showed a single band at 6400-6700 cm^{-1} which probably originates from a trapped electron. The EPR spectra

of Cs 18-crown-6 with R = 0.5 consisted of a single line with g-value 2.0022 ± 0.0001. The linewidth changed from 0.36 G at 214 K to 0.54 G at 106 K. Several attempts to produce crystalline alkalides by using 18-crown-6 as the complexing agent failed, perhaps this was due to the use of unsuitable crystallization solvents. In addition, characterization of the cesium 18-crown-6 electrides was fragmentary. Therefore, a thorough investigation was required to prepare and characterize "alkalides" and "electrides" which utilize 18-crown-6 as a complexing agent. The objectives of the present work can be summarized as follows.

1. Preparation and characterization of powder and/or film electrides which are formed from cesium and 18C6. Several Cs-18C6 systems were prepared by using different solvents and different metal to crown ratios. The properties of these systems were studied by optical and EPR spectroscopy, microwave conductivity and magnetic susceptibility. These properties will be discussed in Chapter III.

2. Attempts to prepare and characterize alkalides by using 18C6 as a complexing agent resulted in the preparation of two crystalline sodide salts $Cs^{+}18C6 \cdot Na^{-}$ and $K^{+}18C6 \cdot Na^{-}$. The properties of these new alkalides will be discussed in Chapter IV.

3. Explore the possibility of preparing alkalides

and electrides by direct vapor phase deposition. Preliminary experiments showed this to be possible and the films prepared were characterized by optical spectroscopy. The experimental procedure and the optical spectra will be presented in Chapter V.

4. Finally, the major breakthrough in this research was the first successful preparation of a crystalline electride, $Cs^{+}18C6 \cdot e^{-}$. This experiment opens the door for the preparation of other new crystalline electrides. The synthesis and properties of this crystalline electride will be discussed in Chapter VI.

CHAPTER II

EXPERIMENTAL

II.A. Materials

II.A.1. Complexing Agents

18-crown-6. IUPAC: 1, 4, 7, 10, 13, 16-hexaoxacyclooctadecane (18C6). (Purchased from PCR, Inc. or Parish) was recrystallized from warm acetonitrile to give the crown-acetonitrile complex (93). The crown ether obtained by vacuum decomposition of the acetonitrile complex was then sublimed under high vacuum at 60°C and stored for further use. It is recommended that the purified 18C6 be stored in the dark *in vacuo* or under an inert atmosphere.

II.A.2. Solvents

After purification, all solvents were stored in vacuum storage bottles and were degassed by freeze-pump-thaw cycles before use.

Ammonia: Ammonia (anhydrous, 99.99% Matheson) was treated twice with Na-K alloy, ratio 1:3 then transferred to a vacuum storage bottle.

Methylamine (MA): Methylamine (98% Matheson) was stirred over calcium hydride for about 48 hours. It was then treated with Na-K alloy until the characteristic deep blue color remained for at least 48 hours at room temperature. The solvent was then vacuum transferred to a vacuum storage bottle.

Ethylamine (EA). Ethylamine (anhydrous, Eastman Kodak) was treated in the same way as methylamine.

Isopropylamine (IPA). (Anhydrous, Eastman Kodak) was first dired over calcium hydride, then degassed by freeze-pump-thaw cycles. It was then treated with excess Na-K alloy over benzophenone until the characteristic violet color remained for at least 72 hours at room temperature. The solvent was then vacuum transferred immediately to a vacuum storage bottle. The violet benzophenone ketyl served both as a drying agent and a dryness indicator.

Diethyl Ether (DEE). Ether (Fisher) was treated in the same way as isopropylamine.

II.A.3. Metals

Cesium. This metal (a gift from Dow Chemical Co.) had been previously transferred into sealed glass ampoules with breakseals. The metal was stored under vacuum in measured small diameter glass tubes (2-8 mm O-D) with sealed

ends. Vacuum transfer of the metal to these tubes was accomplished as follows. The ampoule with breakseal was attached to the distribution apparatus shown in Figure 3. After evacuating the apparatus ($<1 \times 10^{-5}$ torr) and breaking the breakseal, the metal was heated and allowed to run into the reservoirs after which vacuum seal-offs were made at the constrictions. The metal was heated and allowed to run down into each of the tubes which had known internal diameters. Due to the possible contamination of cesium with sodium from sodium borosilicate glass, it is recommended that the final distillation of cesium should be made in a fused silica apparatus (94).

Sodium, Potassium, and Rubidium. These metals (Alfa-Ventron) were supplied under argon in sealed glass ampoules with breakseals. Total purities were 99.95%, 99.45%, and 99.93% respectively according to the supplier. These metals were treated in the same way as cesium.

Lithium: (Automergic Chemical Co. 99.99%). Lithium was treated in an argon-filled dry box (95). A clean knife was used to cut small pieces of lithium which were then weighed on a model RTL Cahn Electrobalance inside the dry box. Then each of the pieces was loaded into a 5 mm tube sealed at one end. A cap to which polyolefin heat-shrinkable tubing (Alpha-wire Corporation) had been previously attached, was sealed onto the sample tube, providing a gas-tight seal. After removal from the dry box, the end of the

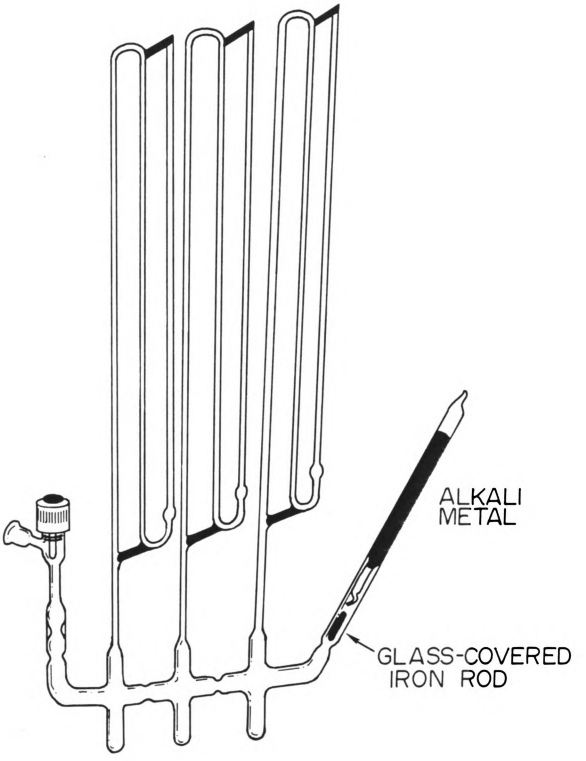

Figure 3. Apparatus for distribution of alkali metal under vacuum.

tube containing the lithium was placed in liquid nitrogen and a seal was made to remove the heat-shrinkable tubing.

II.B. Glassware Cleaning

A general method was used for all glassware cleaning. The apparatus was first filled with an HF cleaner. This cleaner contains 33% HNO_3, 5% HF, 2% acid-stable detergent, and 60% H_2O by volume (96). After thorough rinsing, the apparatus was filled with aqua regia and allowed to stand overnight. The apparatus was then rinsed thoroughly with doubly distilled water and dried overnight in an oven at ∿150°C.

II.C. Sample Preparation and Instrumental Techniques

II.C.1. General Preparative Methods

(a) Electrides (CS-18C6) - The apparatus shown in Figure 4 was used to prepare samples for the study of optical and EPR spectra and magnetic susceptibilities. This procedure permitted the same preparation to be used for all studies in order to eliminate differences in behavior which might arise from different preparations (for example, different crown-to-metal ratios). A known mass of 18C6 equivalent to the amount of Cs metal used was introduced into the apparatus. The small glass tube which contained cesium metal was scored around the middle and introduced

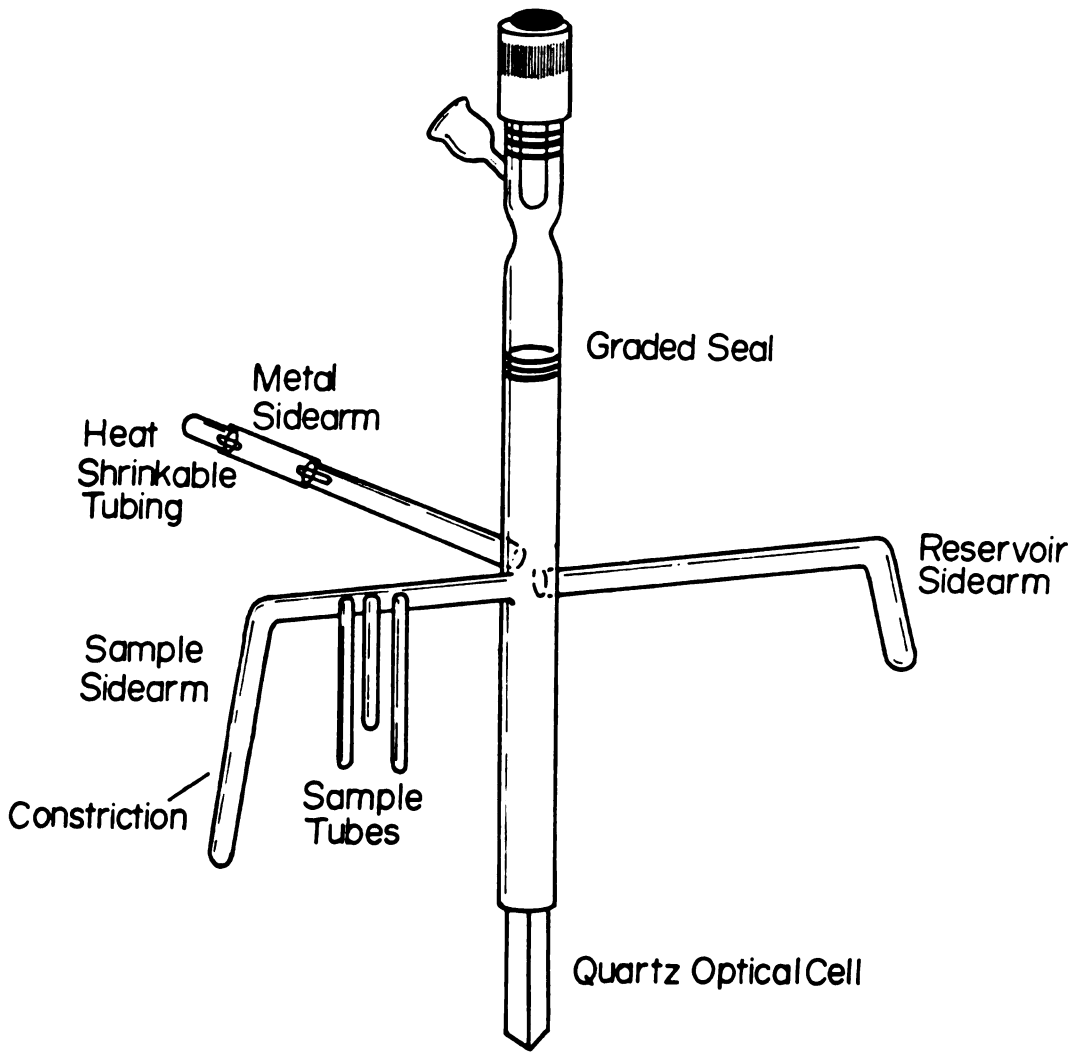

Figure 4. Apparatus for preparation of powders and films of $Cs^{+}18C6 \cdot e^{-}$.

into the apparatus sidearm. A piece of Teflon shrinkable tubing was heated gently and sealed at the end of the sidearm. The other end of the shrinkable tubing was then sealed onto a short piece of glass tubing which had been sealed at one end. Then the apparatus was connected to the vacuum line. To avoid contamination of the manifold, the connection was made through a tee and the tee was connected to the manifold via an intervening liquid nitrogen trap. The apparatus was evacuated to $\sim 1 \times 10^{-5}$ torr and then removed from the vacuum tee with the valve closed. The cesium ampoule was broken. (It was necessary to cool the cesium prior to breaking since the melting point of cesium is low and molten cesium reacts with the shrinkable tubing). After breaking the ampoule, the two pieces were shaken down into the sidearm and a glass seal-off was made behind the pieces in order to remove the shrinkable tubing. The cesium was distilled, and another seal was made at the constriction in order to remove the pieces of glass. The solvent bottle was then connected to the tee and the connecting tubes were evacuated to $\sim 1 \times 10^{-5}$ torr. The solvent was distilled into the apparatus by keeping the temperature of the apparatus lower than the temperature of the solvent bottle. After introducing a reasonable volume of solvent, the valves were closed and the apparatus was removed from the vacuum line to an isopropanol bath at a temperature of -40°C. The apparatus was allowed to stand for a period of time with occasional shaking to dissolve the metal and

the crown and to ensure complexation. Once the solution had been prepared, it was poured gently into the sample tubes for EPR and magnetic susceptibility measurements. The solvent was evaporated slowly to avoid "bumping" by keeping the temperature of the bulk solution in the main stem at -78°C and that in the sample tubes at ∿-60°C. For some unstable electrides such as $(CS)_2(18C6)$, the main stem were kept at liquid nitrogen temperatures while the sample tubes was kept at a temperature of -78°C. It was necessary to wash the sample tubes several times to bring the sample down to the bottom of the tube. After removing essentially all of the solvent, the bulk solution was frozen with liquid nitrogen, then the samples were dynamically pumped for about 45 minutes to insure that the samples were solvent-free. The sample tubes were then sealed-off and stored in liquid nitrogen. The remaining solution was used for studies of optical spectra. For systems, such as CS18C6Li in which two metals were used an additional side arm with a frit was added to the apparatus.

(b) Alkalides - The same general procedure used to prepare electride solutions was also used to prepare solutions of the alkalides. The apparatus shown in Figure 5 was used to prepare crystalline alkalides. After distilling the metals and making the seals, methylamine was distilled into the apparatus. The solution was maintained

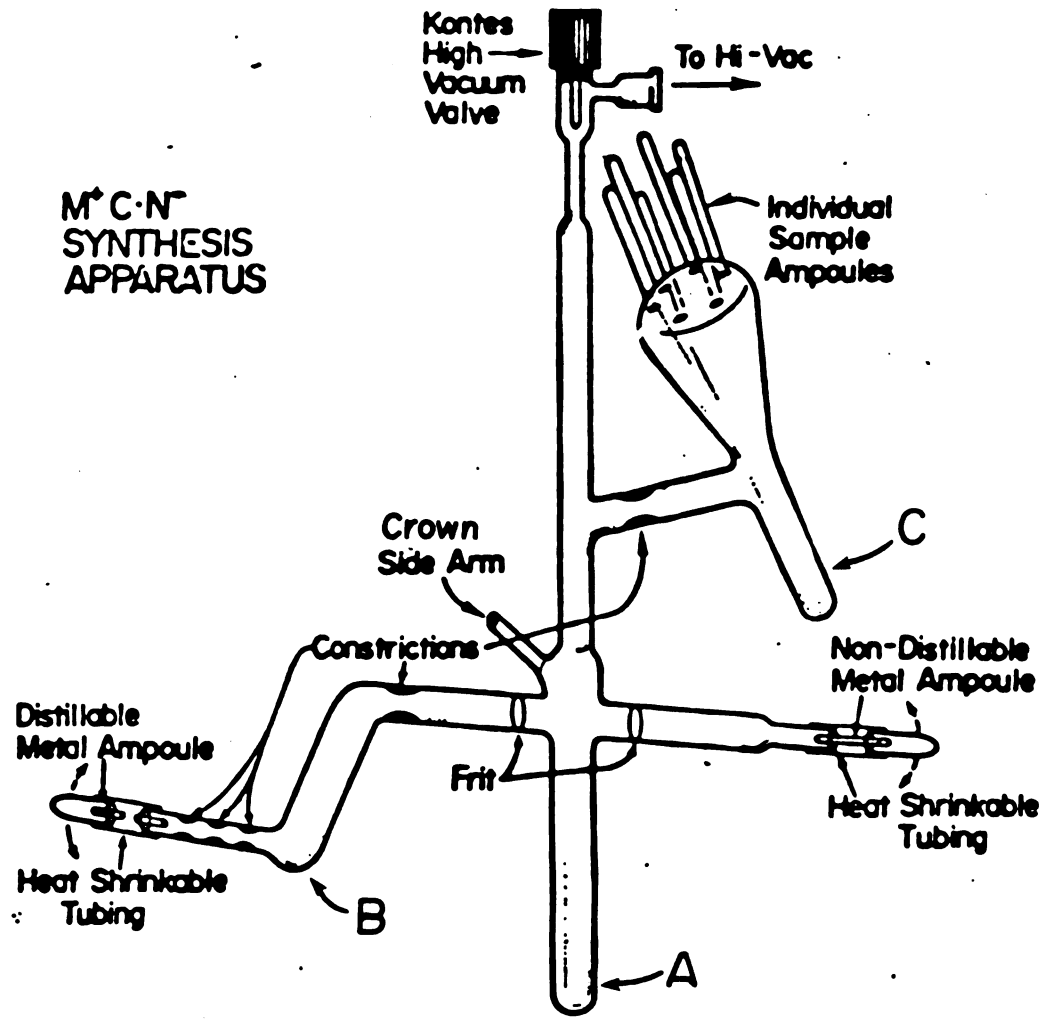

Figure 5. Apparatus for the preparation of crystalline alkalides.

at temperatures of about -25°C, the methylamine was poured back and forth between the main chamber A and chamber B in order to dissolve the metals and the crown. After that, the whole solution was poured into the main chamber A. The methylamine was distilled out of the apparatus into an evacuated empty bottle. Isopropylamine, which served as a crystallization solvent was then distilled into the apparatus. The solution was kept initially at ∿-15°C to dissolve all of the alkalide, and then cooled slowly to -78°C and allowed to stand overnight during which time the crystals precipitated from the solution. The supernatant isopropylamine solution was poured into chamber B, frozen with liquid nitrogen and a seal was made at the constriction. Then diethylether was distilled into the apparatus to wash the crystals and transfer them to part C. The diethylether solution was poured back into the main chamber A, redistilled onto the crystals several times to wash them and finally frozen in the main chamber A with liquid nitrogen and the final seal-off was made at the constriction. The crystals were then distributed into the sample tubes which were sealed-off and stored at dry-ice temperatures. In the preparation of $K^{+}18C6 \cdot Na^{-}$ a co-solvent of isopropylamine and diethylether in a ratio of about 2:1 was used for the crystallization rather than pure isopropylamine.

II.C.2. Optical Spectra

Solutions were prepared in the apparatus shown in Figure 4. However, films for optical spectra were formed in the apparatus which consisted only of the main stem and the reservoir side arm, all other arms having been sealed-off. With the exception of the graded seal and the borosilicate glass vacuum valve, the apparatus was constructed of fused silica in order to avoid sodium exchange contamination of the alkali metal solutions by contact with sodium borosilicate glass (97). Films were formed in the optical cell by leaving 0.2 ml of the solution in the cell, while the bulk solution in the reservoir arm was frozen in liquid nitrogen. During this process, the optical cell was kept in a cold isopropanol bath and was shaken rapidly from side to side about the axis through the side arm. This rapid shaking splashed the solution onto the cell walls where the film formed during the flash evaporation of the solvent. It was necessary sometimes to repeat this process to obtain films of proper thickness and uniformity.

Because of the nature of this method of film preparation, films were often non-uniform, especially when a solvent of high vapor pressure such as ammonia was used. It was noticed also that slow evaporation of the solvent resulted in more uniform films. In general, all films from methylamine solutions were more uniform than those from ammonia

solutions. Some of the films, classified as damp and wet films were prepared by bringing the temperature of the reservoir up to temperatures about 5-20°C below the optical cell temperature. All optical spectra were recorded on a double beam recording spectrophotometer (Beckman DK-2), modified to permit control of the sample compartment temperature between -65°C and 0°C. An ethanol cooling bath (Neslab Model LTE-9) provided rough temperature control for the compartment and was augmented by nitrogen gas which flowed through a coil immersed in liquid nitrogen. A copper-constantan thermocouple placed near the cell provided the signal for temperature readout (Doric Model DS-350). Spectra were recorded from 4000 cm^{-1} (2500 nm) to 25,000 cm^{-1} (400 nm) for standard fused silica cells and from 3125 cm^{-1} (3200 nm) to 25000 cm^{-1} (400 nm) for infrasil cells. The reference beam passed through air. The spectra were normalized to a scale of 0.0 to 1.0 by subtracting a baseline correction, setting the lowest absorbance to zero and the maximum to 1.0 and then scaling the measured absorbance at 500 cm^{-1} intervals. The baseline was obtained by using the spectrum of an empty cell. It was necessary to use a new baseline correction for each new run.

II.C.3. EPR Spectra

EPR spectra were recorded on an x-band spectrometer (Varian Model E-4 or Bruker Model 200) over the temperature

range 3.6-225 K. Above 100 K, a variable temperature controller (Varian) was used which utilized a stream of temperature-regulated cold nitron gas. The temperature setings were calibrated with a copper-constantan thermocouple with digital readout (Doric Model DS-350). Temperatures between 3.6 and 77 K were provided by a continuous flow liquid helium system (Oxford Instrument Co., Ltd., Model ESR 9). Digital temperature readout was based on an (Au + 0.03% Fe/chromel) thermocouple just below the sample.

II.C.4. Magnetic Susceptibility

Samples for magnetic susceptibility were prepared in 4-6 mm o.d. "Spectrosil" fused silica (Thermal American fused quartz). The sample was located in the bottom of the tube. A seal was made about 1 cm above the sample while the sample was immersed in liquid nitrogen. A small fused silica hook was attached to the top of the sample tube ("bucket"). Care was taken to avoid contamination of the bucket and the hook during seal-off and handling. For example, handling the hot quartz with metallic forceps can lead to contamination. Magnetic susceptibility measurements were made with a SQUID (Superconducting Quantum Interference Device) magnetometer purchased from S.H.E. Company. Since most of the electrides decompose at temperatures of -30°C and above, it was necessary to load the samples into the SQUID while keeping them cold. This was achieved

by using a copper block that fit into the airlock of the SQUID. This block had a central hole of 7 mm diameter so that the sample could pass through it. To avoid SQUID contamination with air and moisture, a glove bag was placed around the airlock and purged with a continuous helium flow. Prior to loading the sample, a thread 15-20 cm long was attached to the hook of the bucket. While the sample was kept in liquid nitrogen, the copper block was cooled to liquid nitrogen temperatures, then placed in the airlock and the thread was hooked to the tape of the drive motor. The sample was placed into the hole in the copper block, the airlock cover was put back and the airlock was rapidly evacuated and pressurized with helium gas three times. Then the sample was loaded into the SQUID. It is essential that the loading process be completed as rapidly as possible so that the copper block does not warm up with resulting sample decomposition. Measurements were made over the temperature range 1.7 - 280 K. To correct for the diamagnetism of the bucket, it was ejected from the SQUID and allowed to remain in the airlock at room temperature long enough to decompose the sample. Then the bucket and decomposed sample were loaded back into the SQUID for further measurement. The reading given by the SQUID is the total magnetic moment in e.m.u. The magnetic susceptibility is calculated by using the formula

$$\chi_{gm} = \frac{\text{magnetic moment}}{\text{(SF) x field in Gauss x mass in gm.}}$$

where SF is the total scale factor which equals the scale of the SQUID control multiplied by the scale of sample measurement control. The magnetic susceptibility of the sample was calculated by subtracting the diamagnetism of the bucket and decomposed sample from the total magnetic susceptibility.

II.C.5. Pressed Powder Conductivity

Conductivity measurements were made in an apparatus designed by J. L. Dye and Michael R. Yemen (98). A powder sample was placed between two stainless steel electrodes inside a 2 mm I.D. heavy wall fused silica tube. A steel spring whose force constant had been measured was used to compress the sample. A variable temperature controller (Varian Model V-4540) was used to control the sample temperature. Powdered samples under vacuum which had been stored at dry-ice temperatures were broken in an inert atmosphere glove bag. The sample was transferred to the pre-cooled conductivity sample chamber. After the sample had been loaded, the current at various voltages was measured to determine whether Ohm's law was obeyed. Then the current through the sample was measured at a constant voltage at

a number of different temperatures.

II.D. Analysis

To begin the analysis of samples they were first decomposed with doubly distilled water in a closed vacuum system (95). The hydrogen evolved was collected and measured and the unreduced water which had been distilled into a trap was analyzed for amine solvent content in the crystalline sample. An aqueous solution of the decomposed material was made and divided into two parts, one for titration with a standard acid, the other for metal determination by flame emission spectrometry. Finally, the solution was evaporated to dryness and the residue was dissolved in D_2O so that quantitative proton NMR could be used to determine the amount of complexant present. Potassium hydrogen phthalate (KHP) was used as an internal reference for the NMR integration.

II.D.1. Hydrogen Evolution

The sample tube was scored and sealed into a glass apparatus with Teflon heat-shrinkable tubing. This apparatus was then connected to the hydrogen collection apparatus. The entire system was evacuated to $\sim 3 \times 10^{-5}$ torr and the conductance water used to decompose the sample was degassed several times through freeze-pump-thaw cycles until

no detectable gas remained. The sample tube was then broken and the conductance water was condensed onto the sample very slowly and at a low temperature. The sample was decomposed by reacting with water according to

$$M^+C\cdot N^- + 2H_2O \rightarrow M^+ + C + H_2 + N^+ + 2OH^-.$$

The hydrogen evolved was pumped through two liquid nitrogen traps with a manually operated Toepler pump and collected in a calibrated pipet. After repeated cycles of a mercury leveling bulb, the height of mercury, the atmospheric pressure and the temperature at the pipet were measured and the number of moles of evolved hydrogen was calculated by using the ideal gas law.

II.D.2. pH Titration

The decomposed solution was evaporated during hydrogen collection by condensing the water in a trap at liquid nitrogen temperature. The water was analyzed for amine solvent by measuring its pH. The residue vessel was removed, and under a nitrogen atmosphere in a glove bag a known amount of conductance water was added and a measured portion was then titrated with standard HCl solution by using a pH electrode (Corning, catalog number 476050) and digital pH meter (Orion Research Model 701A) which had been calibrated with pH buffer solutions. However, it was not possible to

calculate the exact hydroxide ion concentration in the presence of 18C6 because of the instability of the pH meter, especially in the vicinity of the end point. This behavior was verified by titration of a solution of cesium hydroxide and 18C6.

II.D.3. Flame Emission

Part of the solution was used for flame emission. The flame emission instrument (Jarrell Ash) was adjusted for the estimated parts per million (ppm) concentration of the unknown sample. Standard solutions of the appropriate metal(s) were run followed by the unknown solution. The emission value was read from a digital averager. The reading from conductance water was determined between all measurements which yielded a background emission or noise level. Calibration curves for the standards were prepared by plotting the emission output versus concentration in ppm. The concentration of the unknown was then calculated from the calibration curve.

II.D.4. ^{1}H NMR

The solution was evaporated to dryness in a partially evacuated desiccator with "Drierite" as a drying agent followed by dynamic pumping to be sure that no water was left. Then the residue was dissolved in 2 ml of a known

concentration of KHP solution in D_2O, which was used as a reference. Measurements were done on a Bruker 250 MHz NMR instrument. The integrated areas of the KHP and the unknown were compared and the number of moles of the unknown sample was calculated.

CHAPTER III

CESIUM 18-CROWN-6 ELECTRIDES

The optical spectra of films of composition $Cs^{+}18C6 \cdot e^{-}$ have been reported previously. The results indicated non-metallic behavior since the optical spectrum was quite similar to that of dilute metal ammonia solutions. However, since the earlier investigations of the nature of these electrides were only fragmentary, further investigation, using different techniques, was undertaken to better understand the nature of these electrides. The abbreviation $Cs^{+}18C6 \cdot e^{-}$ indicates the materials from which the films or powders are made (Cs and 18C6). The symbol $Cs^{+}18C6 \cdot e^{-}$ does not represent the nominal stoichiometry or the metallic or insulator character of the electrons. The ratio of the moles of metal to moles of 18C6, R, will identify the stoichiometry of a particular preparation. The characterization of the nature of these electrides was done by optical spectra, EPR, microwave conductivity and magnetic susceptibility. In some cases the characteristics are similar to those of metal-ammonia compounds, though there are many differences. The various methods of study and their results are detailed below.

III.A. Optical Spectroscopy

III.A.1. Cs-18C6 Films From Ammonia

The spectra of dry films made from ammonia solution containing Cs and 18C6 with R = 0.5 and 1 are similar. In the spectrum shown in Figure 6 with R = 1, the main peak at 7000 cm^{-1} is presumably due to trapped electrons (e_t^-). A shoulder at 8500 cm^{-1} is also observed, probably due to interaction of e_t^- with the cation Cs^+18C6 or else to the presence of different traps for the electron because of inhomogenities in the solid.

III.A.2. Films From Methylamine

Due to the inhomogenity and instability of dry films produced from ammonia solutions, it was difficult to characterize the nature of the electrides. However, using methylamine as a solvent produced more homogenity and enhanced the stability of the films. Figure 7 shows the spectrum of a dry film from methylamine solution with R = 0.5. The main peak at 7000 cm^{-1} is due to the trapped electron e_t^-, the peak is somewhat broad and there is no absorption in the far-infrared region. The damp film shows the same features except that the peak is less broad. Dry films from methylamine solution with R = 1 give a single peak at 6500 cm^{-1} (shown in Figure 7) due to trapped electrons. Interaction of these films with methylamine vapor causes

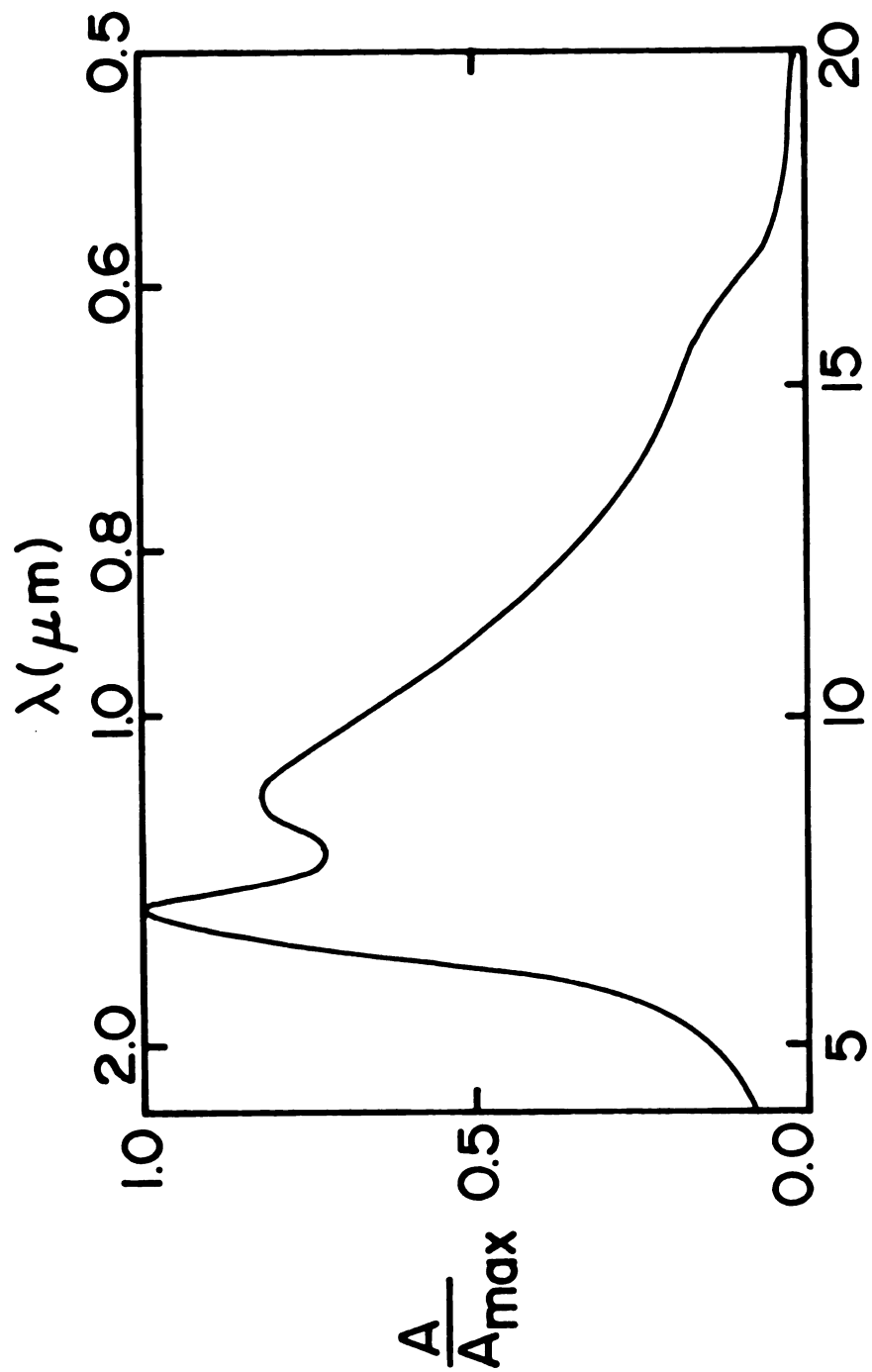

Figure 6. Optical spectrum of a dry film of Cs18C6 (R = 1) from ammonia solution.

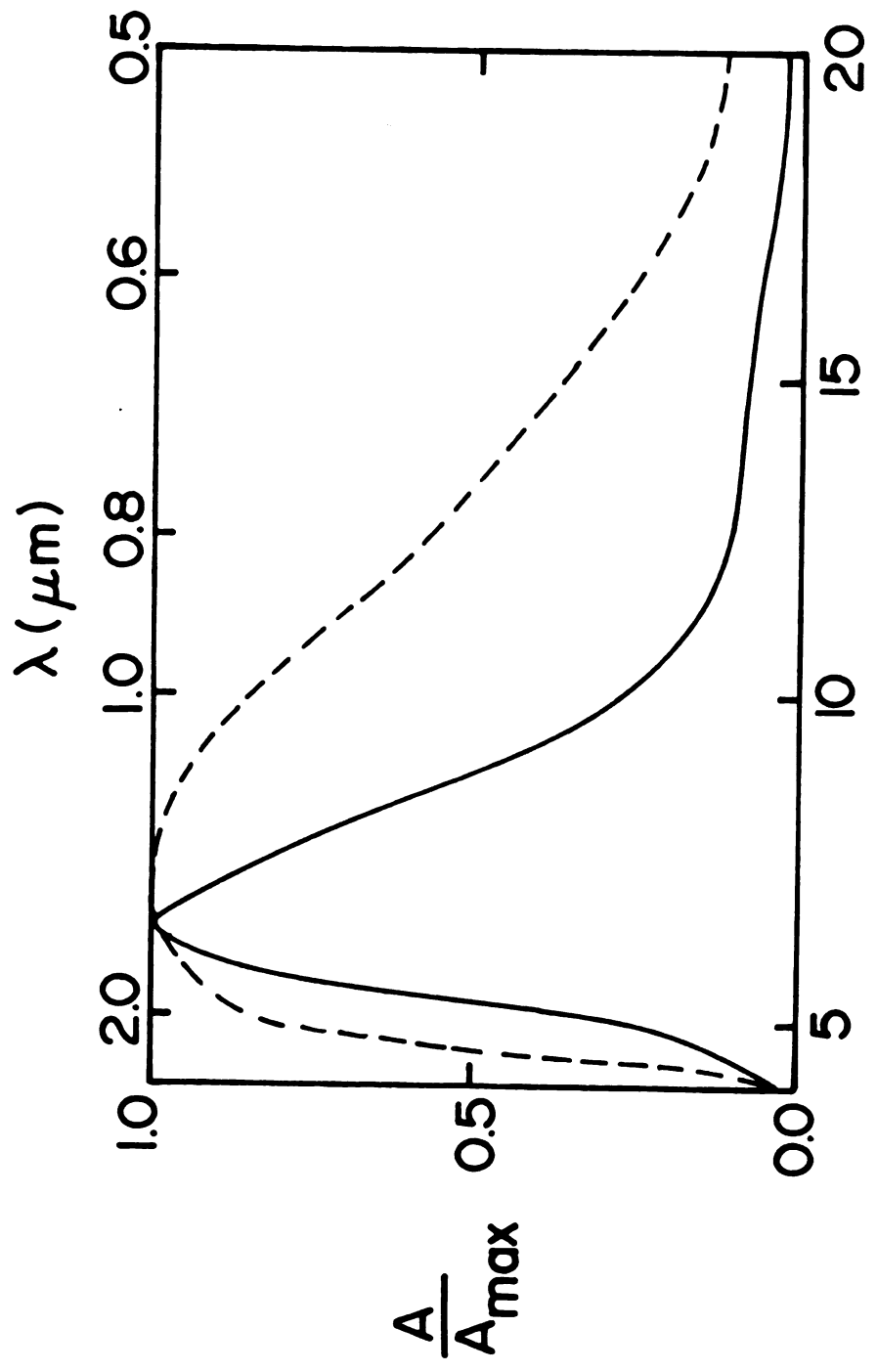

Figure 7. Optical spectra of dry films of Cs18C6 from methylamine solutions (——— R = 1), (---- R = 0.5).

a shift in the peak position towards shorter wavelength and produces shoulders on both sides of the peak. This might be due to more interaction between the electron and the cation and the presence of more than one site for the electron. These two systems show almost the same optical properties and are similar to dilute metal ammonia solutions indicating the presence of localized electrons. However, making the film richer in crown ether destabilizes the films and produces more heterogenity. In order to permit comparison with the lithium-cryptand (C211) systems which always give absorptions in the infrared region even up to R = 2 (79), a series of methylamine solutions which contained cesium metal and 18C6 in different ratios, R = 1.25, 1.5, 1.75 and 2 were prepared. The optical spectra of dry films formed from these solutions were studied. Figure 8 shows the spectrum of a dry film made at a temperature of -42°C with R = 1.5. There are two peaks, one at 10500 cm^{-1} probably due to Cs^- and a second peak at 8500 cm^{-1} due to trapped electrons. However, the Cs^- peak is a little more intense than the e_t^- peak. The position of the e_t^- peak is shifted (compared with the e_t^- peak from Cs18C6, R = 1) towards shorter wavelength, probably due to the interaction of the trapped electron with Cs^-. Another characteristic of the spectrum is the high absorption in the far-infrared region compared with the spectrum of a film of Cs 18C6 R = 1. The optical spectra for this system were also recorded when the films

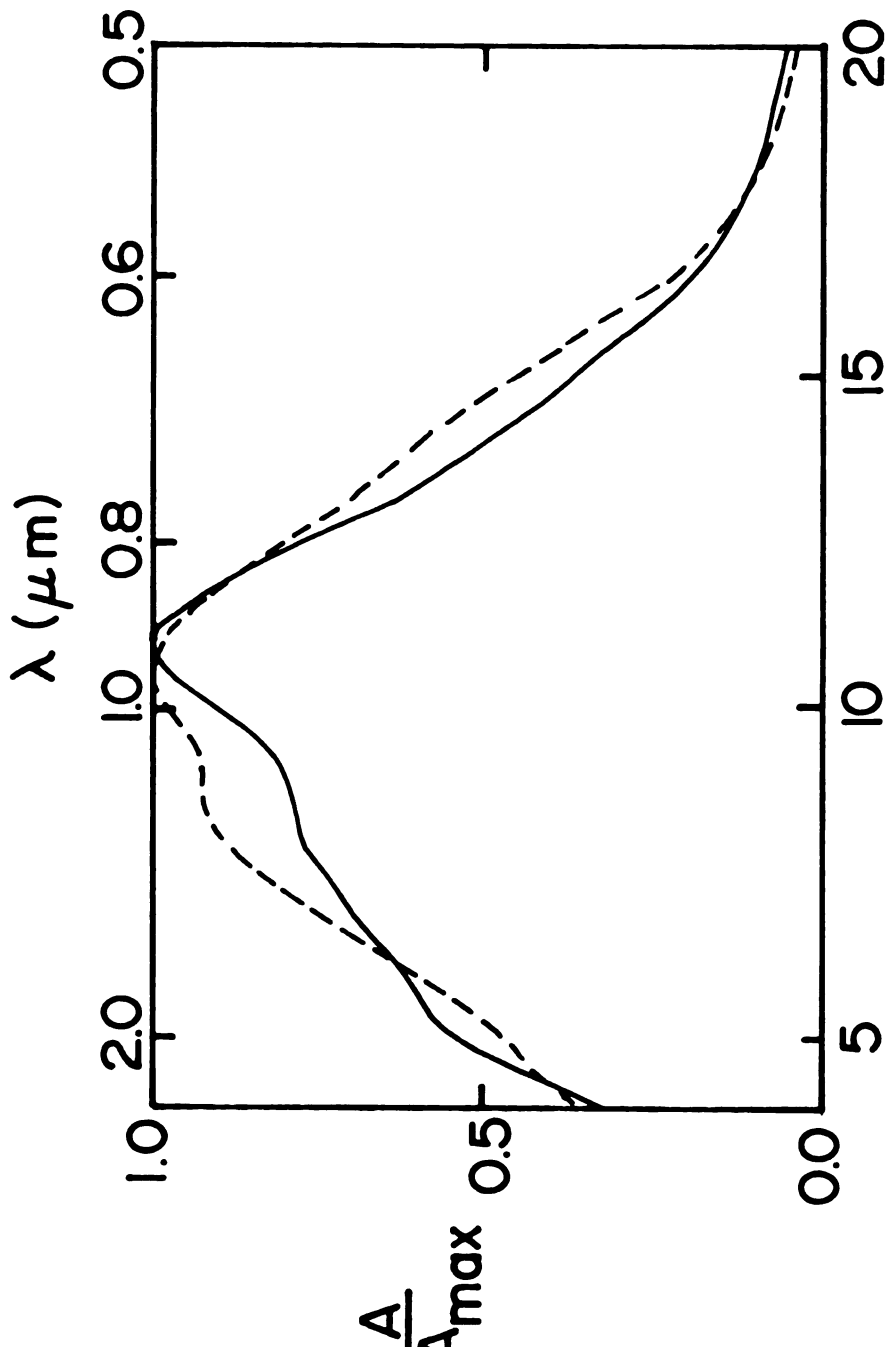

Figure 8. Optical spectra of Cs18C6 (R = 1.5) from methylamine solution (----- film made at -42°C) (——— film made at -55°C).

were made at lower temperatures. Figure 8 shows the optical spectrum of a dry film made at a temperature of -55°C. As the spectrum indicates, there is a major peak at 11000 cm^{-1} (probably caused by Cs^-) and an ill-defined broad shoulder at 8000 cm^{-1}. From these spectra we can conclude that in the range $1 < R < 2$ there are two species e_t^- and Cs^- and that they are temperature dependent. High temperatures favor the formation of the trapped electron over Cs^-. However, once the film has been formed, temperature does not affect the relative concentrations of e_t^- and Cs^-. When these films are made wet with methylamine vapor they shift to give a localized peak due to the solvated electron. However, these systems are difficult to characterize since there is more than one species. This was not the case with Cs18C6 when R = 2. Figure 9 shows the spectrum of a dry film made at a temperature of -52°C of Cs18C6 with R = 2. The main feature of the spectrum is the high absorbance in the infrared region and the apparent metallic "plasma" character similar to that of concentrated metal ammonia solutions. When the film was made at a temperature of about -45°C or higher the spectra show some changes. Figure 9 shows the spectrum of such a dry film with R = 2. The major characteristic of this spectrum is the high absorption in the far-infrared region which looks "plasma" like and two peaks at 7000 cm^{-1} and 8500 cm^{-1}. These multiple peaks are probably due to different

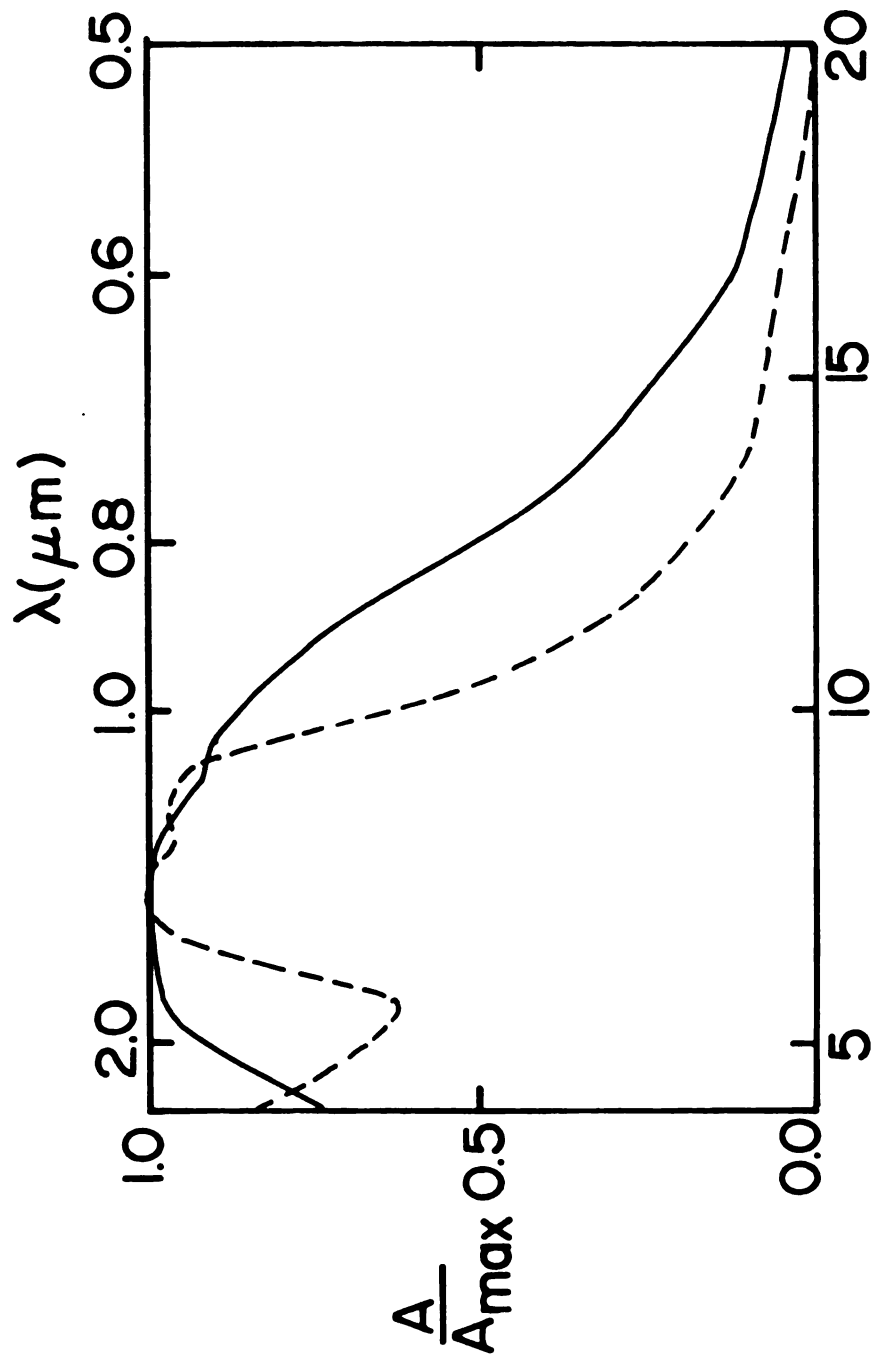

Figure 9. Optical spectra of films of Cs18C6 R = 2 from methylamine solution (——— temperature of the film -52°C), (---- temperature of the film - 45°C).

environments of the electron. Making these films "damp" with methylamine vapor tends to localize the electron peak. In spite of these complexeties, all of the above mentioned spectra were reproducible. It was also noticed that the intensities of the spectra increase dramatically at a certain temperature which depends on the ratio R. As R increases that temperature decreases. This is probably due to melting or annealing of the film which then produces more homogeneous and uniform films.

III.B. EPR

Electron paramagnetic resonance spectroscopy (EPR), in contrast to other techniques such as magnetic susceptibility detects the local environment of the unpaired spins. When a magnetic field is applied to a spin system, the energy levels of an unpaired electron are separated due to the Zeeman effect

$$\Delta E = g\beta H_0 \qquad (6)$$

where β is the Bohr magneton, g is the Landé g-factor and H_0 is the applied field. Transitions between the Zeeman levels can be achieved by radiation of appropriate frequency according to the equation

$$\Delta E = h\nu.$$

For an electron with a spin angular momentum $\frac{1}{2}$ and L = 0, so that there is no spin-orbit interaction, g = 2.0023. The g-value is used as a measure of the electron's interaction with its environment. The lineshape is determined by the type of coupling between the spins and their environment. However, there are two theoretical expressions commonly used to describe the EPR spectra which have symmetrical lineshapes (53). For systems where the spin-lattice and exchange effects predominate, the lineshape is Lorentzian. The Gaussian shape usually applies to systems where spin-spin couplings predominate. The linewidth of the EPR line is determined by the degree of coupling of the unpaired electrons to their environment. If such coupling is strong, i.e., the relaxation times are short, then the electrons spend only a small time Δt in the upper energy level. This time Δt corresponds to an uncertainty ΔE in the energy given by $\Delta E \Delta t \sim h$. Therefore, there will be a broadening of the lines observed in the EPR spectrum. In addition, there are other sources of line broadening which can be divided into two major groups. The inhomogeneous broadening, in which the unpaired electron is subjected to slightly different effective fields. Therefore, the observed line is a superposition of a number of individual components referred to as "spin packets". The reasons for inhomogeneous broadening are, inhomogeneous field, anisotropic interaction in randomly oriented systems and unresolved hyperfine structure. The

other kind is homogeneous broadening caused by non-uniformity of the instantaneous magnetic field at each dipole. There are several mechanisms which account for this homogeneous broadening. These include (a) electron spin-electron spin dipolar interaction which depends on the concentration of the paramagnetic centers; (b) electron spin-nuclear spin interaction, caused by the random local field produced by magnetic nuclei in the vicinity of the electron; and (c) electron exchange where the electrons in different sites exchange their spin states. This exchange-narrowing is important in bimolecular reactions. For dilute samples the spectra could have more than one line and as the concentration increases, these lines coalesce to a single line which becomes narrower at even higher concentrations. In solids this exchange-narrowing arises from the overlap of molecular wave functions (99).

III.B.1. Results and Discussion

III.B.1.a. Solids From Cs-18C6 Ammonia Solution

The EPR spectra of films and/or powders obtained by evaporating ammonia from solutions which contained Cs and 18-crown-6 with a ratio of R = 0.5 or 1 where (R = $\frac{\text{moles of metal}}{\text{moles of crown}}$) were studied in the temperature range 4.2 to 230 K. In general both systems showed the same lineshape and the value of $\frac{A}{B}$ (the ratio of the low-to high-field

peak amplitudes in the EPR spectrum) was always greater than 1. The variation of $\frac{A}{B}$ with temperature is shown in Figure 10 for the solid Cs-18C6 with R = 1. This high value of $\frac{A}{B}$ might be due to inhomogenities of the system which give more than one trapping site for the electron, resulting in closely-spaced peaks. The g-value determined by calibration with a standard diphenylpicrylhydrazyl (DPPH) (99) sample is 2.0019±0.0001 for the system with R = 0.5 and 2.0028±0.0001 for the system with R = 1. The g-values determined in the temperature range 230 to 140 K showed no temperature dependence. The g-values for these systems suggest that there is some interaction between the electron and its environment (presumably the Cs^{+}18C6 cation). The possibility of the presence of other phases and excess crown and metal atoms cannot be ruled out. The linewidth was 0.6 Gauss at 230 K and increased to 2.2 Gauss at 4.2 K for Cs18C6 with R = 0.5, and 0.5 Gauss at 230 K which increased to 1.05 Gauss at 4.2 K for Cs18C6 with R = 1. The variation of linewidth with temperature for Cs18C6 with R = 1 is shown in Figure 11. The general behavior is that the linewidth increases with decreasing temperature. The discrepancies in the values of the linewidths in the region of temperature where the values determined in the nitrogen temperature range should overlap with those determined in the liquid helium range might be due to the temperature cycle and to the conditions of the instrument

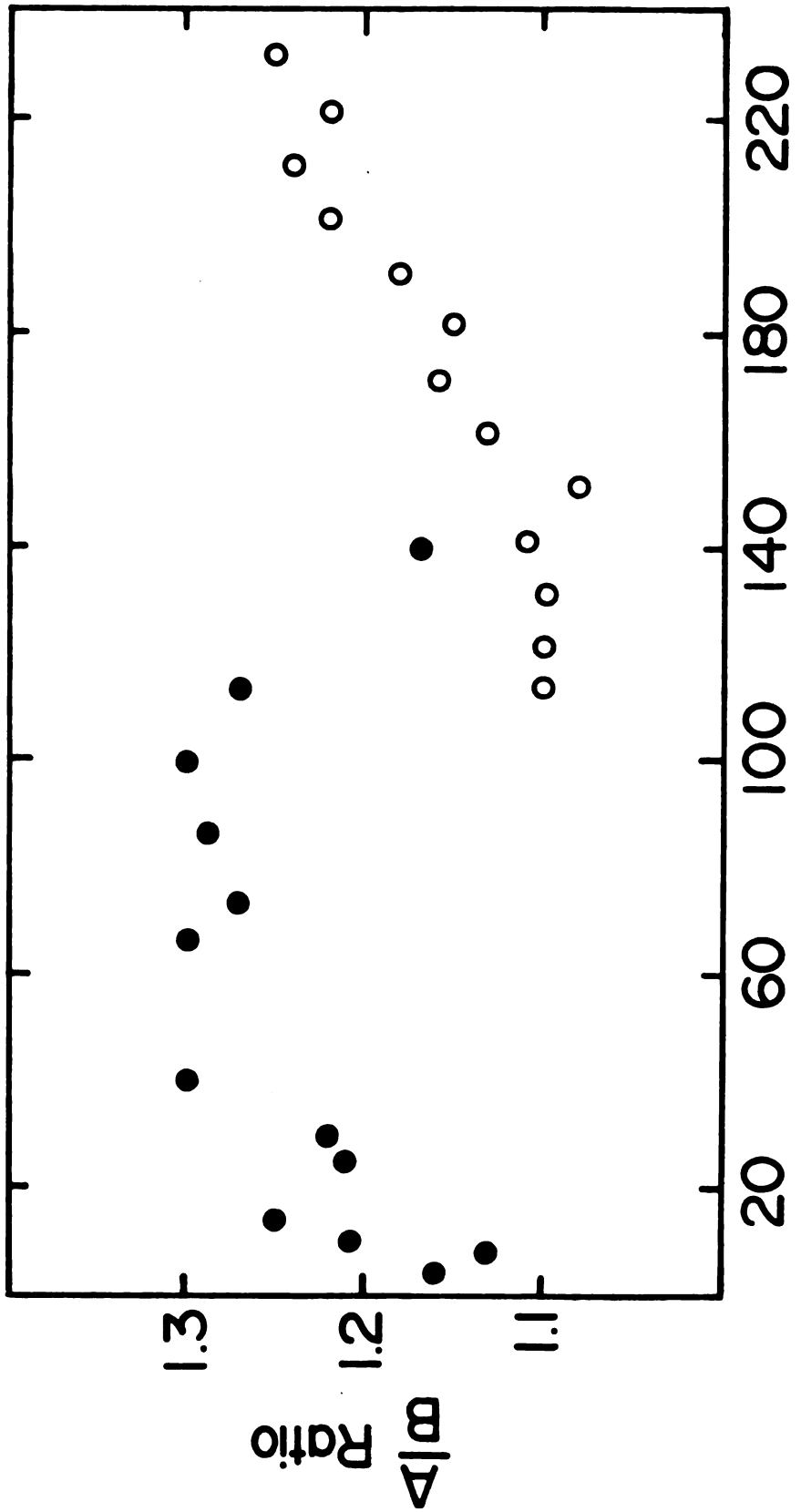

Figure 10. A/B ratios of $Cs^{+}18C6 \cdot e^{-}$ with R = 1 prepared from ammonia solution.

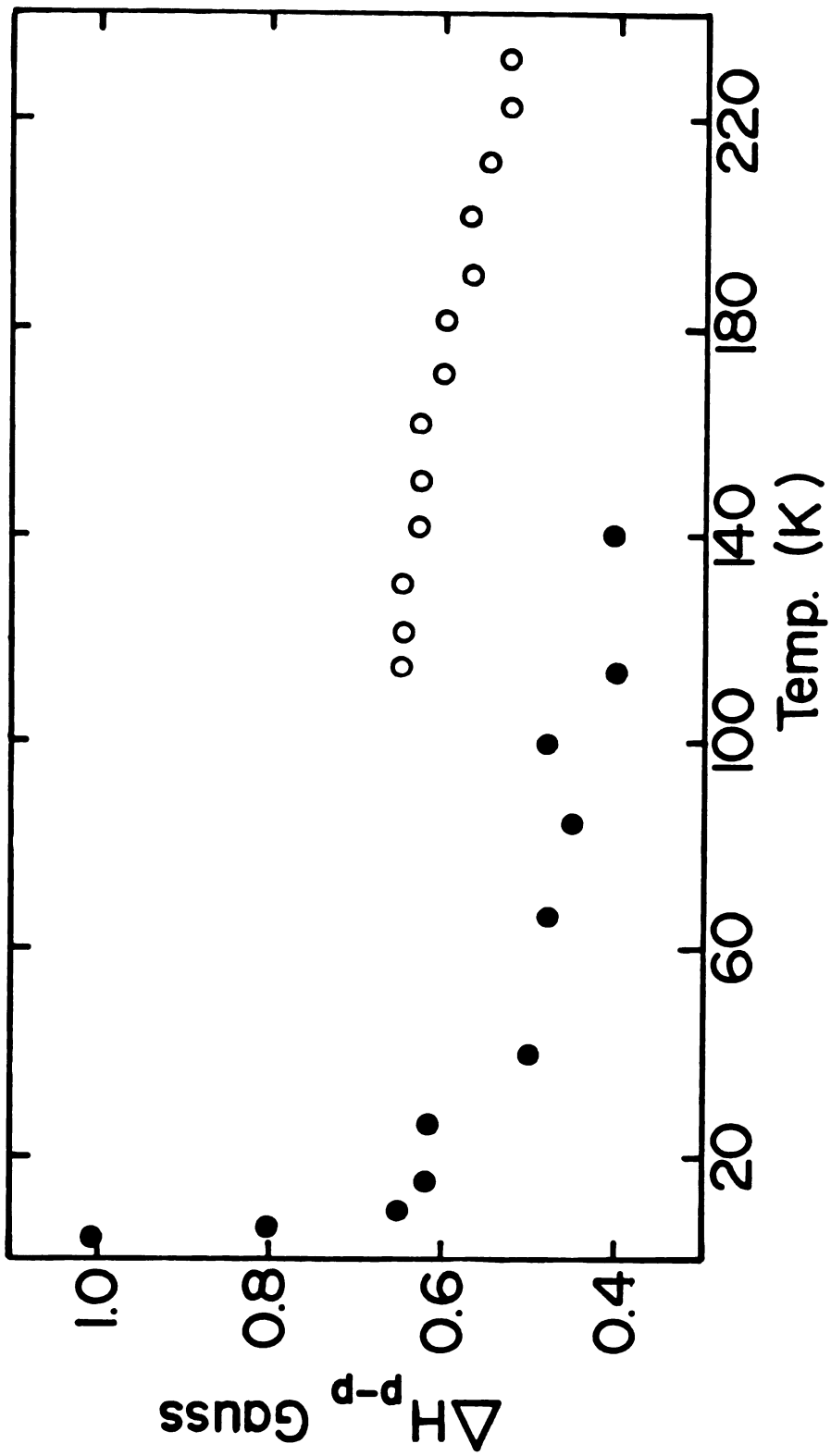

Figure 11. Linewidths of $Cs^{+}18C6 \cdot e^{-}$ (R = 1) from ammonia solution. Solid symbols data collected with ℓ-He cryostat; open symbols ℓ-N_2 cryostat.

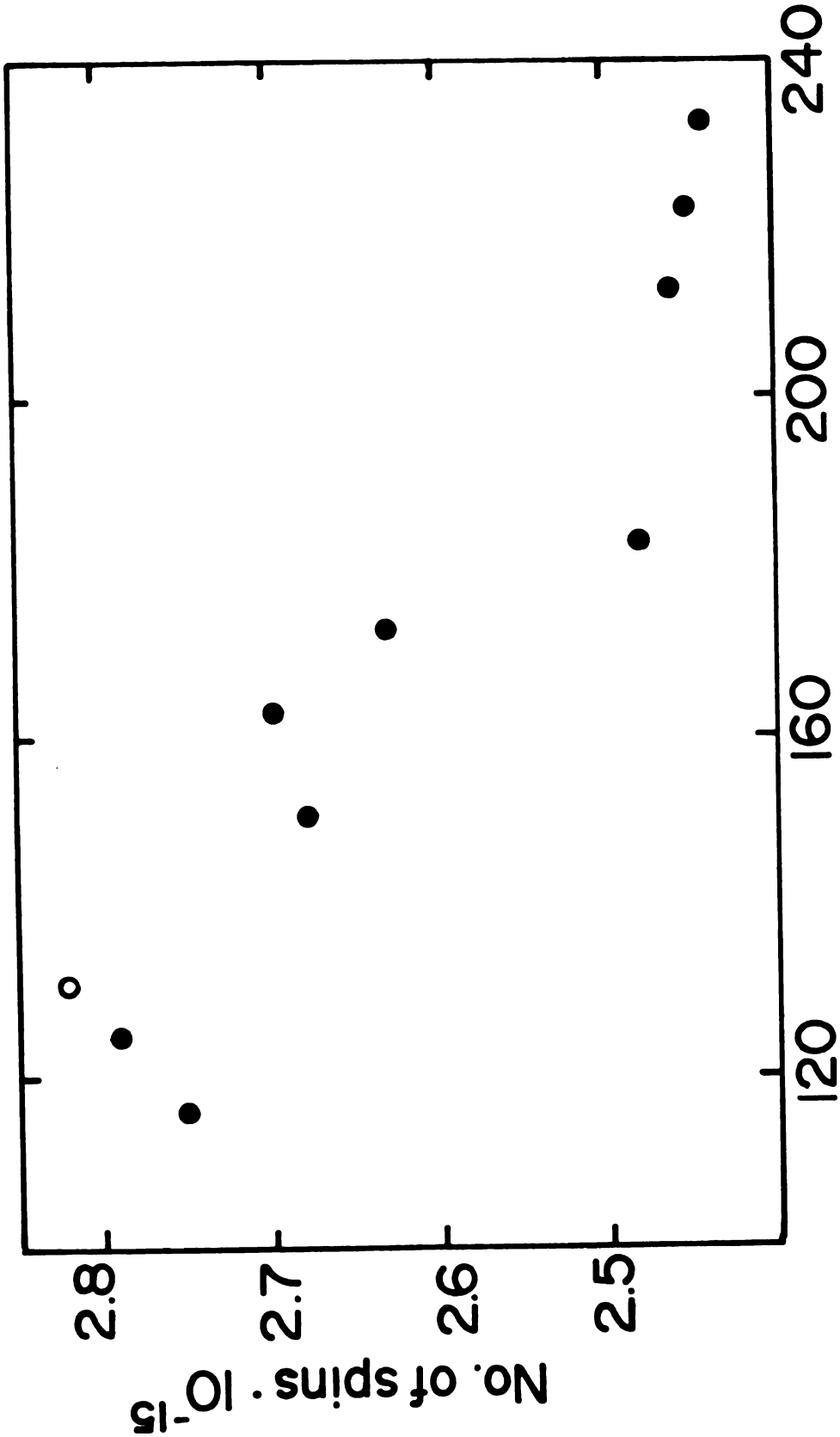

Figure 12. Number of spins vs. temperature for $Cs^{+}18C6 \cdot e^{-}$ (R = 1) from ammonia solution.

since the two runs were done separately. The number of spins calculated by using a spin standard Ruby sample (Al_2O_3 Cr^{3+}) (100) indicated that the number of spins increases with decreasing temperature. Figure 12 shows the plot of the number of spins with temperature for Cs18C6 with R = 1. However, the inhomogenity of the films and/or powders obtained from ammonia solutions made it difficult to further characterize these systems.

III.B.1.b. Solids from Cs-18C6 Methylamine Solutions

A series of methylamine solutions which contain cesium and 18-crown-6 were prepared with different ratios of metal to crown. The EPR spectra of the solid with R = $\frac{\text{metal}}{\text{crown}}$ = 0.5 were recorded in the range 4.2 to 230 K. The g-value was found to be 2.0023±0.0001 which is close to the free electron value and suggests little interaction between the electron and its environment. The variation of linewidth with temperature is shown in Figure 13, which shows that the linewidth increases gradually from 0.45 Gauss at 230 K to 2.0 Gauss at 4.2 K. The $\frac{A}{B}$ ratio (shown in Figure 14) was always greater than 1, probably due to the presence of several peaks originating from different trapping sites of the electron. This was also indicated by the broadness of the infrared peak in the optical spectra. The number of spins calculated using a spin standard Ruby as a function

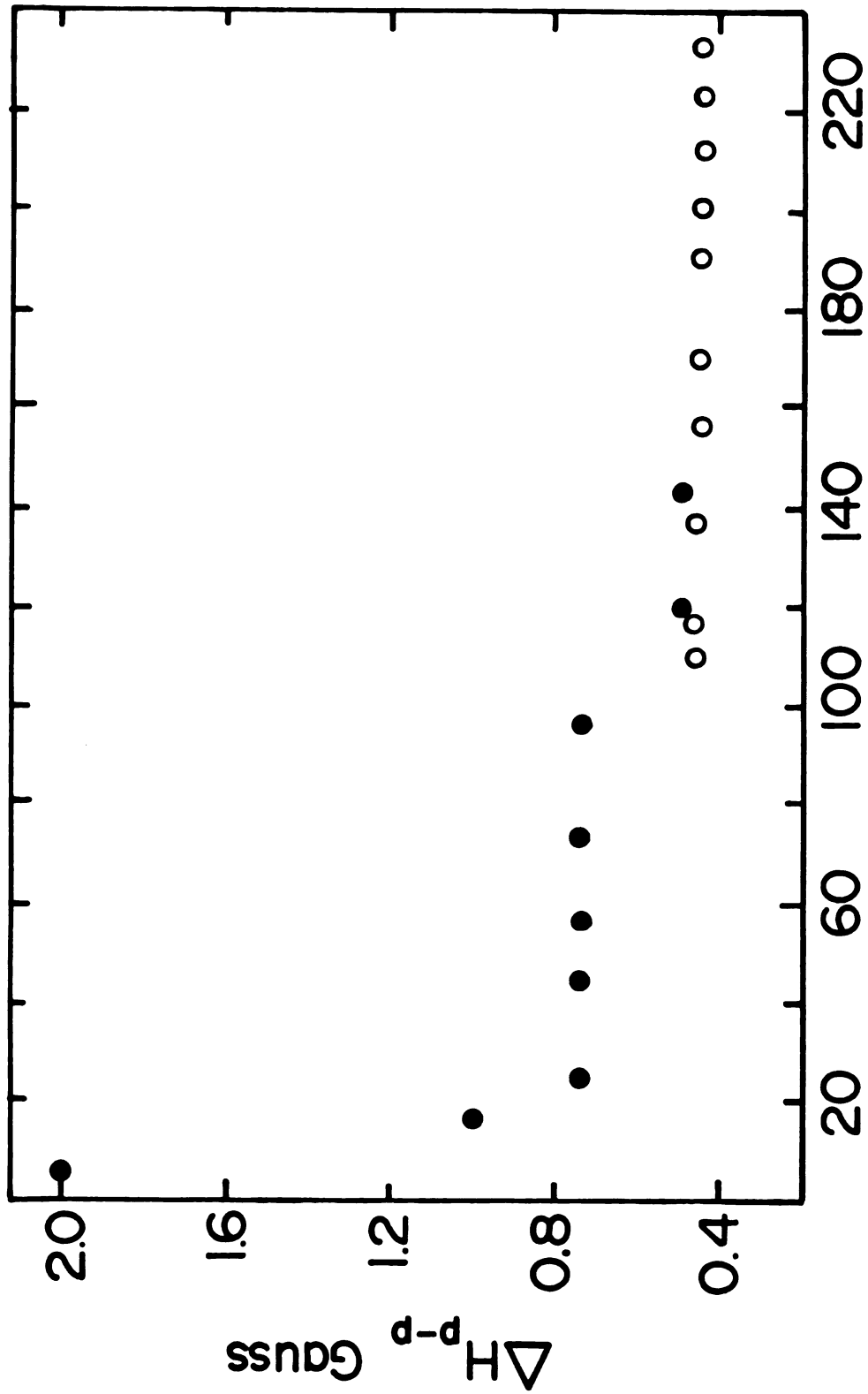

Figure 13. Linewidth of $Cs^{+}18C6 \cdot e^{-}$ with R = 0.5 from methylamine solution. Solid symbols - data collected with ℓ-He cryostat; open symbols - ℓ-N_2 cryostat.

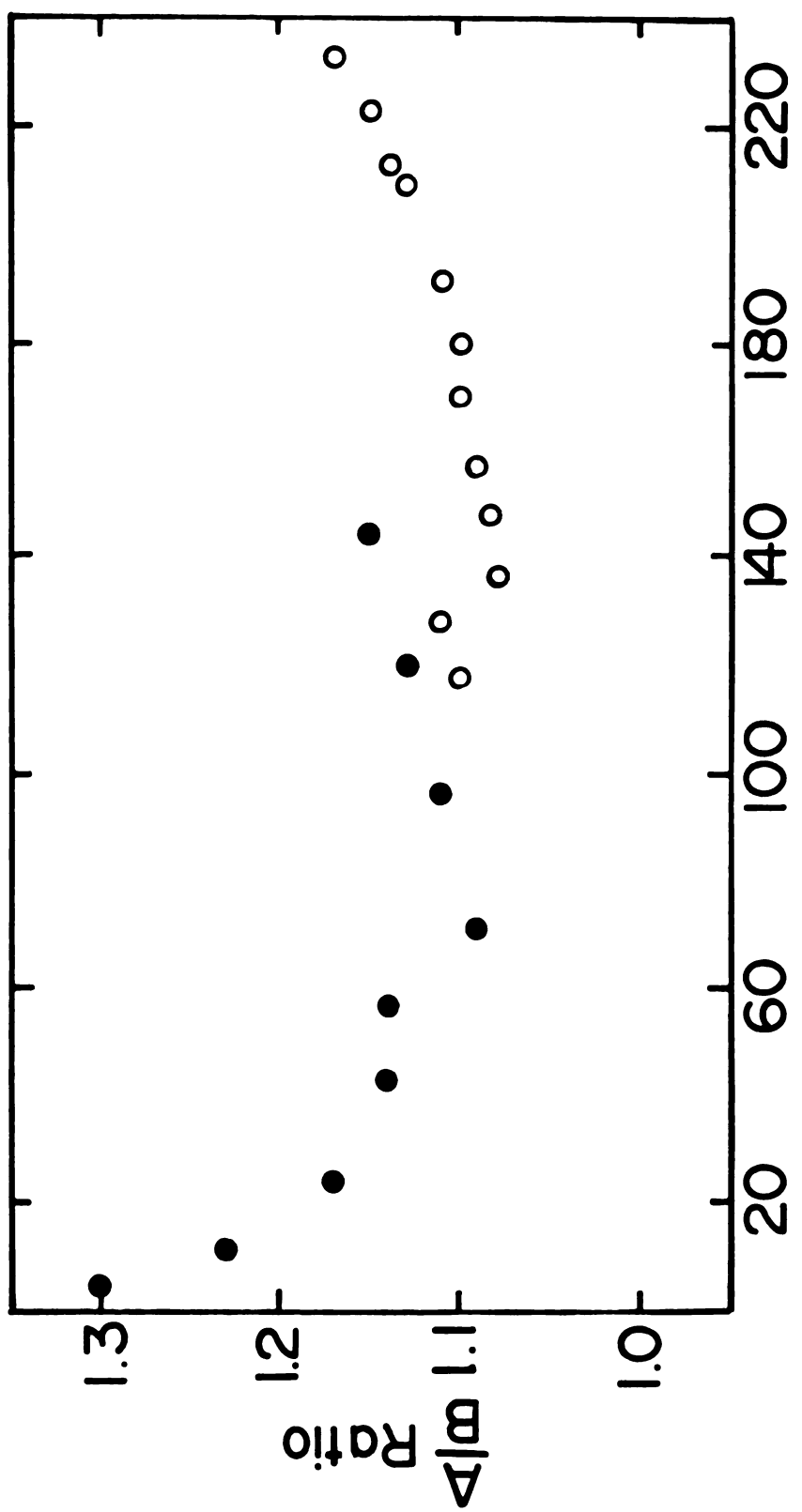

Figure 14. A/B ratios of $Cs^{+}18C6 \cdot e^{-}$ R = 0.5 from methylamine solution. Solid symbols - data collected with the ℓ-He cryostat; open symbols - ℓ-N_2 cryostat.

of temperature is shown in Figure 15. The figure shows that the number of spins increases with increasing temperature. We found the system Cs-18C6 with R = 1 to be more attractive in terms of homogenity and stability than with R = 0.5. Films and/or powder samples of Cs18C6 with R = 1 were prepared and studied by EPR spectroscopy. The g-value calculated for this system is 2.0024 0.0001 which is close to the free electron value and might suggest very little interaction between the trapped electron and the Cs^{+}18C6 cation. The linewidth, as shown in Figure 16, changes with temperature. It is 0.6 Gauss at 230 K and increases to about 1.5 Gauss at 4.6 K. This increase in linewidth might be explained by the presence of more than one peak. The fact that the lineshape has a structure at about 4 K (Figure 17) supports this, while at higher temperatures these peaks overlap to form a single line. The $\frac{A}{B}$ ratio shown in Figure 18 in the liquid nitrogen temperature range is about 1.15, while in the liquid helium temperature range it is about 1 at 4 K which decreases gradually to about 0.71. A possible explanation for values which are less than 1 is the presence of more than one peak. As shown from the figures, the two samples showed essentially the same behavior. Figure 19 shows the variation of the number of spins calculated by using a spin standard Ruby. It is difficult to conclude any specific behavior, but the general behavior is that the number of spins is less at higher temperatures.

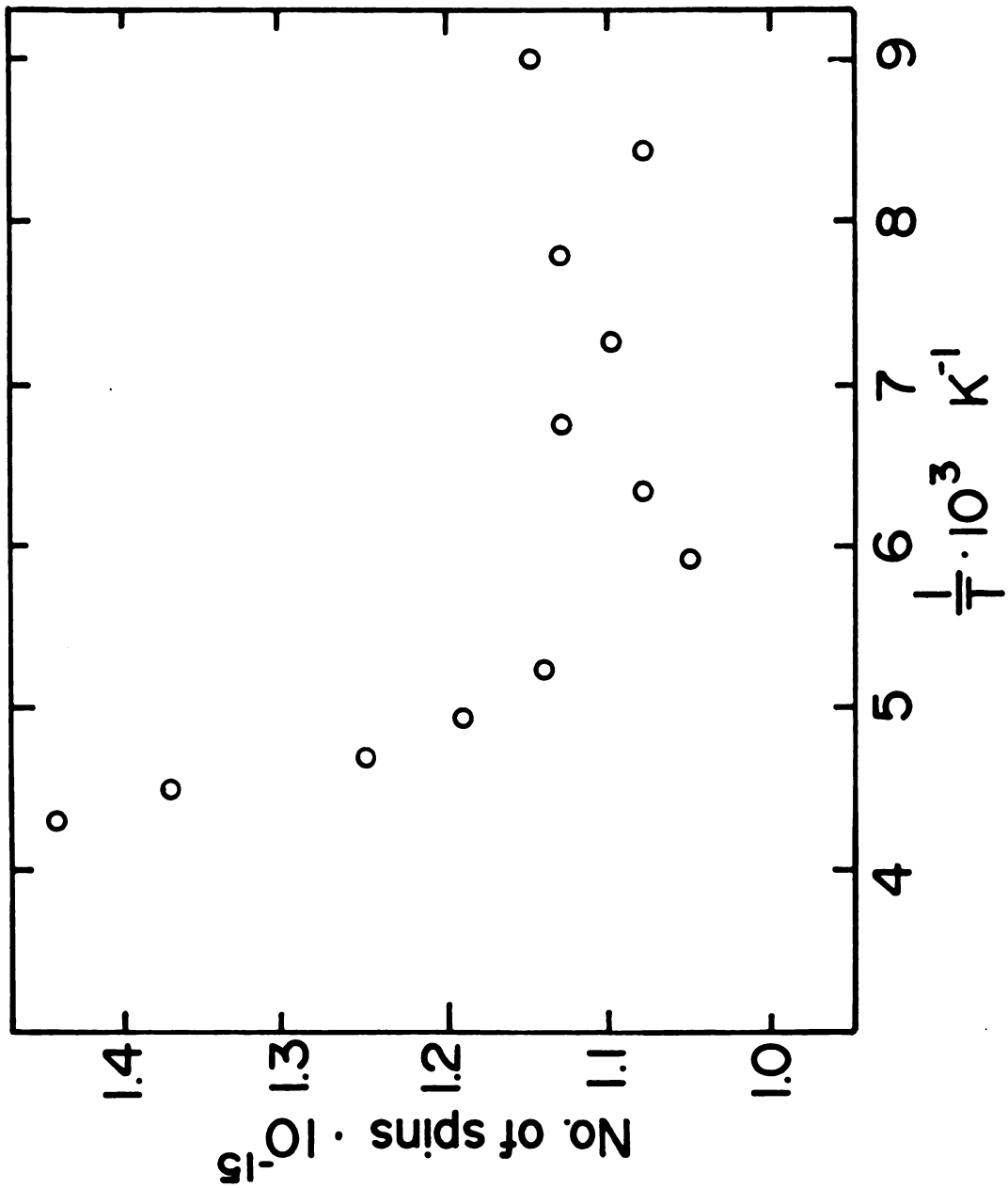

Figure 15. Number of spins against reciprocal temperature for $Cs^{+}18C6 \cdot e^{-}$ with (R = 0.5) from $MeNH_2$ solution.

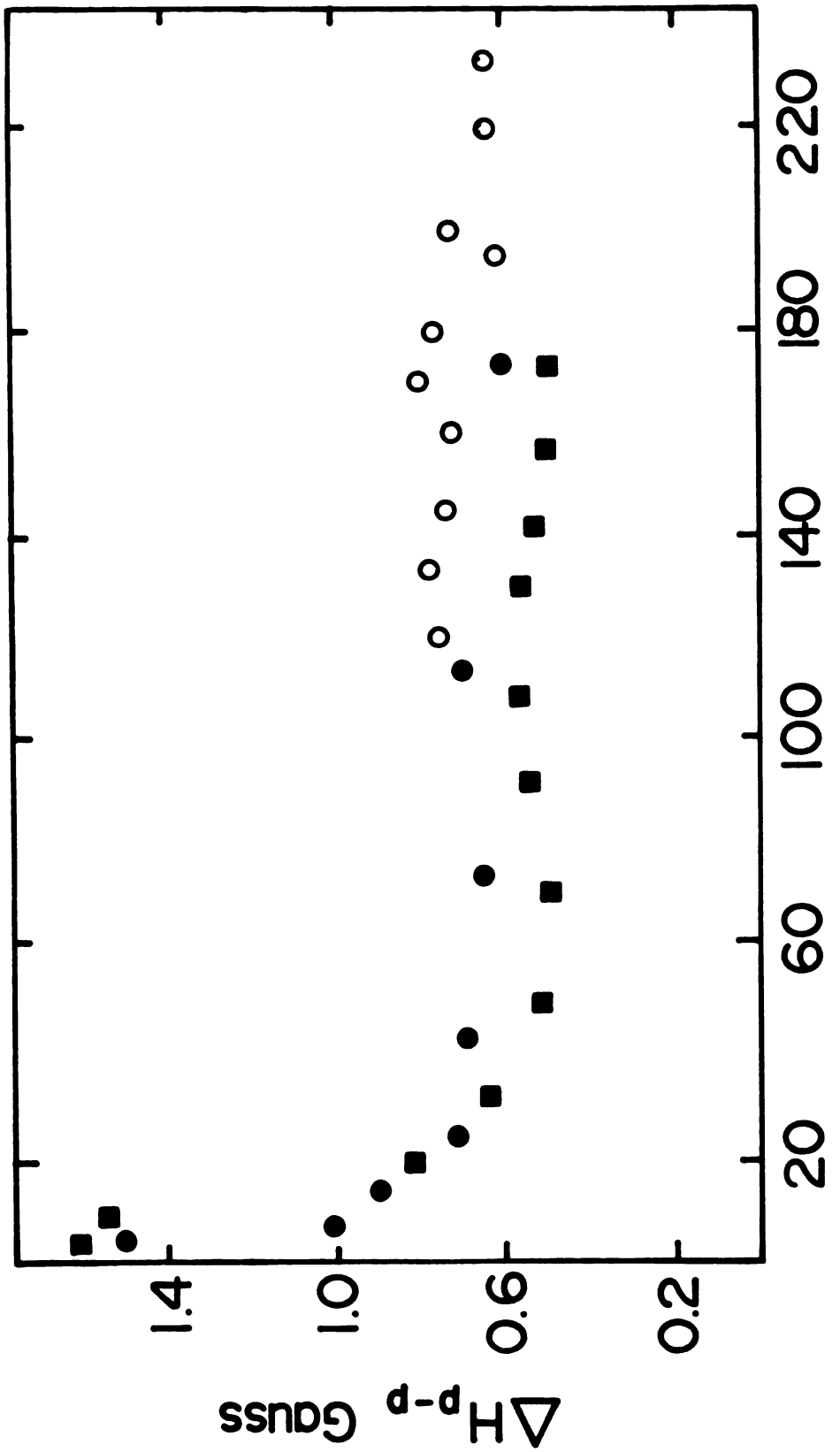

Figure 16. Linewidth of $Cs^{+}18C6 \cdot e^{-}$ with R = 1 from methylamine solution. Solid symbols - data collected with ℓ-He cryostat, open symbols - ℓ-N_2 cryostat, solid squares data collected on another sample from different preparation.

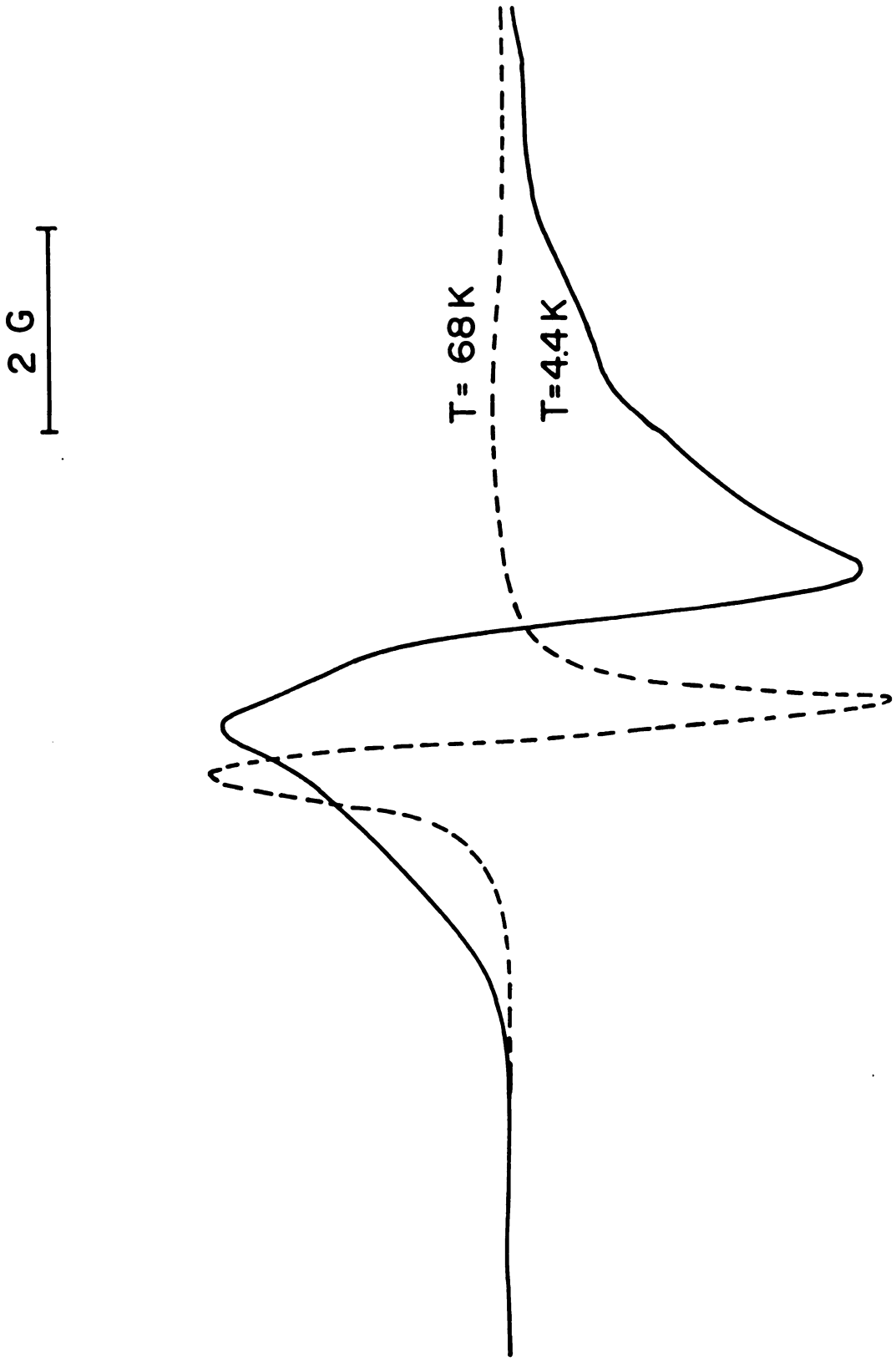

Figure 17. EPR spectra of $Cs^{+}18C6 \cdot e^{-}$ (R = 1) from methylamine at two different temperatures.

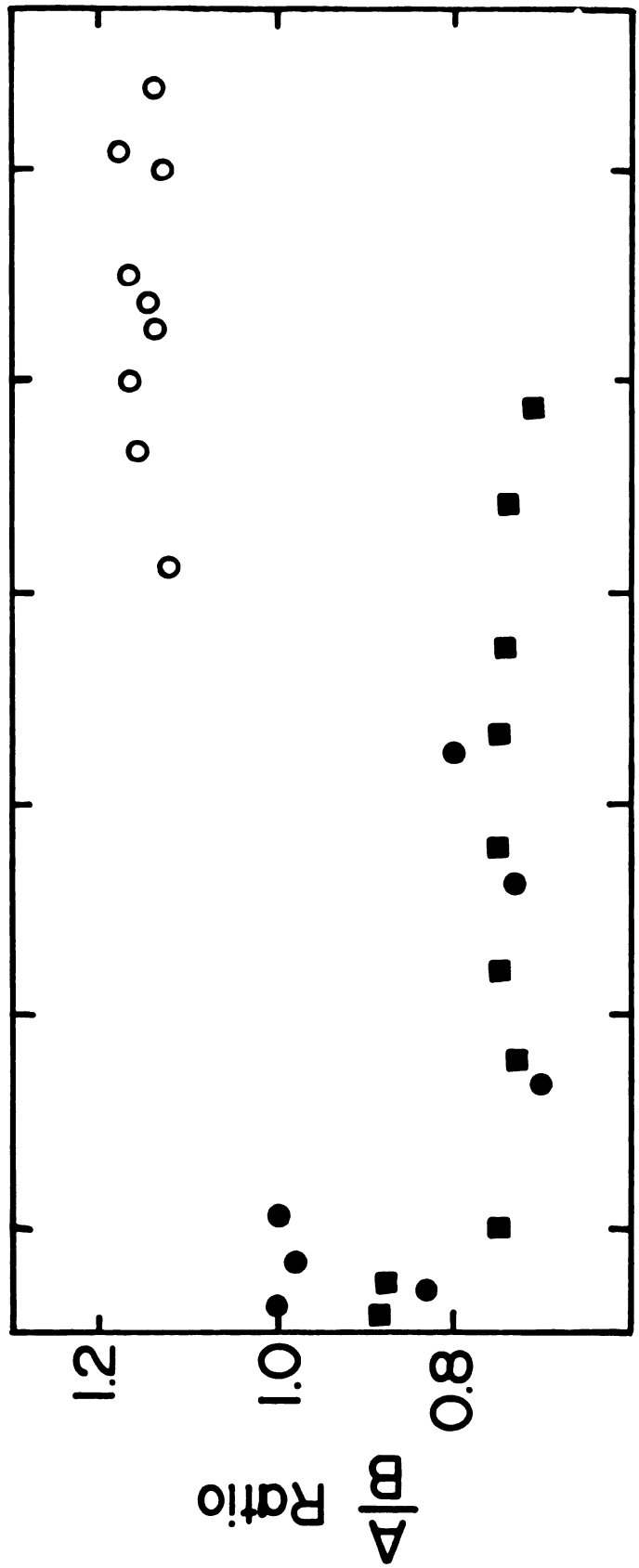

Figure 18. A/B ratios for $Cs^{+}18C6 \cdot e^{-}$ (R = 1) from methylamine. Solid symbols - data collected with ℓ-He cryostat; open symbols - ℓ-N_2 cryostat; squares - data collected on another sample from different preparation.

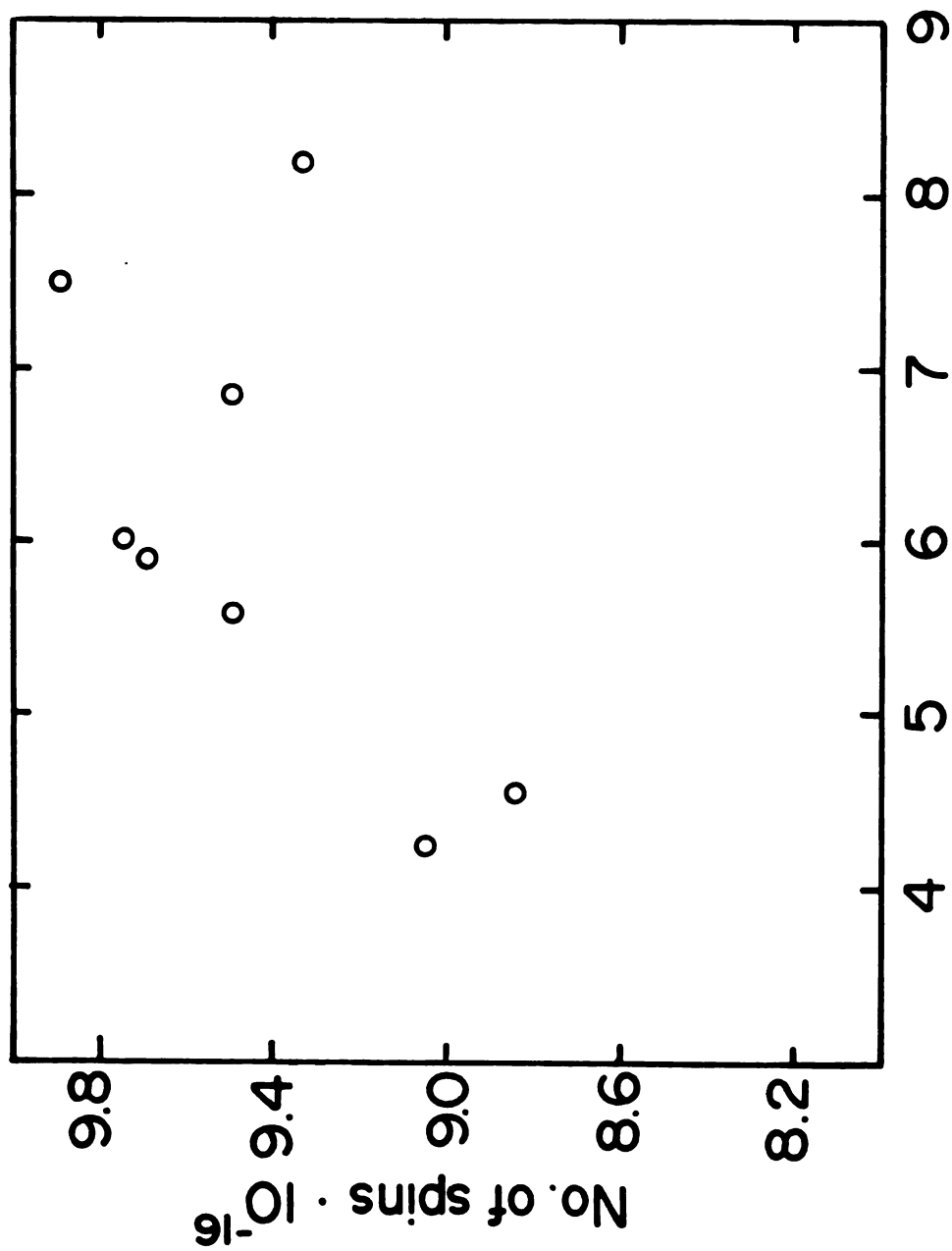

Figure 19. Number of spins vs. reciprocal temperature for $Cs^{+}18C6 \cdot e^{-}$ (R = 1) from methylamine solution.

However, since the possibility of the existence of two kinds of material is demonstrated by the linewidth and $\frac{A}{B}$ ratio. The calculated number of spins could be distorted by changes in lineshape. The system Cs-18C6 with R = 1.5 was also studied by EPR in the liquid nitrogen temperature range. The $\frac{A}{B}$ ratio was less than 1, which suggests the presence of more than one peak. The g-value is 2.0022±0.0001, which is close to the free electron value and suggests little interaction between the trapped electron and its environment. The linewidth in the liquid nitrogen range is about 0.5 to 0.6 Gauss. The number of spins calculated indicates that only about 4% of the available electrons contribute to the EPR signal. However, due to the presence of at least two kinds of species, the trapped electron, e_t^- and Cs^- as indicated by the optical spectra it is very difficult to characterize this system. On the other extreme, the system Cs-18C6 with R = 2 showed completely different properties as indicated by its optical and EPR spectra and other techniques. The average g-value in the temperature range 118-200 K is 2.0026±0.0001. The g-value showed some dependence on temperatures. While the g-value is 2.00247 at 118 K it shifted to 2.00253 at 171 K and to 2.0027 at 201 K. This indicates that the interaction between the electrons and their environment is greater at high temperatures. The $\frac{A}{B}$ ratio is about 1.3, a possible indication of Dysonian lineshape which represents

metallic systems (25). The optical spectra of films made for this system also showed this metallic behavior. The linewidth in the liquid nitrogen temperature range is about 0.5 Gauss. The percentage of the free spins (calculated by using a spin standard Ruby) which participate in the EPR absorption is only about 0.05%. This calculation is only approximate because it is valid only for systems which have Lorentzian lineshape. The EPR spectra in the liquid helium range were measured on two samples from two different preparations. The first sample which appeared to be a powder gave $\frac{A}{B} \simeq 1.1$ and a linewidth of about 37.5 Gauss at 4.3 K which decreased to 28.5 Gauss at 120 K. As the temperature increased the linewidth decreased gradually until the temperature reached about 140-150 K, at which point there was a sudden change in the spectrum. The linewidth dropped to about 5 Gauss. This change was reversible with respect to temperature. Reducing the temperature once again yielded large linewidths. The lineshape below 140 K indicates the presence of one peak and two shoulders at the ends of the peak (Figure 20), while above 140 K there is only one single peak (Figure 20). The other sample, which appeared to be a film on the walls of the EPR tube, showed qualitatively the same EPR spectral behavior. $\frac{A}{B}$ was about 1 and the linewidth was about 25 Gauss at 4.2 K. It remained almost constant at this value up to $\sim$140 K. At 140 K the EPR spectrum changed to

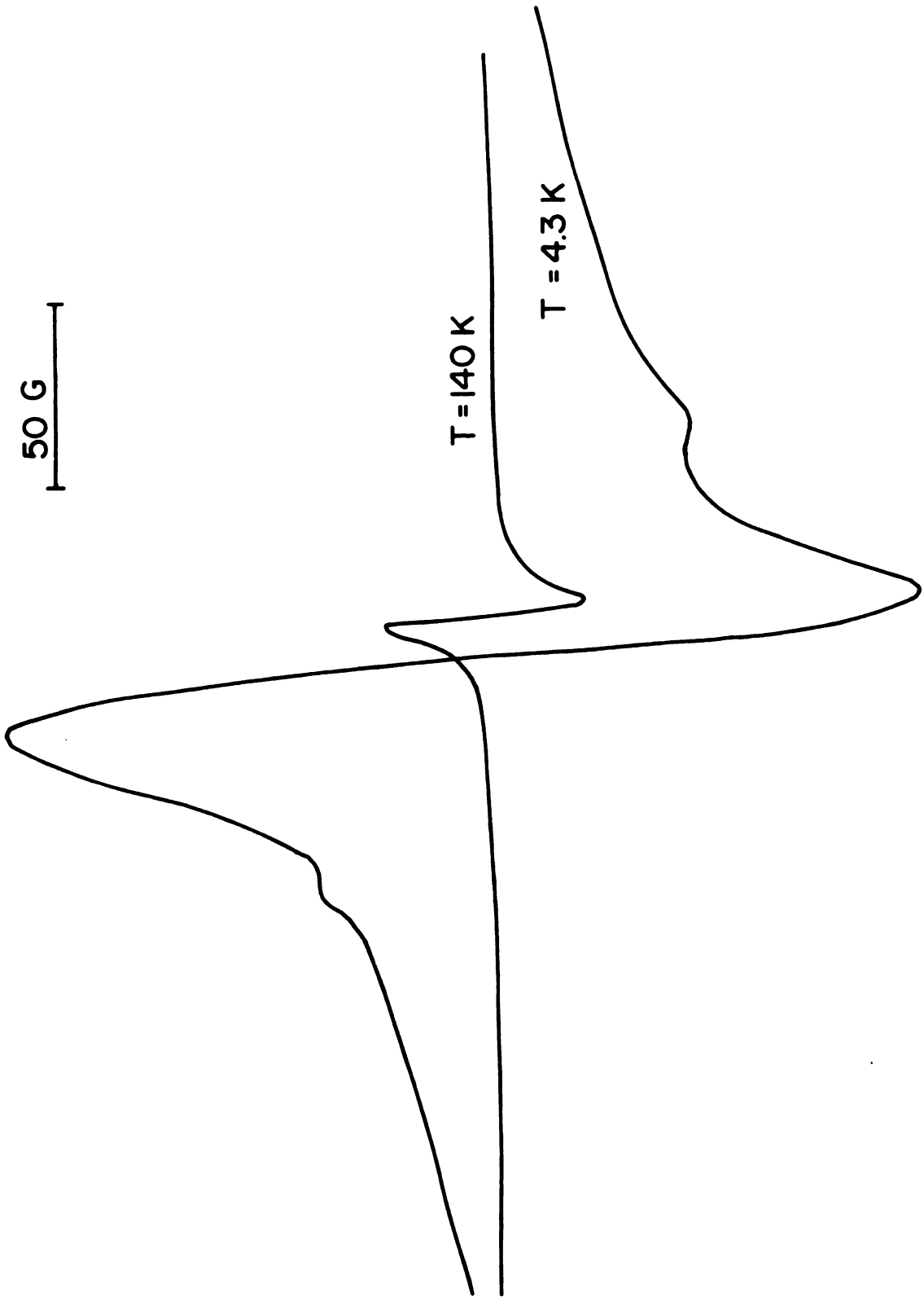

Figure 20. EPR spectra of Cs18C6·e^- with R = 2 from methylamine solution.

give a more symmetrical lineshape and a smaller linewidth. This behavior might be due to an electron exchange process (99) which participates in the broadening of the peak and there might be several unresolved peaks which overlap at higher temperatures to give a single symmetrical line. The dependence of the g-value on temperature supports this explanation. However, possible phase change cannot be ruled out. This system looked crystalline under the microscope. However, the instability and the reactivity of this system made it impossible at this point to prepare temperature stable powders or crystals.

III.C. Magnetic Susceptibility

Magnetic susceptibility is determined by the response of the material to an applied external magnetic field. When a substance is placed in a magnetic field of strength $\bar{H}$, the magnetic induction $\bar{B}$ in the substance is given by the equation

$$\bar{B} = \bar{H} + 4\pi\bar{M} \qquad (7)$$

where $\bar{M}$ is the intensity of magnetization or the magnetic moment per unit volume. For an isotropic material $\bar{M}$ is proportional to $\bar{H}$ and the proportionality constant is the volume magnetic susceptibility

$$\chi_V = \frac{M}{H} \qquad (8)$$

Quite frequently the susceptibility is referred to unit mass or to a mole of the substance. The gram susceptibility is given by

$$\chi_{gm} = \frac{\chi_V}{\rho} \tag{9}$$

where ρ is the density. If M is the molecular weight, the molar susceptibility is given by

$$\chi_M = M\chi_{gm} \tag{10}$$

All materials have diamagnetic contributions to their susceptibility which results from the orbital motion of the electrons. If the net susceptibility is negative, the substance is diamagnetic. Substances with a positive susceptibility are paramagnetic. Paramagnetism occurs only in materials in which individual atoms or molecules have permanent magnetic moments. The paramagnetism arises from several sources. The free spin paramagnetism which is due to non-interacting unpaired electrons can be described by the Curie-Law

$$\chi = \frac{M}{H} = \frac{NP^2\mu_\beta^2}{3kT} = \frac{C}{T} \tag{11}$$

where N is Avogardo's number, k is Boltzmann constant, μ_β is the Bohr magneton (eh/4 Me) and P is the effective

number of Bohr magnetons and is defined as

$$P = g[J(J+1)]^{\frac{1}{2}} \qquad (12)$$

where J is the total angular moment quantum number and g is the Landé g-factor. For a system with single spin and no spin-orbit interaction $P = g[S(S+1)]^{\frac{1}{2}}$, where S is the spin quantum number. For the case $S = \frac{1}{2}$, the Curie constant, C, calculated from the above equation is 0.37604 cm^3 k $mole^{-1}$ for a mole of free spins. Equation 12 must be modified when internal interactions occur between the magnetic atoms, which tend to align the spins. Weiss first postulated such interactions and it was shown later by Heisenberg that this interaction can be described as a result of quantum mechanical exchange interactions (101). The exchange energy of a two electron system is written as $-2J_{12}(S_1 \cdot S_2)$, where J is the exchange integral and is related to the overlap of the charge distribution of the atoms 1 and 2. For a ferromagnetic system in which the magnetic moments tend to align parallel to each other the exchange integral J is positive while for antiferromagnetic systems it is negative. In the temperature range where antiferromagnetic and ferromagnetic interactions are too weak to lead to spontaneous ordering, the susceptibility can be described by the Curie-Weiss Law

$$\chi = \frac{C}{T-\theta} \qquad (13)$$

where θ is a temperature characteristic of the material generally called the Weiss constant. θ is positive for ferromagnets and usually, but not always, negative for antiferromagnets. Another type of paramagnetism is due to conduction electrons in a metal. Pauli explained this phenomenon by the application of the Fermi-Dirac distribution (102). In this model, which is called the Fermi-gas model, the net magnetization of the conduction electrons is given by $N\mu^2H/k_BT$ and only the electrons within the range k_BT of the Fermi energy are likely to change spin in an applied field. Therefore, only a fraction T/T_F (where T_F is the Fermi temperature) of the total number of electrons contribute to the susceptibility, hence

$$\chi_M = \frac{N\mu_B^2}{k_BT_F} \qquad (14)$$

This result is the net magnetic susceptibility for conduction electrons after making the Landau's correction for diamagnetism.

III.C.1. Results and Discussion

III.C.1.a. $Cs(18C6)_2$ Solid From Methylamine Solution

Magnetic susceptibility measurements were done on solid powder, produced by evaporation of the solvent from methylamine solution with the composition Cs and 18C6 in a ratio

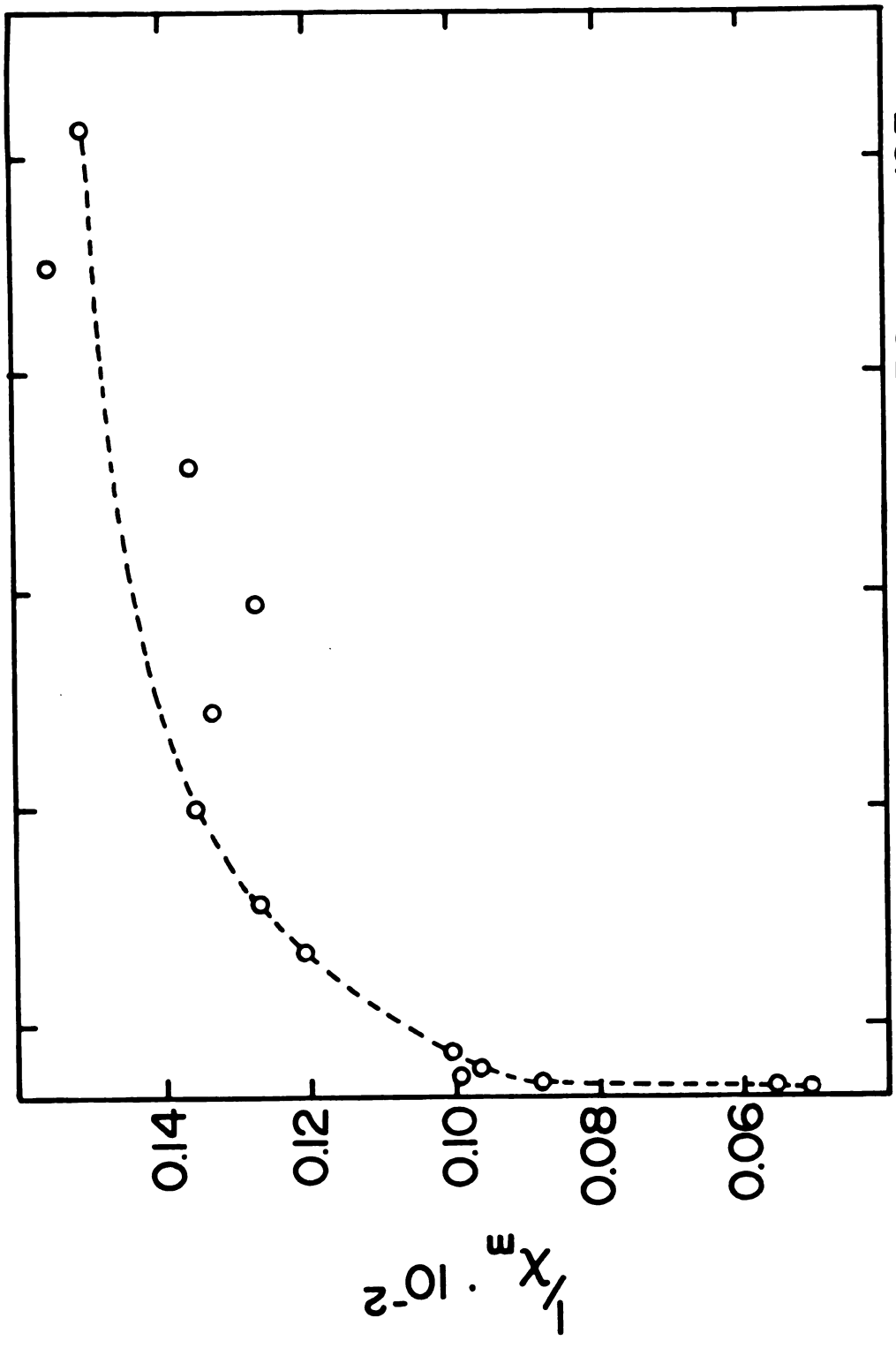

Figure 21. Plot of reciprocal molar susceptibility vs. temperature of $Cs^{+}18C6 \cdot e^{-}$ (R = 0.5) from methylamine solutions.

1:2. The measurements in the temperature range 1.7 to 200 K showed a temperature dependent paramagnetism. The plot of $\frac{1}{\chi_m}$ vs. T (Figure 21) does not follow the Curie-Weiss Law. This behavior was also observed in another more stable system, Cs-18C6 in a ratio 1:1 (see below). Because of this behavior and other reasons such as the possible presence of different phases in the solid, this system was not studied further.

III.C.1.b. $\underline{(Cs)\text{-}(18C6)_1}$:

Several samples from methylamine solution of composition Cs-18C6 in a ratio 1:1 were prepared and their magnetic susceptibilities were measured in the temperature range 1.7 to 250 K. All the samples showed the same qualitative behavior, but quantitatively there were some differences which might be due to partial decomposition which is likely to occur to different extents in different samples because of difficulties in handling these reactive compounds. The results reported here are those for the most stable samples determined by its blue color and the absence of white color due to decomposition after ejecting the sample from the SQUID when the run had been completed. The reciprocal molar susceptibility $\frac{1}{\chi_m}$ was plotted <u>vs</u> temperature as shown in Figure 22. The plot does not follow the Curie-Weiss law in any of the samples over the whole temperature range. A possible explanation is the

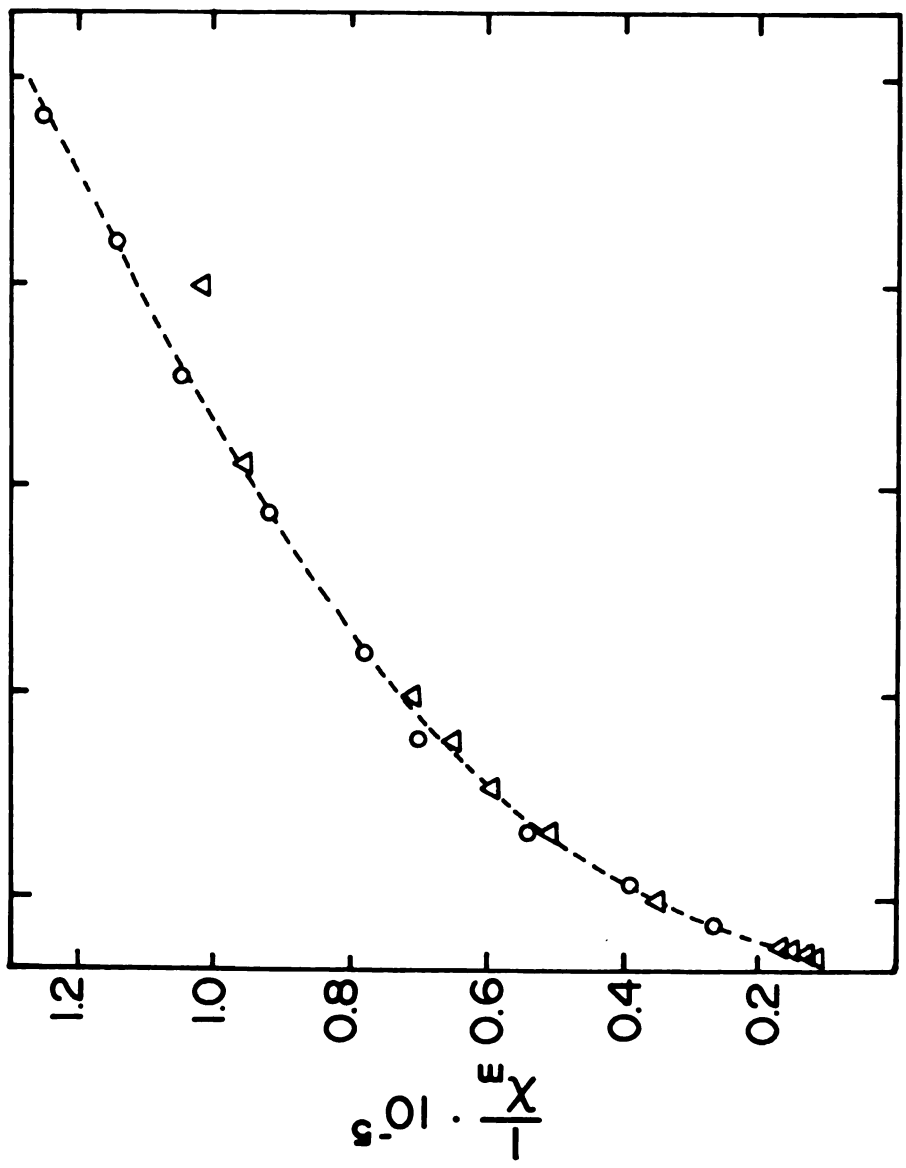

Figure 22. Plot of reciprocal molar susceptibility vs. temperature for $Cs^{+}18C6 \cdot e^{-}$ (R = 1) from methylamine solutions - Δ data taken as temperature increases; o - data taken as temperature decreases.

presence of two non-interacting magnetic sites or two types of materials. In this case the susceptibility would be the sum of two individual susceptibilities. The results were fitted to the following equation by using the non-linear least squares program KINFIT (103).

$$\frac{1}{\chi_m} = \frac{C_1}{T-\theta_1} + \frac{C_2}{T-\theta_2}$$

The fit of the measurements on the three samples gave almost the same qualitative behavior, but they differed quantitatively. The values of the parameters from the fit are tabulated below:

Table 1. Values for the Parameters in the Fit of the Static Susceptibility for Three Different Samples with Two Non-Interacting Centers.

Sample	C_1	θ_1	C_2	θ_2
1	0.033±0.003	-2.06±0.35	0.275±0.061	-262±85
2	0.012±0.001	-1.44±0.16	0.095±0.260	-798±247
3	0.023±0.002	-1.82±0.25	1.330±0.480	-725±309

The values of θ_1 and θ_2 suggest that the sample exhibit antiferromagnetic behavior.

III.C.1.c. $\underline{(Cs)_2(18C6)_1}$

This system showed very different behavior. Figure 23 shows a plot of the molar magnetic susceptibility vs temperature. The sample has almost a temperature-independent paramagnetism above 30 K and a temperature dependent paramagnetism below 30 K. The behavior above 30 K can be interpreted as the Pauli paramagnetism for conduction electrons in a metallic system. The optical and EPR spectra indicate such metallic behavior. The behavior at low temperatures might be due to some magnetic impurities. To be certain about this behavior, reproducibility of these results should be demonstrated, but the high reactivity and instability of this system made it very difficult to prepare.

III.D. Microwave Conductivity - Results and Discussion

The microwave conductivity measurements of several Cs-18C6 systems were conducted in the microwave region (x-band) following the method of Lok (104). In this method the relative power absorption of the sample was compared with known standards ranging from metals to insulators. The samples were prepared in 3 mm O.D. fused silica tubes, placed in a microwave cavity (TE_{103}) and the power transmitted was measured with a power meter (Hewlett-Packard Model 432 A) attached to a 10 db coupler. All standard samples were commercially available and were used without

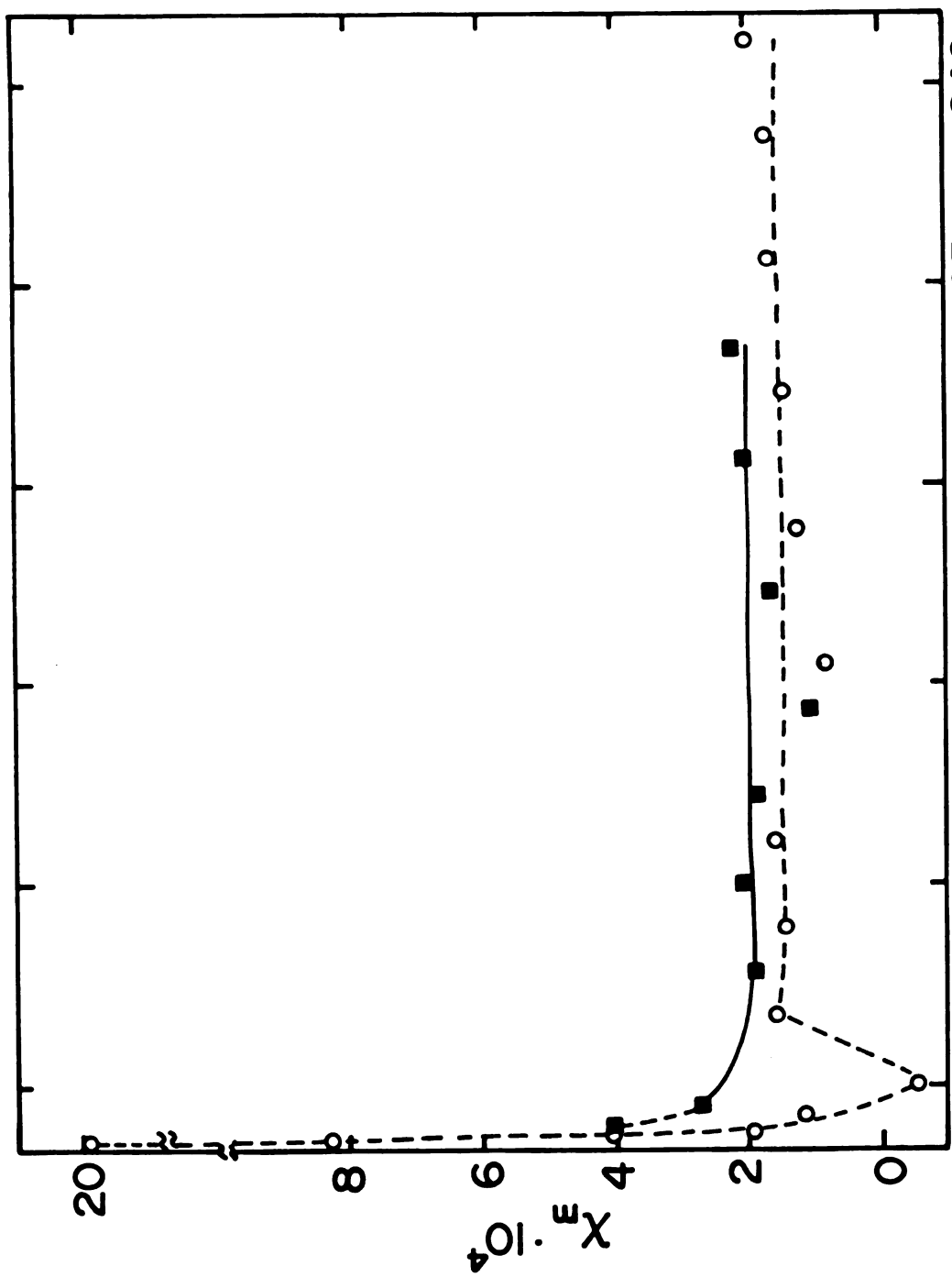

Figure 23. Plot of molar susceptibility vs. temperature for $Cs^+18C6 \cdot e^-$ (R = 2) from methylamine solution. Circles resemble data taken as temperature increases; squares resemble data taken as temperature decreases.

further purification. Because of the unknown skin depth of the Cs-18C6 samples and because the cavity filling factor varied between samples and standards, this method gives only qualitative results, but it can certainly distinguish qualitatively between metals, low-gap semiconductors and insulators. It should be noted that for band gaps much larger than k_BT the results are indistinguishable from those obtained with insulators. Tables 2 and 3 summarize the results of the microwave conductivity measurements of Cs-18C6 systems compared with the standards. The measurements showed that solids prepared from ammonia and methylamine solutions with R = 0.5 and 1 are poor conductors. The solids from methylamine solutions with R = 1.25 and 1.5 also showed similar behavior in spite of the fact that there is some optical absorption in the I.R. region at 4000 cm^{-1}. The solid Cs-18C6 with R = 2 which shows a "plasma" type absorption in the optical spectra did not show truly metallic character by the microwave conductivity measurement, but it certainly was different from the rest of the systems. The power absorbed by this sample was of comparable value to that of a low band-gap semiconductor. However, by the method we used we were not able to distinguish between the other electrides prepared from Cs-18C6 with different proportions.

Table 2. Microwave Conductivity Measurements of $Cs^{+}18C6 \cdot e^{-}$ Compared with the Standards.

Sample	Voltage	Power Transmitted mA	Sample	Voltage	Power Transmitted mA
Copper <1 μ	904	0.024	$(Cs)_1(18C)_1/NH_3$	966	1.45
Pallidium (full)	932	0	$Cs(18C6)_2NH_3$	975	1.45
Pallidium (0.65)	936	0.022	$Cs(18C6)_2/MeNH_2$	962	1.30
Pallidium (0.35)	960	0.073	$Cs(18C6)_2MeNH_2$	965	1.35
Triphenylmethane (full)	966	1.45			
Empty glass	967	1.45			

Table 3. Microwave Conductivity Results of $Cs^{+}18C6 \cdot e^{-}$ Electrides Compared with the Standards.

Sample	Voltage	Power Transmitted mA	Sample	Voltage	Power Transmitted mA
Copper <1 μ	606.25	0.075	$(Cs)_1(18C6)_1/MeNH_2$	606.8	0.52
Pallidium (full)	606.5	0.08	$(Cs)_{1.25}(18C6)_1$	606.55	0.52
Pallidium (0.65)	606.25	0.054			
			$(Cs)_{1.5}18C6$	606.4	0.52
Pallidium (0.35)	606.55	0.46			
Q_3Me	606.6	0.54	$(Cs)_2(18C6)_1$	606.6	0.48
Empty Glass	606.7	0.54			

CHAPTER IV

ALKALI METAL 18-CROWN-6 ALKALIDES

Since the preparation and characterization of the first crystalline salt ($Na^+C222 \cdot Na^-$) of an alkali metal anion in 1974 (66,67) the formation of other alkali metal anions was observed in the film spectra (75,78). The first synthesis (105) and characterization of two sodide salts which use 18-crown-6 is reported here.

The synthesis of alkalide salts has been greatly aided by the ability to measure the transmission spectra of thin solvent-free films produced by rapid solvent evaporation. These spectra permit the identification of the alkali metal anion and also indicate when trapped electrons are likely to be present. Besides that, they provide information about the stability of alkalides in the presence of the complexing agents. The preparation procedure of the alkalides has been discussed in the experimental section. The properties of these alkalides will be reviewed in the following sections.

IV.A. Optical Spectroscopy

IV.A.1. Films of CsNa18C6

Figure 24 shows the optical spectrum of a dry film made from a methylamine solution which contained equimolar amounts of cesium, sodium and 18-crown-6. As the spectrum shows, there is a sharp peak at 16500 cm^{-1} which corresponds to the Na^- anion. This peak is slightly shifted compared to the Na^- peak (16000 cm^{-1}) produced from the Na 18C6 system with R = metal/crown = 2 (78). The spectrum showed no changes with time or temperature.

IV.A.2. Films of K Na 18C6

The spectrum of a dry film made from methylamine solution which contains equimolar amounts of potassium, sodium and 18C6 is shown in Figure 25. There is a broad peak at 13000 cm^{-1} and a shoulder at 10000 cm^{-1}. If the major peak is due to Na^- then the presence of K^+18C6 causes a red-shift of 3000 cm^{-1}. On the other hand, if it is due to K^-, then the presence of Na^+18C6 causes a blue-shift of 800 cm^{-1}. This contrasts with the behavior of K^+C222·Na^- films in which the peak shifted only 300 cm^{-1} from that of Na^+C222·Na^- (78). The shoulder is attributed to a trapped electron shifted to shorter wavelength probably due to interaction with the cation and anion. The spectrum of K-Na 18C6 films showed no change with time or temperature.

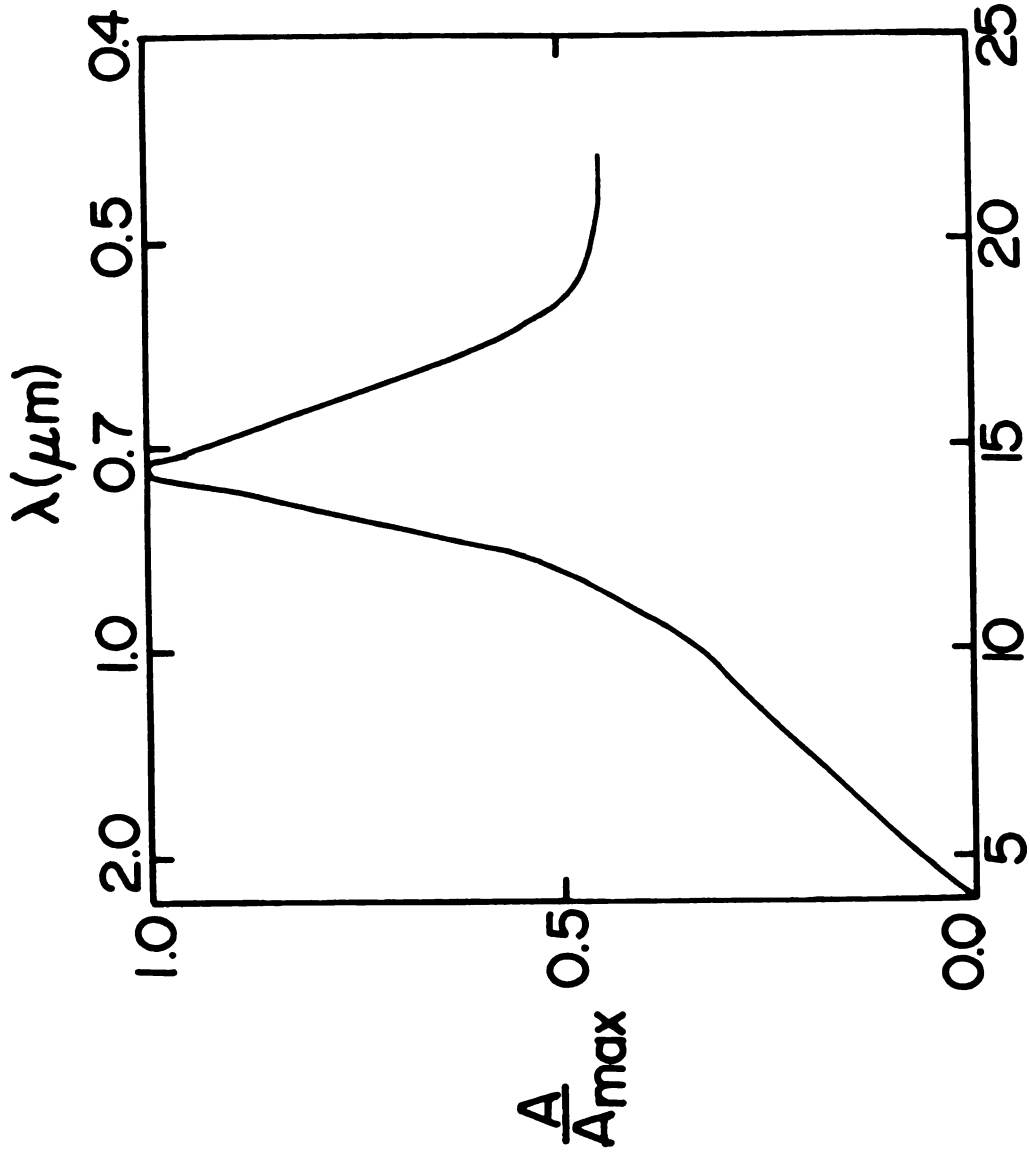

Figure 24. Optical spectrum of dry film of $Cs^{+}18C6 \cdot Na^{-}$ from methylamine solution.

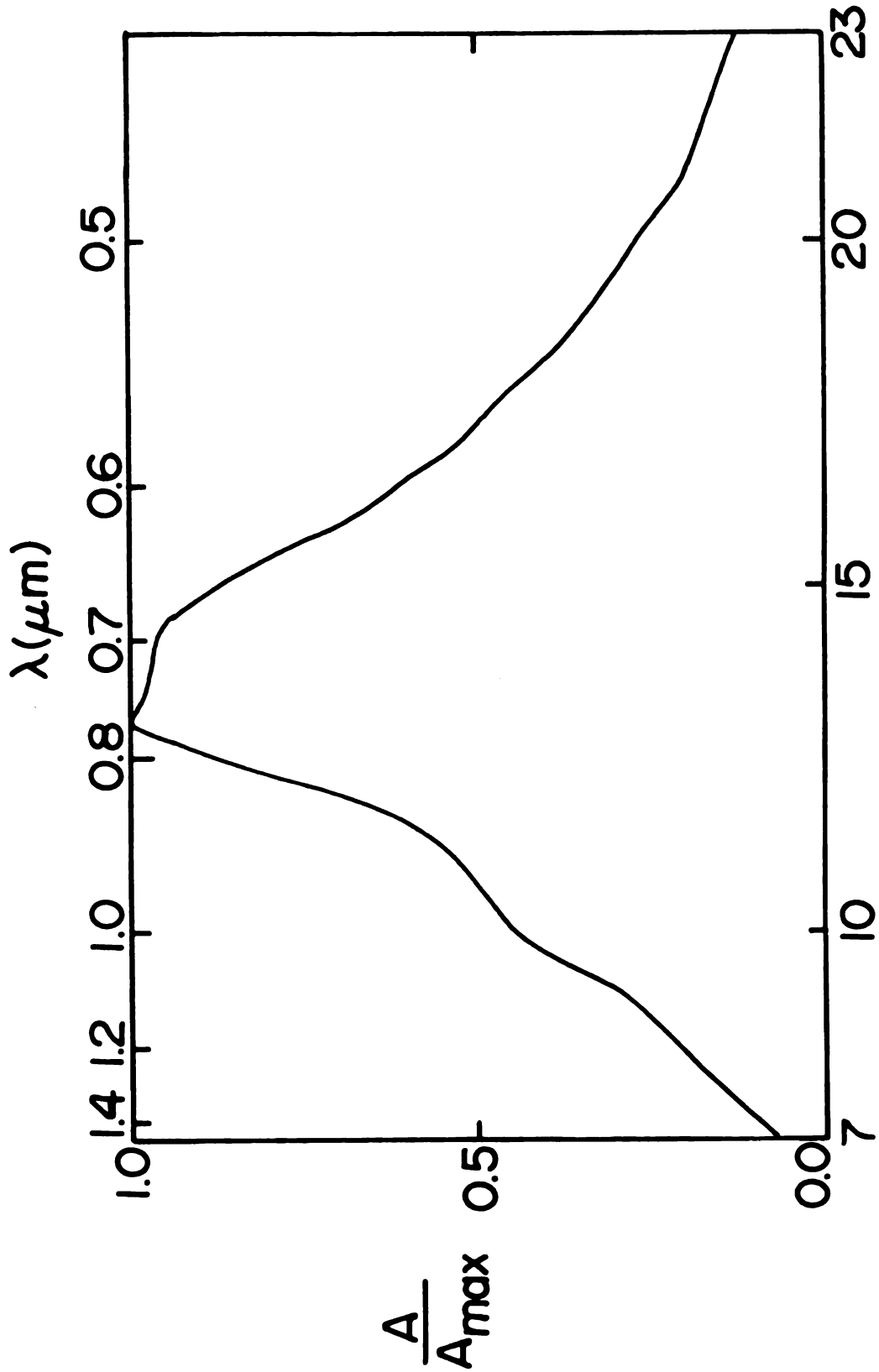

Figure 25. Optical spectrum of a dry film of KNa18C6 from methylamine solution.

We expect the major peak to be due to Na^- and not K^-. This is because the complexation constant of K^+18C6 is greater than Na^+18C6 in solution (88) and Na^- is generally much more stable than K^-. However, the observed peak might be due to a mixture of K^- and Na^-.

IV.A.3. Films of Cs Rb 18C6

The spectrum of a dry film made from a methylamine solution which contained equimolar amounts of cesium, rubidium and 18C6 is shown in Figure 26. There are two peaks, the major peak is at 11500 cm^{-1} and it is very broad, extending over a 1000 cm^{-1} range. The center of the peak is at 12000 cm^{-1} which corresponds to Rb^- observed in the spectrum of Rb 18C6 with R = metal/18C6 = 2 (78). The second peak at 9000 cm^{-1} assigned to the trapped electron is shifted to higher energies than expected, probably because of interaction with the anion Rb^-. However, the presence of the Cs^- anion cannot be excluded since these films showed different behavior at different temperatures. When the films are made at lower temperatures the absorption is very broad and probably includes Cs^-, Rb^- and trapped electron. This system was difficult to characterize and attempts to prepare crystals from this system have failed.

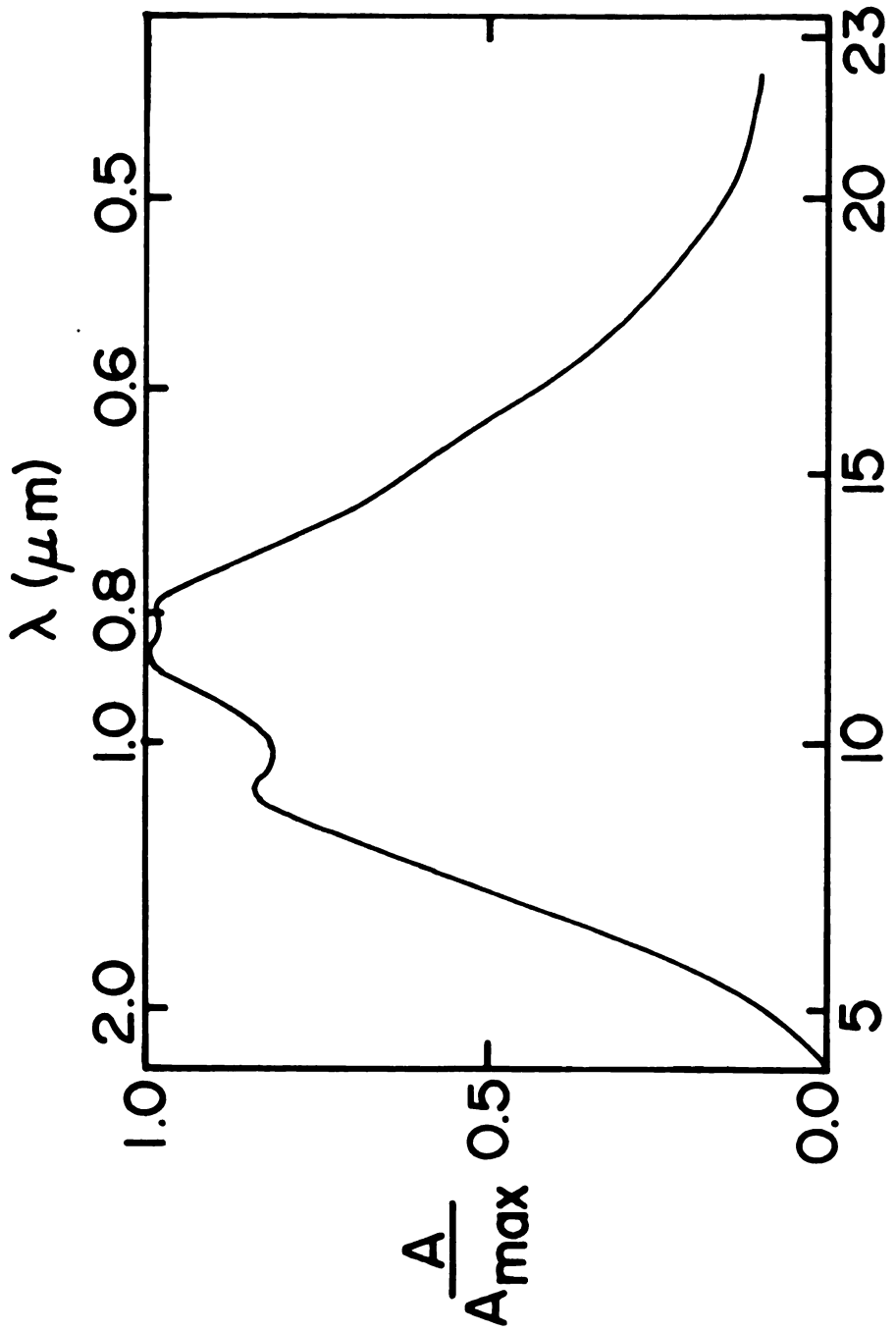

Figure 26. Optical spectrum of a dry film of CsRb18C6 from methylamine solution.

IV.B. Sample Analyses

The procedure and the analysis scheme have been discussed in the experimental section. Several different samples of the alkalides $Cs^+18C6 \cdot Na^-$ and $K^+18C6 \cdot Na^-$ were analyzed. The samples were analyzed according to the reaction

$$M^+18C6\ N^- + 2H_2O \rightarrow M^+ + N^+ + 18C6 + 2OH^- + H_2\uparrow$$

The number of moles of hydrogen was calculated by using the ideal gas Law and the number of moles of hydroxide ion was determined by titration with standard HCl solution. The number of moles of M^+ and N^+ were determined by flame emission. The amount of crown ether was determined by integration of the ^1H NMR signal compared with a known concentration of potassium hydrogen phthalate (KHP). Table 4 gives the results of analysis of $Cs^+18C6 \cdot Na^-$ and the percentage deviation from the amount of sample present as determined by hydrogen evolution. As shown from Table 4, the stoichiometry of the compound is Cs18C6·Na. Since the optical spectrum shows only the peak of Na^-, the formula of the compound must be $Cs^+18C6 \cdot Na^-$. The 5% deviation for OH^- is higher than for the metals. This is due to the difficulty in the titration of OH^- in the presence of crown ether which causes instability of the pH meter especially near the end point. The pH of the water distilled

Table 4. Results of the Analyses of $Cs^{+}18C6 \cdot Na^{-}$. The Values in the Parenthesis are the Percent Deviation From the Predicted Stoichiometry.

Sample No.	Moles of $H_2 \cdot 10^4$	Moles of $OH^- \cdot 10^4$	Moles of $Cs^+ \cdot 10^4$	Moles of $Na^+ \cdot 10^4$	Moles of $18C6 \cdot 10^4$
1	0.471	0.889	0.473	0.483	
	(-)	(-5)	(0)	(+3)	
2	0.197				0.198
	(-)				(0.5)

from the sample after the hydrogen evolution step showed that there was no solvent associated with the crystals.

Table 5 shows the results of the analysis of $K^{+}18C6 \cdot Na^{-}$.

Table 5. Results of the Analyses of $K^{+}18C6 \cdot Na^{-}$. The Numbers in the Parentheses are the Percent Deviation from Predicted Stoichiometry.

Sample No.	Moles of $H_2 \cdot 10^4$	Moles of $OH^- \cdot 10^4$	Moles of $K \cdot 10^4$	Moles of $Na \cdot 10^4$	Moles of $18C6 \cdot 10^4$
1	0.858	1.645	0.900	0.813	
	(-)	(-4)	(+4.9)	(-5)	
2	0.171				0.186
	(-)				(8.8)

The analysis of the water after hydrogen evolution showed that the crystals contained about 16% amine even though they had been vacuum-dried before decomposition.

IV.C. Powder dc Conductivity

Conductivity measurements were performed on alkalide compounds. This was done first by checking Ohm's Law by reading the current versus voltage at different temperatures. Then at a certain voltage the current was measured with changing temperature. The resistance was calculated and a plot of log R vs $\frac{1}{T}$ shown in Figures 27 and 28 for $Cs^+18C6 \cdot Na^-$ and $K^+18C6 \cdot Na^-$ gave a straight line from which the band gap was calculated. A fit of the data to a linear relationship using the non-linear least-squares KINFIT program (103) gave the relation log R = -5.579±0.637 + (4.541±0.172) x $10^3(\frac{1}{T})$, the average band gap calculated is 1.7 eV. The conductivity measurements of $K^+18C6 \cdot Na^-$ yielded the relation log R = -1.397±0.169 + 2.287±0.042 x $10^3(\frac{1}{T})$ which gives an average band gap of ∿.93 eV. As the values of the band gaps indicate, these compounds are semiconductors.

IV.D. Magnetic Susceptibility of $Cs^+18C6 \cdot Na^-$

Crystals of $Cs^+18C6 \cdot Na^-$ are diamagnetic in the temperature range 1.6 and 300 K and there is no evidence for any

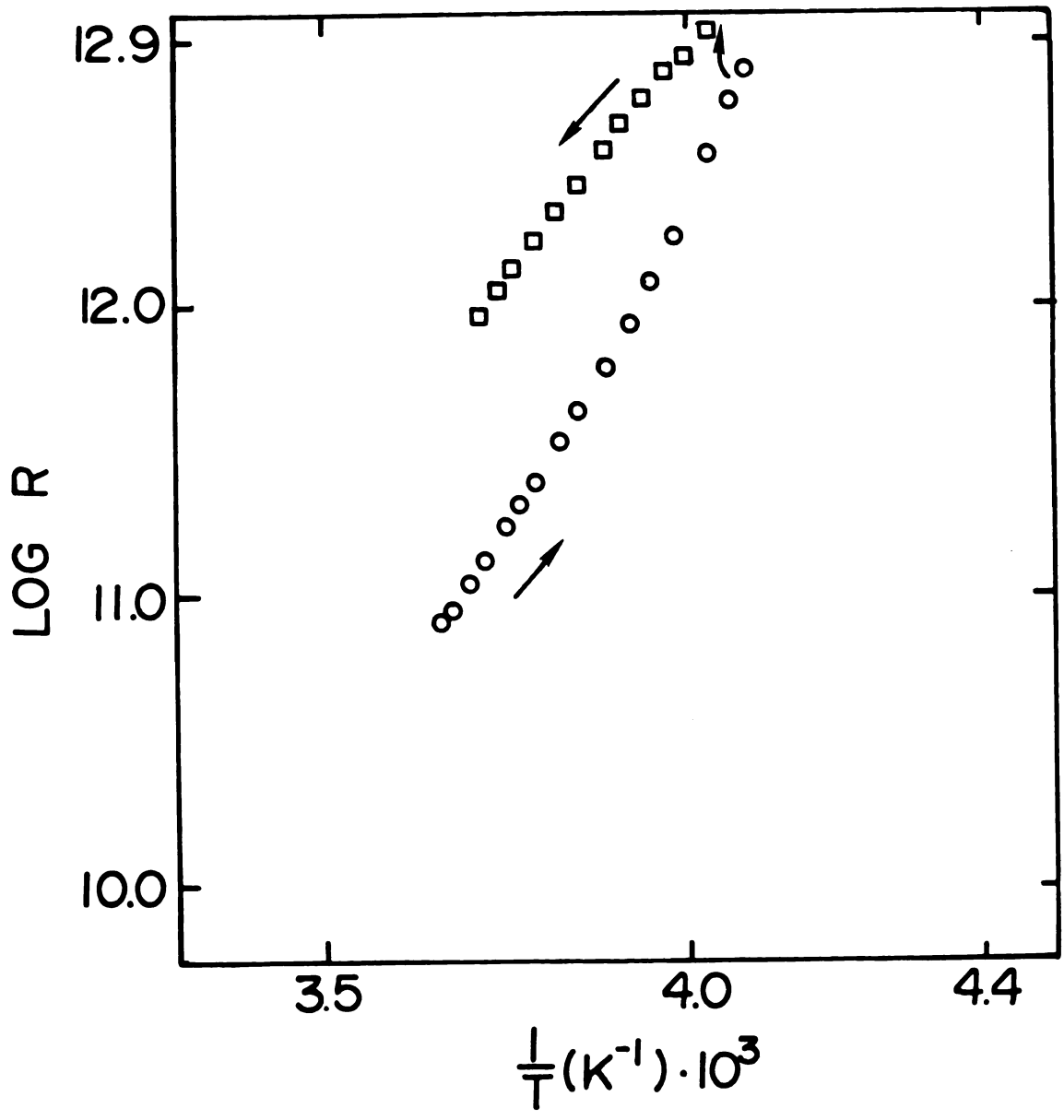

Figure 27. Plot of log resistivity vs. reciprocal temperature for polycrystalline $Cs^{+}18C6\cdot Na^{-}$.

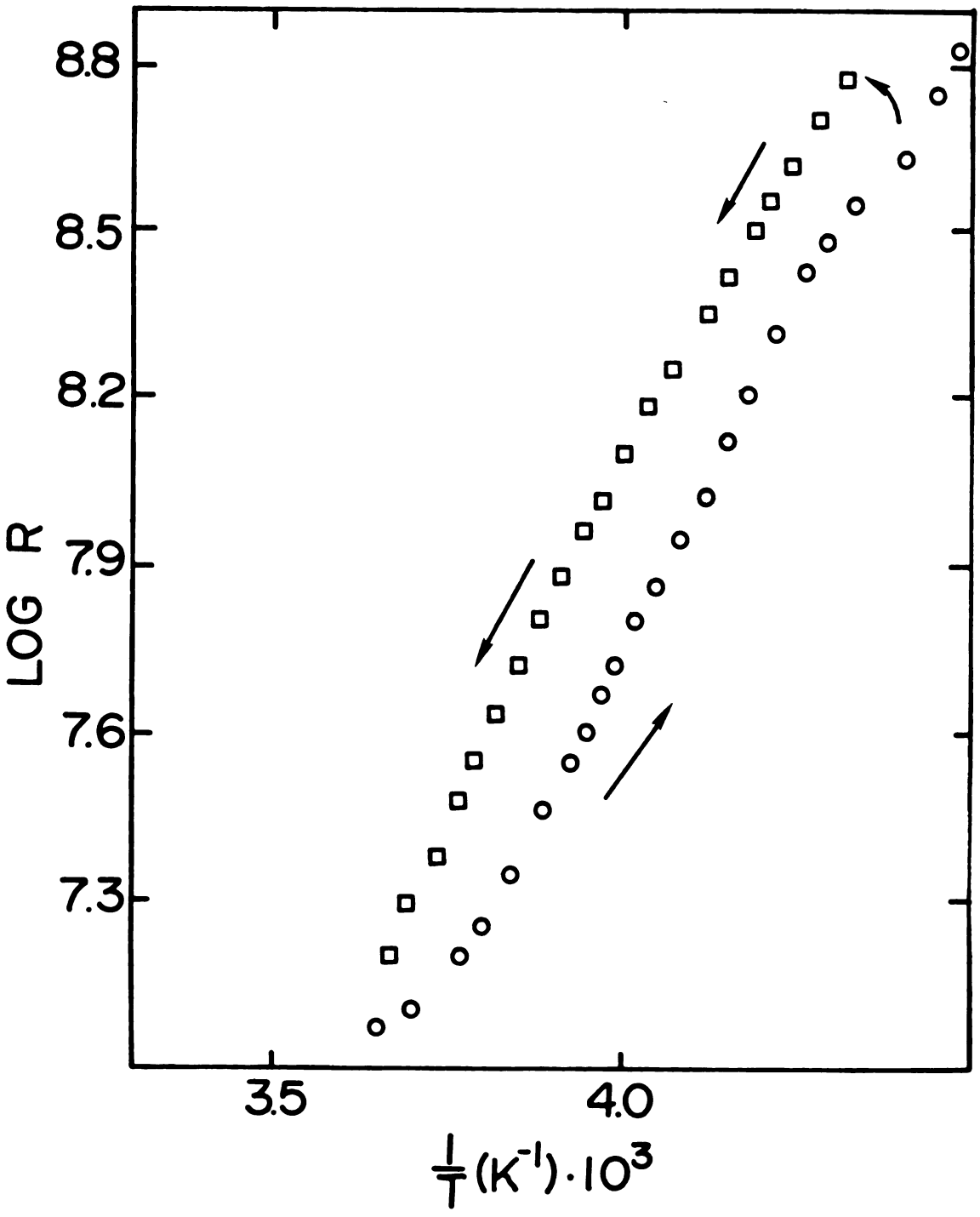

Figure 28. Plot of log resistance vs. reciprocal temperature for polycrystalline $K^{+}18C6\cdot Na^{-}$.

magnetic ordering. The observed molar magnetic susceptibility can be compared to that calculated using Pascal's constants for diamagnetic susceptibility. The summation of the atomic susceptibilities (Pascal's constants) give the molar susceptibility (106). Therefore, the calculated molar susceptibility for $Cs^+18C6 \cdot Na^-$ is

$$\chi_{Cs^+18C6 \cdot Na^-} = \chi_{Cs^+} + \chi_{18C6} + \chi_{Na^-} \qquad (15)$$

The diamagnetic susceptibility of Na^- can be approximated to be equal to that of Cl^- (since the radius of Cl^- is close to that of Na^-) according to Langevin equation for diamagnetism which states that the diamagnetic susceptibility is proportional to the mean square distance of the electrons from the nucleus. Then the calculated molar susceptibility value 2.27×10^{-4} emu/mole. This value is in the same range of the experimental value 1.72×10^{-4} emu/mole within the experimental error.

IV.E. X-ray Study of $Cs^+18C6 \cdot Na^-$

IV.E.1. Single Crystal Isolation

The crystalline compound $Cs^+18C6 \cdot Na^-$ is stable at room temperature in an inert atmosphere. Single crystals were loaded in small thin wall capillary tubes (107) in the argon atmosphere box (dry box). The crystals were loaded with the help of a microscope mounted outside the

box. Due to difficulties in adjusting the microscope, the crystals which were loaded were not all of good quality. After loading the crystals in the capillary tubes (0.3-0.2 mm D), they were sealed inside the box by using resistively heated nichrome wires. After that the crystals were taken out of the box and examined under the microscope to assess their quality. However, this technique has its faults. The compound is extremely reactive and the crystals are degraded by any impurities in the inert atmosphere box. Temperature changes may also alter the quality of the crystals. Problems also have occurred because of the movement of the crystal in the capillary. Furthermore, there were many problems with twinned crystals, unfavorable crystal dimensions and irregular shapes. Because of all these difficulties only a few crystals satisfied all of the necessary conditions for X-ray structure determination and even these gave fewer reflections than would have been desired.

IV.E.2. Results of X-ray Study

Different procedures were used by Dr. Donald Ward for data collection from three different crystals. All of them gave essentially the same results, but the structure could not be solved. A summary of the information obtained about the crystalline compound $Cs^{+}18C6 \cdot Na^{-}$ will be given.

Crystal symmetry: monoclinic.

Unit Cell parameters:

a = 13.895 (11) Å

b = 15.501 (24)

c = 8.932 (7)

β = 93.25 (5)

V (volume) = 1920.7 A^3, and assuming Z = 4.

the number of molecules per unit cell, the density D = 1.453 g cm^{-3}. Possible space groups: C2, Cm, C2/m. Patterson map peaks are (no. U, V, W, height)

1.	0.000	0.000	0.000	999
2.	.500	.000	.500	147
3.	.361	.500	.652	122
4.	.298	.339	.155	105
5.	.420	.332	.697	86
6.	.395	.500	.467	71
7.	.000	.183	.726	67
8.	.000	.000	.500	45
9.	.260	.040	.000	43
10.	.260	.000	.000	41

Remaining peaks are of heights less than 9. The Cs-Cs peaks should be of the type (depending on space group):

0	0	0
0	2y	0
2x	0	2z
2x	2y	2z

and a single-weighted Cs-Cs peak (scaled to the origin = 999) should have a height about 190. The structure making the most "sense" places Cs at: 0, 0, 0; ½, ½, 0; ½, 0, ½; and 0, ½, ½. This is a face-centered arrangement and gives an R-factor of about 55%. (Placing Cs only in the first two positions gives an R-factor of about 25% but is not face-centered and corresponds to only two cesiums per unit cell. The structure could not be extended by repetitions of structure-factor calculations and electron density maps. Direct methods were not successful in solving the structure. We conclude that the microstructure must be more complex than a simple face-centered monoclinic system.

CHAPTER V

PREPARATION OF ALKALIDES AND ELECTRIDES BY DIRECT VAPOR DEPOSITION

The films from solution used to study the optical spectra were always prepared at low temperatures (<-30°C) in order to minimize decomposition. The spectra of some dry films showed changes with time which suggested "annealing" in the solid state. In addition, dark blue films often formed when cesium metal was distilled into a vessel which contained 18-crown-6 at room temperature. These observations lead us to investigate the possibility of preparing alkalides and electrides by direct vapor deposition (108).

V.A. Experimental

The apparatus shown in Figure 29 was used to prepare films of alkalides and electrides by vapor deposition. The crown ether (18C6) and the metal were introduced into the side arms by using Teflon heat-shrinkable tubing. After evacuation to about 1×10^{-5} torr, the glass ampoule containing the metal was broken, moved to the constriction and a seal was made behind it to remove the heat-shrinkable tubing. The side arms were then

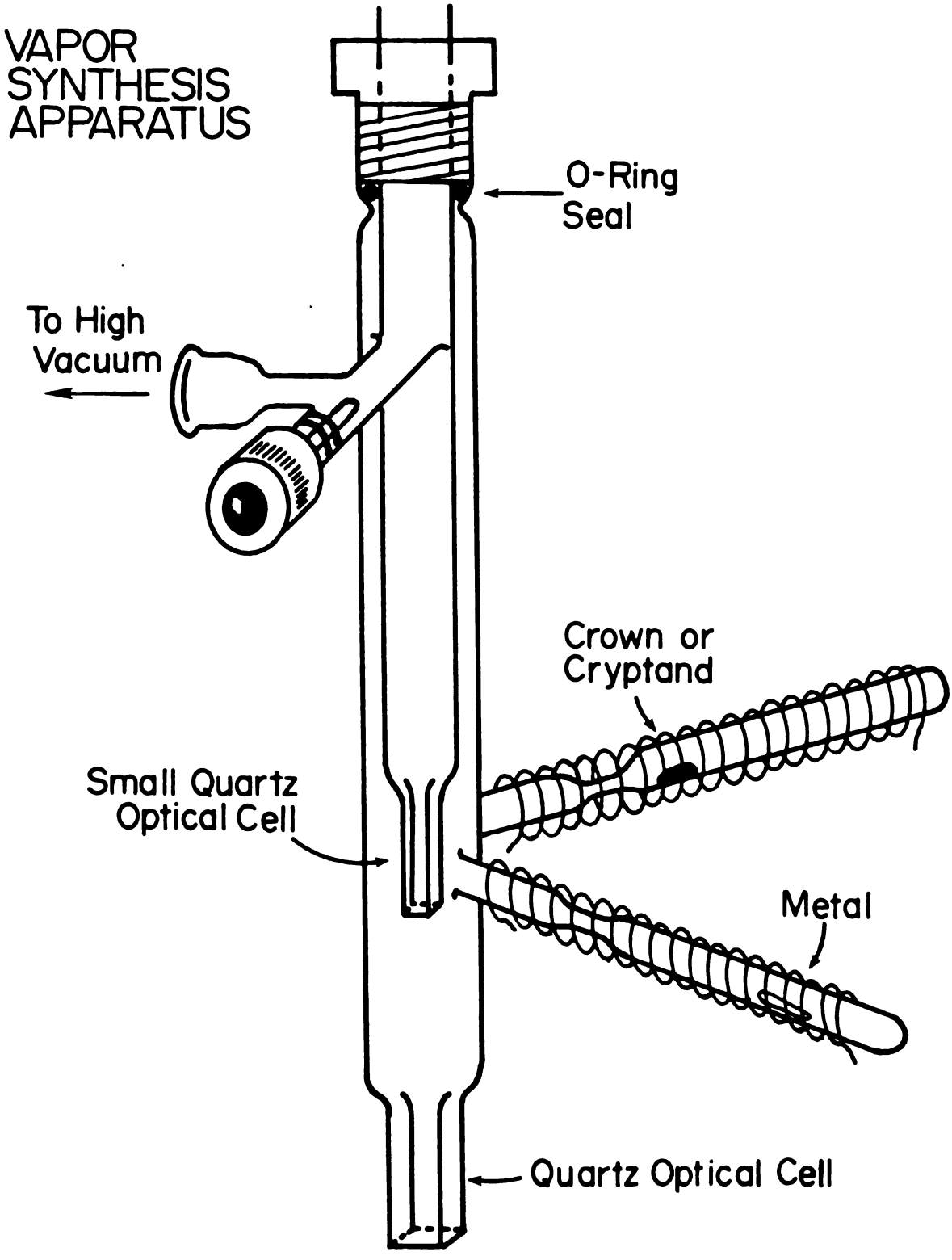

Figure 29. Apparatus for preparation of films of electrides and alkalides from vapor deposition.

electrically heated to the appropriate temperature by adjusting the voltage across the Nichrome wire coils. While the inner cell was above the side arms, a film was first deposited on the inside of the outer vessel. When an appropriate film was formed (judged by the appearance of the film), the inner cell was lowered so that the optical part was facing the two side arms. After the film had been formed, the inner cell was lowered down into the optical portion of the outer cell, the apparatus was closed, removed from the vacuum line and the spectra were recorded with a Beckman DK-2 Spectrophotometer.

Except for the films formed from cesium and 18C6, the films were rather unstable and tended to decompose when formed at room temperature. Therefore, it was necessary to cool the inner cell by inserting powdered dry-ice into the cell while forming the film. After that, the dry-ice was removed and the film was allowed to come to room temperature and the spectra were recorded.

V.B. Results and Discussion

The optical spectra of films made from the alkali metals (Na, K, Rb and Cs) with 18C6 are shown in Figure 30. The spectrum of Cs-18C6 shows a sharp peak at 5250 cm^{-1} in the IR region attributed to the trapped electron and a very intense peak which was out of scale in the visible region probably due to the Cs^- anion. In the spectrum of

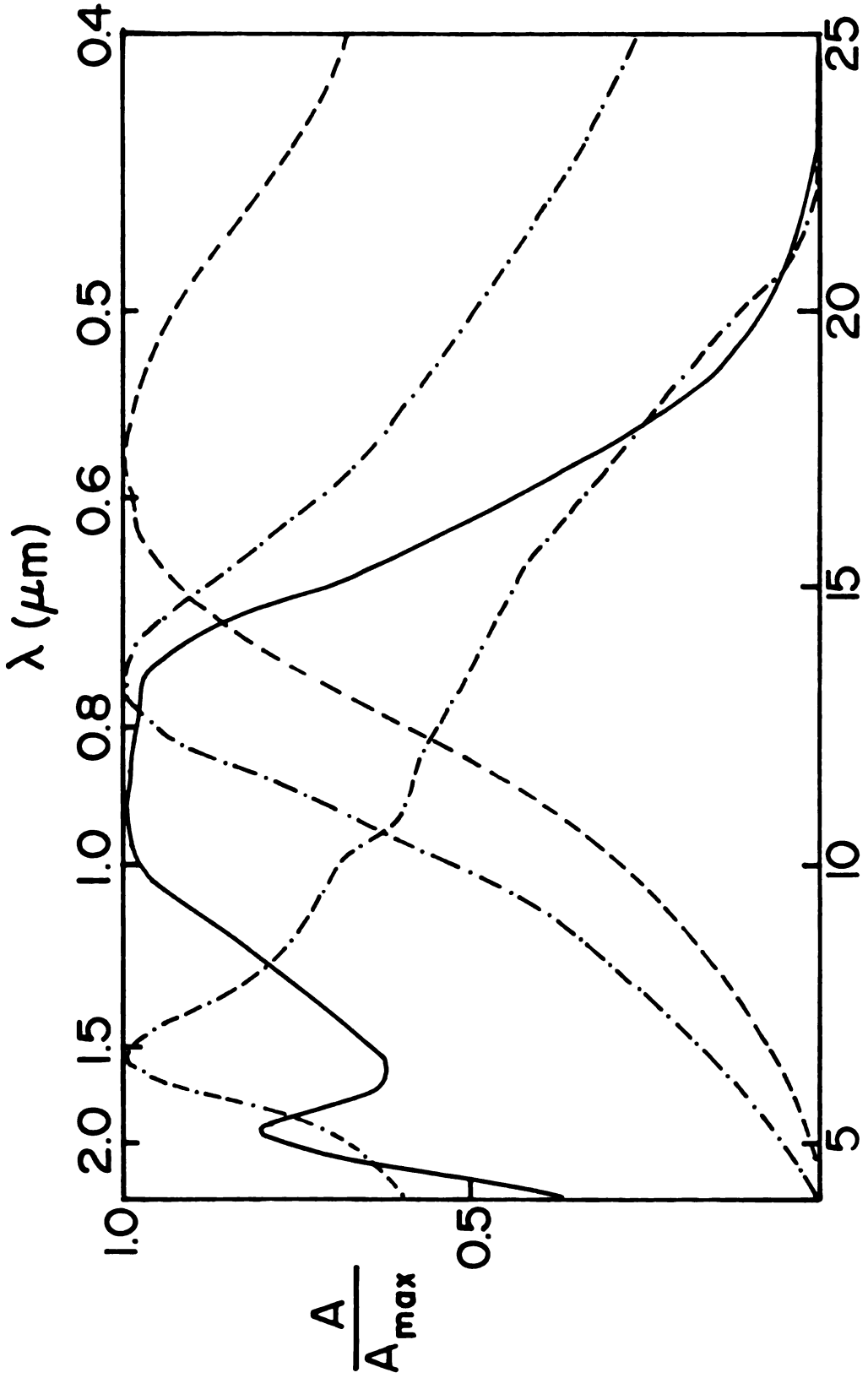

Figure 30. Optical transmission spectra of 1) —— Cs18C6; 2) -·- Rb18C6; 3) -·- K18C6; 4) --- Na18C6 by direct vapor deposition.

Rb-18C6 film there is only a major peak at 6500 cm^{-1} due to the trapped electron. However, this peak is broad with extensive tailing in the visible region. For the films of Na-18C6 and K-18C6, the peaks are at 17500 cm^{-1} and 13250 cm^{-1} probably corresponding to Na^- and K^-, respectively. These peaks were very broad. The spectra of all films made from vapor deposition were compared with the corresponding known spectra of films made from solution. Blank experiments were also done, in which only films of metals were formed. Their spectra were recorded and compared with spectra which have been previously reported (109). The inability to control the stoichiometry and thickness often caused interferences from light scattering, absorption by excess metal and absorbances which were out of range. With the apparatus we used it was impossible to prepare a uniform homogeneous film. Therefore, some films (for example that with Cs-18C6) showed two kinds of peaks, one due to the trapped electron and the second caused by Cs^-. The reason for this behavior is the nature of the film formed. The part of the film which faces the metal side arm is richer in metal and therefore produced Cs^-, while the other part which faces the crown ether is richer in the crown and gives the trapped electron. Depending on the metal to crown ratio, it is possible to prepare either electrides or alkalides and this can be accomplished by increasing the rate of evaporation of either the crown or

the metal. Although it was not possible by this method to prepare films with controlled thicknesses and stoichiometries, these preliminary results clearly show that alkalides and electrides can be prepared by direct vapor deposition.

CHAPTER VI

PREPARATION AND CHARACTERIZATION OF A CRYSTALLINE ELECTRIDE $Cs^{+}18C6 \cdot e^{-}$

Introduction

The major thrust in the research in this laboratory since 1970 has been to prepare and characterize crystalline "electrides" and "alkalides". Successful preparation of the first crystalline alkalide, $Na^{+}C222 \cdot Na^{-}$, came in 1974. Continuous attempts over almost twelve years to prepare crystalline electrides have failed. The extreme reactivity and instability of the electrides has made the synthesis of electrides a very difficult and often frustrating task. The easiest method for the preparation of electrides is the solvent evaporation discussed in Chapter II. It was clear from the beginning that our major problems with this work were due to decomposition. Even with extreme care in cleaning glassware, purification of complexants, metals and solvents, we were able to minimize decomposition but not entirely prevent it. The second major problem with the crystallization procedure is that changing the initial solvent from methylamine to a less polar

crystallization solvent always resulted in decomposition. Even a gradual change of the polarity of the solvent did not help. Recently, after I had prepared powders and films of the extremely reactive electride $Cs^{+}18C6 \cdot e^{-}$ in a mole ratio of up to two moles of metal per mole of crown ether and had shown that it displayed different properties compared with the other systems discussed in Chapter III, a preparation was tried in which I dissolved cesium, lithium and 18-crown-6 in equimolar amounts in methylamine. Surprisingly, the solutions were very stable even at high temperatures (about $\sim$-10°C). The stability of films made from this solution was remarkable. It was clear that the lithium played a major role in stabilizing the solution and preventing decomposition. The lithium probably serves as a scavanger for radicals (such as $\cdot CH_2NH_2$) which may enhance decomposition as chain carriers. Cooling the methylamine solution to dry ice temperatures did not produce crystals. This was expected because the materials are very soluble in methylamine. Finally, crystallization was made possible by using a co-solvent of isopropylamine and diethylether. (It is possible to obtain crystals from isopropylamine solutions alone at low temperatures but the yield is low). However, it is quite possible that the composition of the solvent mixture might be very important because of problems that might arise from precipitation of lithium metal which would contaminate the crystals and give false

analyses. Because of all these problems, a very careful procedure has to be used in order to get metal-free crystals (110). The preparation procedure and characterization and properties of this crystalline electride are discussed in the following sections.

VI.A. Preparation Procedure

The synthesis procedure used here is similar to that used in alkalide synthesis as discussed in Chapter II. The apparatus in this case was constructed of fused silica instead of borosilicate glass in order to avoid sodium contamination of the lithium solutions by contact with sodium borosilicate glass. In the final and most successful preparation the solution was filtered through a coarse frit prior to the crystallization step in order to exclude precipitated lithium.

IV.B. Analyses

The analysis scheme used for alkalides was also used here. This is based on the reaction of the electride with water according to

$$Cs^+18C6 \cdot e^- + H_2O \rightarrow Cs^+ + 18C6 + OH^- + \frac{1}{2}H_2\uparrow$$

The results of the analyses of three samples taken from

Table 6. Results of the Analyses of Crystalline $Cs^{+}18C6 \cdot e^{-}$. The Numbers in Parentheses are the Percent Deviation From Predicted Stoichiometry.

Sample No.	Moles According to Mass	Moles of Evolved H_2	Moles of OH^-	Moles of Cs	Moles of Li	Moles of 18C6
1	---	10.0184×10^{-5} (-)	20.0450×10^{-5} (0)	20.8220×10^{-5} (+4)	7.5688×10^{-6}	21.8787×10^{-5} (+9)
2	6.8026×10^{-5} (-)			6.5010×10^{-5} (-4)	6.0527×10^{-6}	5.9662×10^{-5}
3	2.4616×10^{-4} (-1)	1.2426×10^{-4} (0.0)	2.5200×10^{-4} (+2)	2.5250×10^{-4} (+2)	3.2954×10^{-6}	2.5783×10^{-4} (+4)

three different preparations are tabulated in Table 6. The crystals were free of solvent as indicated by the following results: In two of the analyses the water left after the decomposition step was collected by distillation and its pH was checked. The pH value indicated no amine solvent. In the third analysis the crystalline sample was decomposed with D_2O and the solution was taken for ^1H NMR measurement. The spectrum showed no evidence of contamination of the crystals by solvent.

From the results in Table 6 it is clear that lithium metal is not an essential constituent of the crystals. The percent deviations of the values from those predicted are comparable to the estimated experimental errors of each method. Thus, these results prove that the stoichiometric formula is Cs18C6.

VI. C. Optical Spectra

The films studied here were formed as discussed in the Experimental section but in this case the solutions were prepared by distilling methylamine into the optical apparatus which contained some crystals of Cs18C6. The optical spectrum of a solvent-free film made at a temperature of -50°C is shown in Figure 31. As the spectrum indicates there is high absorption in the IR region which peaks at 6000 - 7250 cm^{-1} but there is also a shoulder at 10250 cm^{-1}. These features are probably due to trapped electrons and

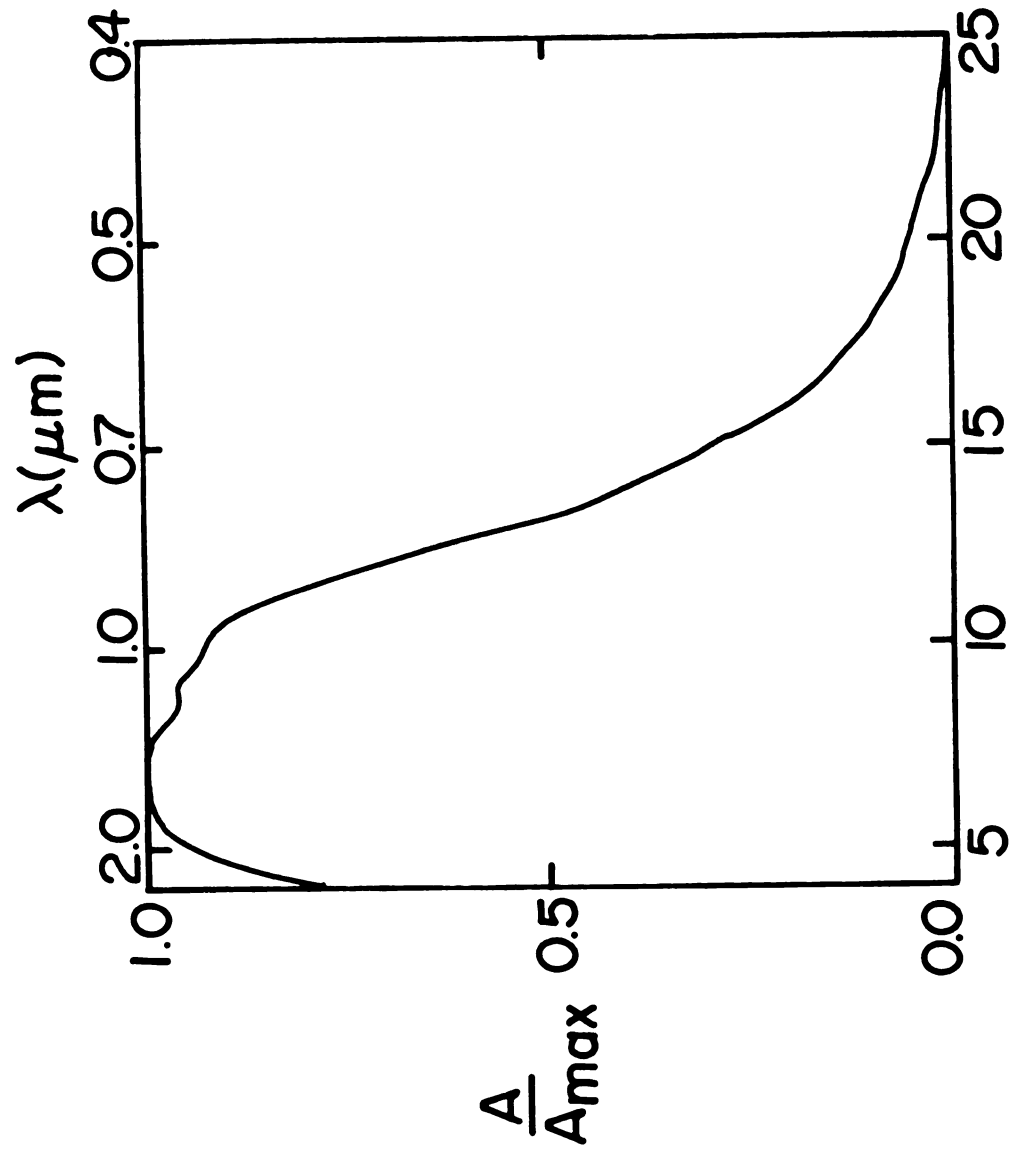

Figure 31. Optical transmission spectra of $Cs^{+}18C6 \cdot e^{-}$ film made at -50°C.

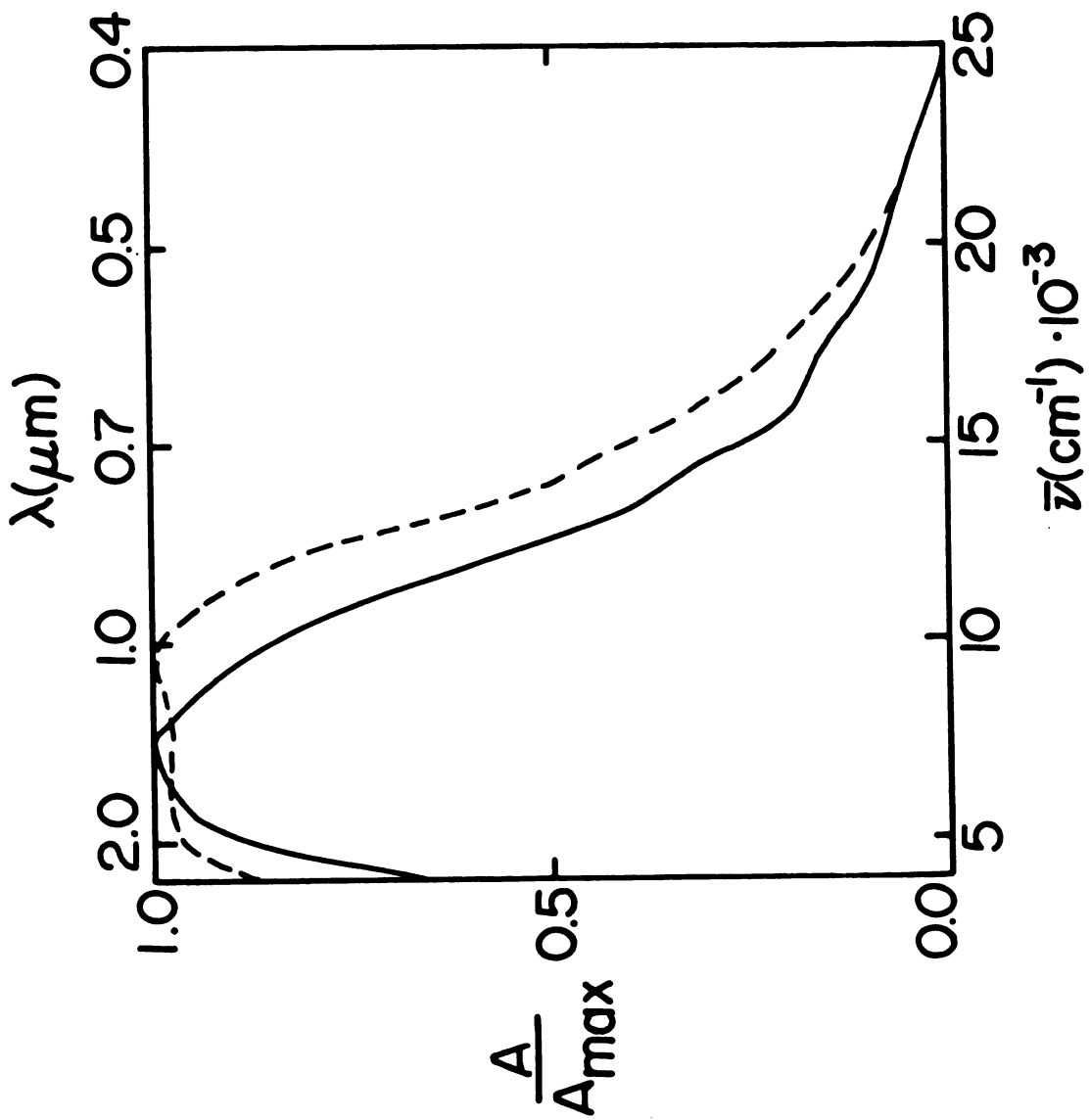

Figure 32. Optical transmission spectra of $Cs^{+}18C6 \cdot e^{-}$ film at temperature -37°C.
1) --- unannealed film at -50°C; 2) —— annealed film at +12°C.

Cs^-. However, this spectrum does not represent the most stable state because it changes upon annealing. Figure 32 shows the spectra of a dry film made at temperature of -37°C. The spectrum (recorded at a temperature of -50°C) shows a high absorption in the IR region and a peak at 10000 cm^{-1}. As the temperature increases, the films "anneal" and the absorption in the IR region drops and the peak tends to localize to give a maximum at 7250 cm^{-1}. Once the film annealed at this temperature its spectrum stays the same and is not affected by time or temperature change. Therefore, this spectrum represents the most stable state produced in the experiment. The absence of a peak due to Cs^- in the annealed film is the strongest evidence for the assignment $Cs^+18C6 \cdot e^-$ rather than $Cs^+(18C6)_2 \cdot Cs^-$ for the crystalline material.

VI.D. Powder dc Conductivity

Powder dc conductivity measurements were made with two samples from different preparations. The Ohm's Law behavior was checked at different temperatures and it was found that $Cs^+18C6 \cdot e^-$ nearly obeys Ohm's Law as shown in Figure 33 although some polarization is evident. The current at various temperatures in the temperature range +10°C to -54°C was measured at constant voltage and converted to resistance. Figure 34 is a plot of log R against reciprocal temperature. A non-linear least-squares fit

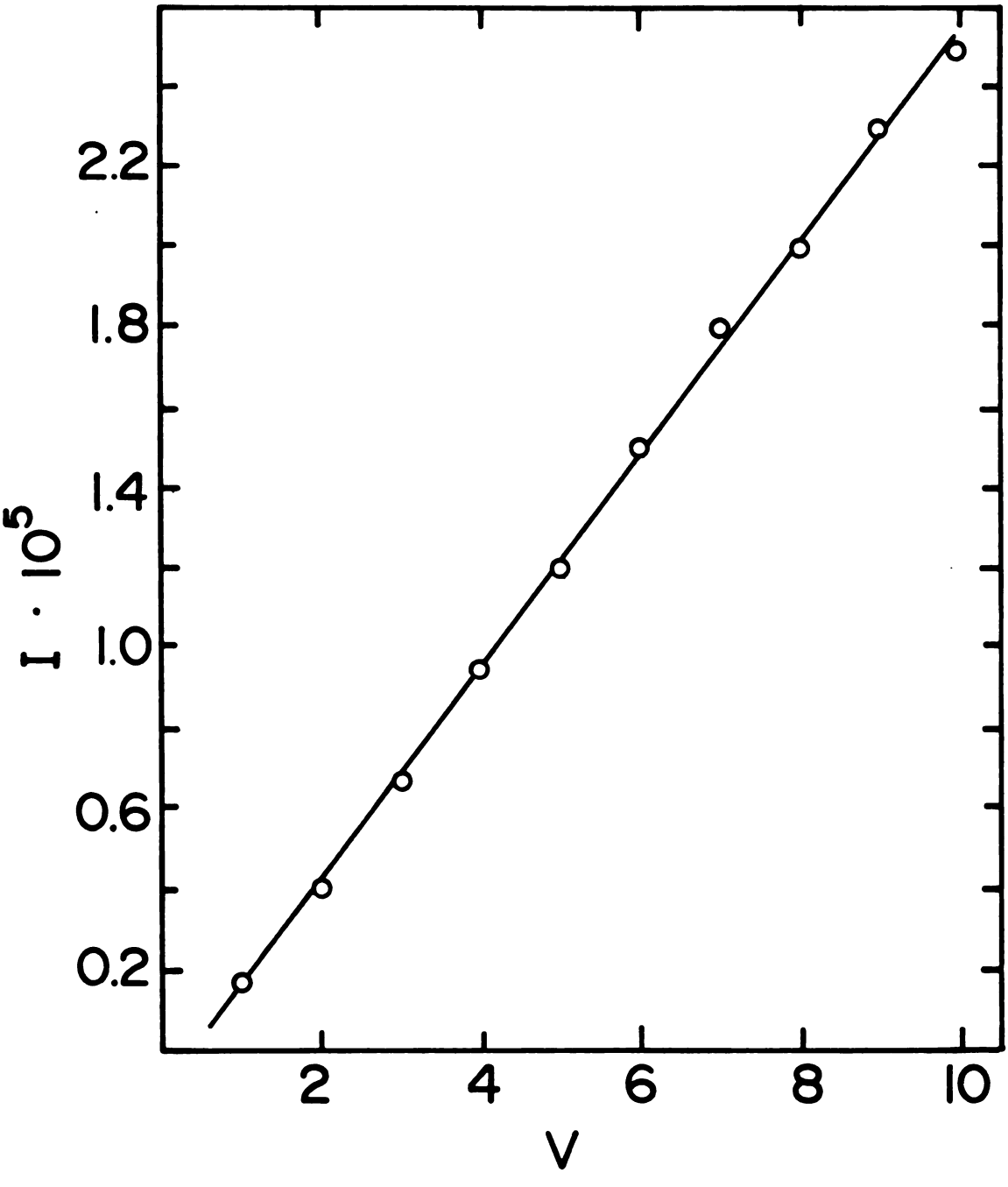

Figure 33. Ohm's Law plot of polycrystalline powder of $Cs^{+}18C6 \cdot e^{-}$.

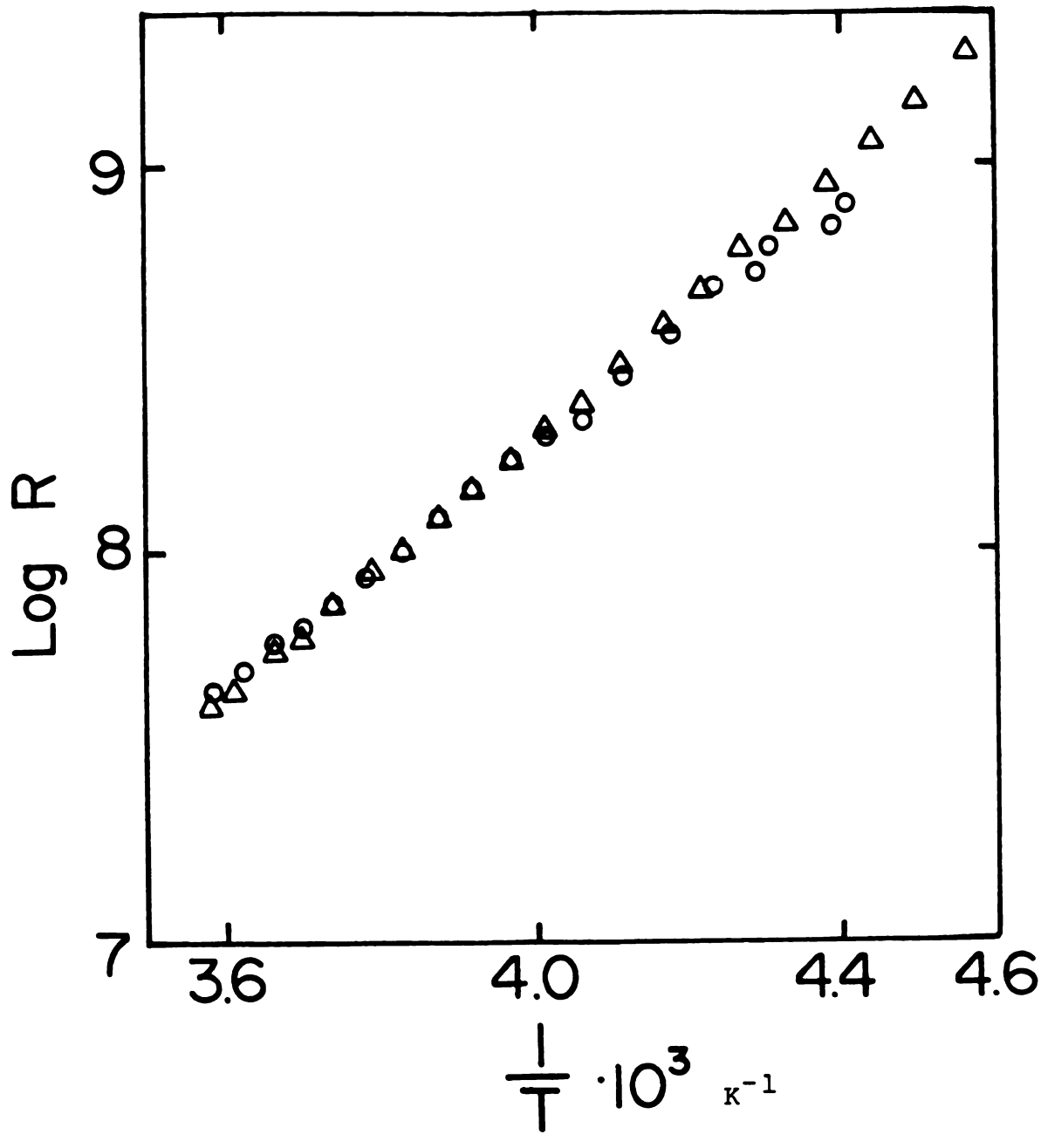

Figure 34. Plot of log resistance vs. reciprocal temperature for a polycrystalline $Cs^{+}18C6 \cdot e^{-}$.

of the line yields log R = 1.850±0.076 + (1.611±0.019) x $10^3 \frac{1}{T}$. The average value of the band gap calculated from this result is ∿0.60 eV in this temperature range. These powder conductivity measurements suggest that the crystalline $Cs^+18C6 \cdot e^-$ is a semiconductor.

VI.E. EPR Study

Both a polycrystalline sample and a single crystal were used in the EPR study. It was found that the spectra show two peaks and the resolution of these peaks depends on the orientation of the crystal with respect to the magnetic field. Figure 35 shows a series of spectra taken at (arbitrary) different orientations. It is clear from these spectra that there are two peaks. Measurements of the g-values showed that one of them is essentially isotropic with g = 2.0023 while the other is anisotropic. The effect of temperature on the peaks was also studied. Figure 36 shows the spectra for a single crystal where the two peaks almost resolved at a temperature of ∿-100°C. As shown in the figure, the isotropic peak was not affected by temperature, while the second anisotropic peak was greatly affected. At lower temperatures the anisotropic peak tends to shift downfield (higher g-values) and the linewidth becomes smaller, while at high temperatures this peak gets broader, decreases in amplitude and vanishes at 51°C.
It is not possible experimentally to separate the peaks

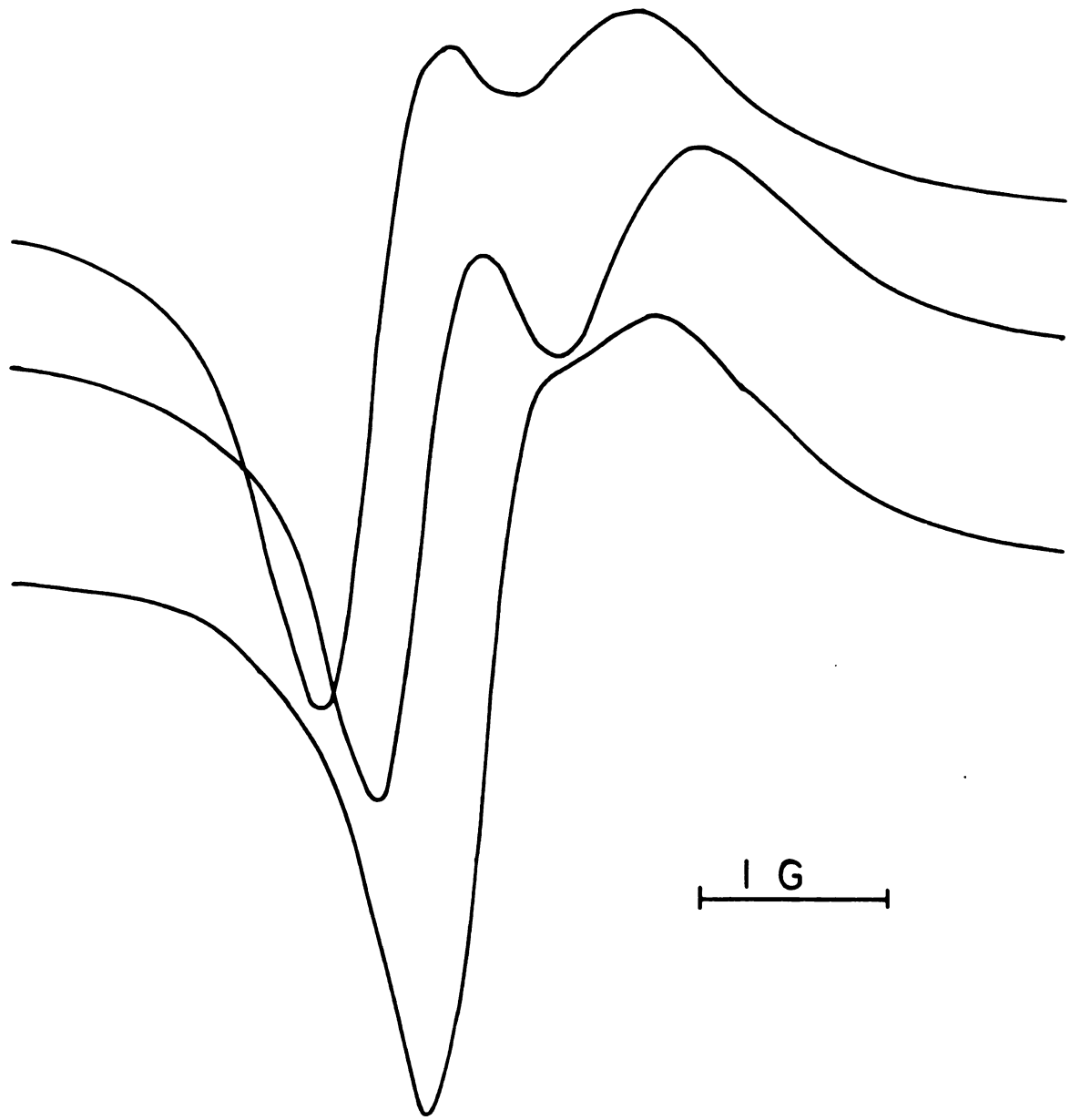

Figure 35. EPR spectra of a single crystal of $Cs^{+}18C6 \cdot e^{-}$ at different (arbitrary) orientations.

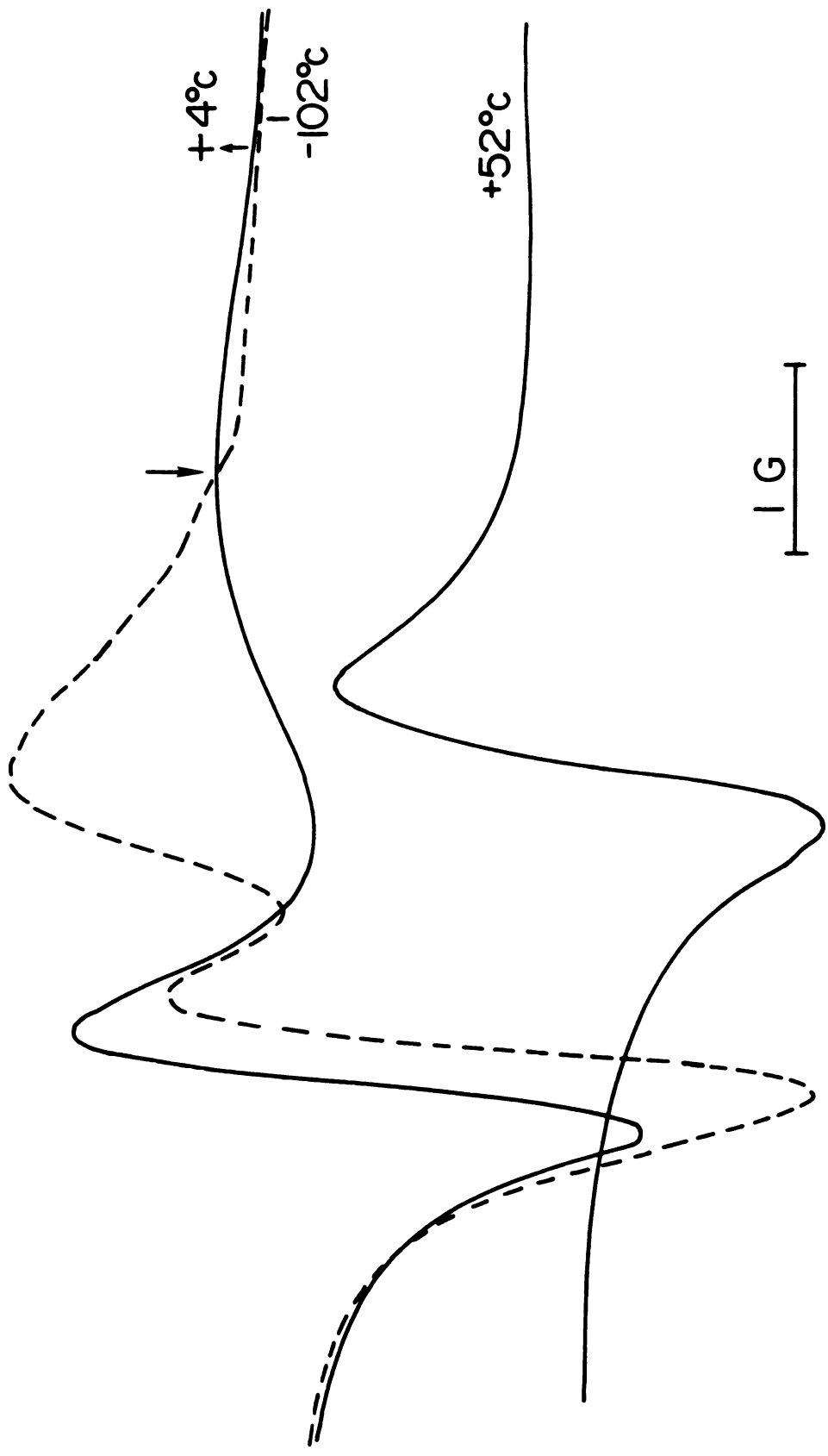

Figure 36. Effect of temperature on the EPR spectra of single crystal ($Cs^{+}18C6 \cdot e^{-}$).

completely. It was possible, however, to measure the g-values by using DPPH as calibrating agent. The g-values indicate that the isotropic peak has a g-value of 2.0023, the free electron value. This suggests no appreciable spin-orbit interaction with the cesium cation. The second anisotropic peak has a smaller g-value indicative of some interaction. This value is temperature-dependent, it varied from 2.0015 to 2.0020 and also depends upon the orientation of the crystal. It was difficult to measure the g-value at high temperatures because this peak is very broad suggesting a short relaxation time. An approximate calculation of the number of spins was done by using a spin standard Ruby crystal. This was accomplished by orienting the crystals so that the two peaks almost overlap which could only be done at low temperatures. The calculations show the presence of less than 1% free spins (in the temperature range 128 K to 240 K).

VI.F. Magnetic Susceptibility Study

The magnetic susceptibility of crystalline $Cs^{+}18C6 \cdot e^{-}$ was measured in the temperature range 1.7 K to 300 K. Figure 37 shows the magnetic behavior *vs.* temperature for the crystalline $Cs^{+}18C6 \cdot e^{-}$ electride. This is a plot of the susceptibility of the electride minus that of the decomposed sample. It is seen that the electronic susceptibility is diamagnetic in the range 130 K to 300 K. Below

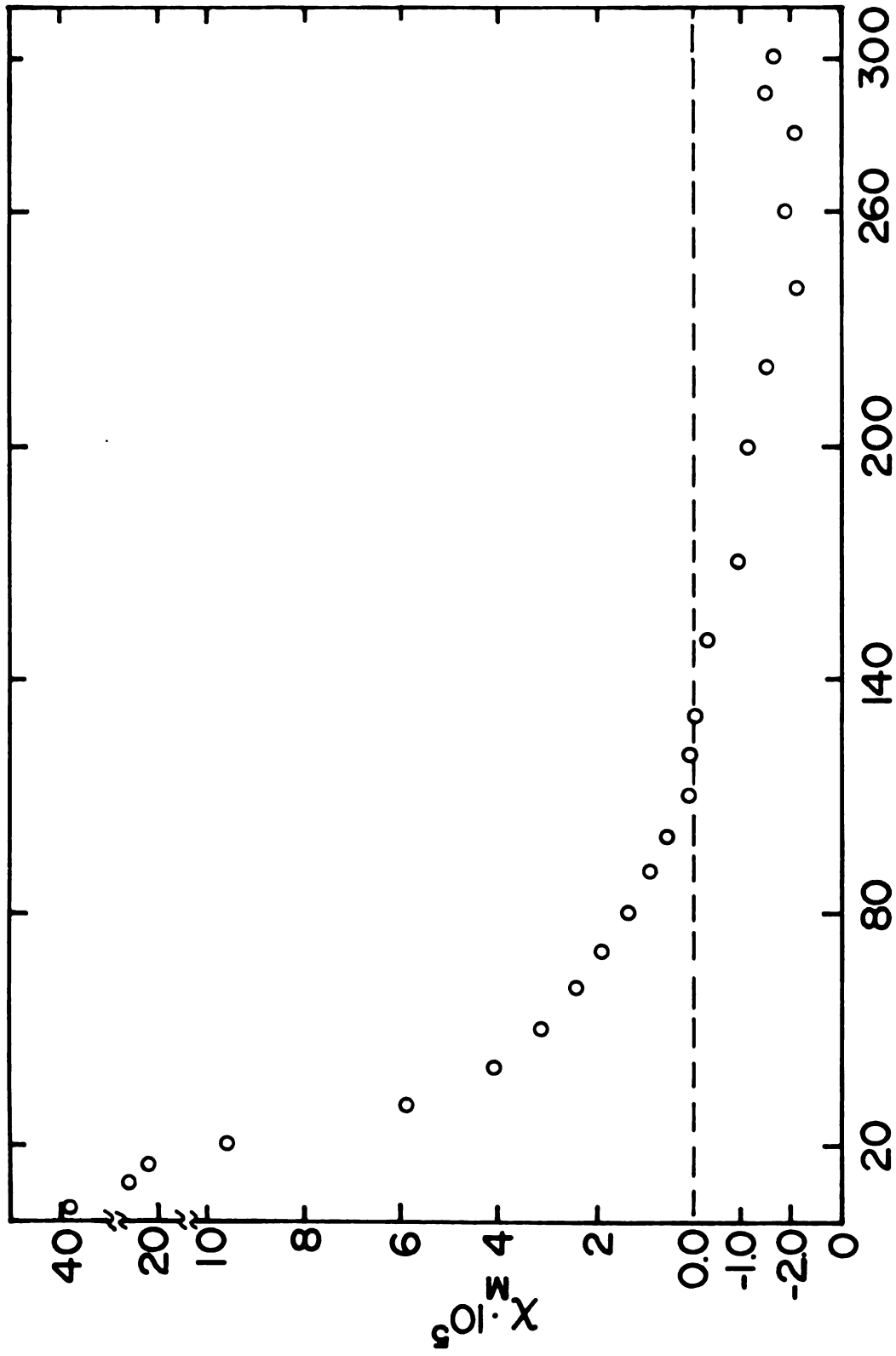

Figure 37. Plot of molar susceptibility against temperature for polycrystalline $Cs^+18C6 \cdot e^-$.

130 K the magnetic susceptibility is paramagnetic and is temperature dependent down to 1.7 K. The fact that $Cs^{+}18C6 \cdot e^{-}$ is nearly diamagnetic rather than strongly paramagnetic is attributed to antiferromagnetic ordering of the electrons in the lower Hubbard band. Cyrot (111) and others pointed out that when electron correlations are taken into account, the singlet ground state is favored over the paramagnetic state.

CHAPTER VII

CONCLUSIONS AND SUGGESTIONS FOR FUTURE WORK

VII.A. Conclusions

Films and/or powders of Cs-18C6 electrides prepared by solvent evaporation showed properties which are dependent on the metal to crown ratio. The properties range from nonmetallic when R = 1 to metallic when R = 2.

Two stable crystalline alkalides, $Cs^{+}18C6 \cdot Na^{-}$ and $K^{+}18C6 \cdot Na^{-}$ were prepared and their properties were investigated. Analyses and the properties of these compounds confirmed the proposed formula.

Films of alkalides and/or electrides were prepared by direct reaction of the alkali metals and 18-crown-6 deposited from the vapor phase. The optical spectra of these films guide their classification.

The first crystalline electride, $Cs^{+}18C6 \cdot e^{-}$, was synthesized and its properties were investigated. These crystals were stable at room temperature, and have a melting point of $\sim$65°C. Analyses of different samples confirmed the stoichiometry Cs18C6. Such properties as optical spectra and powder d.c. conductivities support the formula $Cs^{+}18C6 \cdot e^{-}$. Single crystal EPR spectra showed

two lines, one of which is isotropic and the other anisotropic. Magnetic susceptibilities and EPR spectra indicated a substantial spin-pairing.

VII.B. Suggestion for Future Work

(1) After the success in preparing the first crystalline electride, $Cs^+18C6 \cdot e^-$, further investigation of its properties such as quantitative single crystal EPR spectra and single crystal conductivity should be made. X-ray structure determination is absolutely necessary for a better understanding of the properties of electrides. Therefore, systematic procedure for growing high-quality single crystals should be developed. The synthesis of other electrides which use 18C6 and cryptant C222 might be possible if the stabilization by lithium is a general phenomenon and should be investigated.

(2) Work should continue to solve the crystal structure of the stable alkalide $Cs^+18C6 \cdot Na^-$. This will probably require crystals of better quality. Other properties such as the single crystal conductivity and photoconductivity should also be investigated. Quantitative work should be done to understand the nature of the system $K^+18C6 \cdot Na^-$. Other alkalides such as $Rb^+18C6 \cdot Na^-$, $Cs^+(18C6)_2 \cdot Na^-$, etc., might be feasible to synthesize. If so, their properties should be investigated in order to establish trends in the properties of such sodides.

(3) Quantitative optical and electrical studies should be done on films prepared by vapor deposition using Bell-Jar high-vacuum techniques.

(4) The synthesis of mixed alkalides and electrides $M^{+}C\cdot N_{x}^{-}\cdot e_{1-x}^{-}$ would provide an ideal opportunity to study the influence of electron density on electron-electron interactions and should also be explored.

BIBLIOGRAPHY

BIBLIOGRAPHY

1. J. C. Thompson, "Electrons in Liquid Ammonia", Oxford University Press, Oxford, 1976.

2. G. LePoutre and M. J. Sienko (eds.), "Metal-Ammonia Solutions, Colloque Wey 1", W. A. Benjamin (New York) 1964.

3. J. J. Lagowski and M. J. Sienko (eds.), "Metal-Ammonia Solutions", Butterworth (London) 1970.

4. J. Jortner and N. R. Kestner (eds.), "Electrons in Fluids", Springer-Verlag (New York) 1973.

5. J. Phys. Chem. 79 (26) 1975.

6. J. Phys. Chem. 84 (10) 1980.

7. G. LePoutre and J. P. LeLieur, Reference 3, p. 247.

8. R. A. Ogg, Jr., J. Am. Chem. Soc., 68, 155 (1946), J. Chem. Phys. 14, 114, 295 (1946); Phys. Rev., 69, 243, 668 (1946).

9. J. Jortner, J. Chem. Phys., 30, 839 (1959).

10. D. A. Copeland, N. R. Kestner and J. Jortner, J. Chem. Phys., 53, 1189 (1970).

11. N. R. Kestner and J. Jortner, J. Chem. Phys., 77, 1040 (1973).

12. M. Gold, W. L. Jolly and K. S. Pitzer, J. Am. Chem. Soc., 84, 2264 (1962).

13. J. L. Dye, Reference 3, p. 1.

14. J. V. Acrovis and K. S. Pitzer, J. Phys. Chem., 66, 1693 (1962).

15. J. P. LeLieur, P. DaMay, and G. LePoutre, J. Phys. Chem., 79, 26 (1975).

16. E. Huster, Ann. Phys., 33, 477 (1938).

17. S. Freed and N. Sugarman, J. Chem. Phys., 11, 354 (1943).

18. C. A. Hutchison, Jr. and R. C. Pastor, Rev. Mod. Phys., 25, 285 (1953); J. Chem. Phys., 21, 7959 (1953).

19. A. Demortier and G. LePoutre, C. R. Acad. Sci. Paris, 268, 453 (1969).

20. A. Demortier, M. DeBacker, and G. LePoutre, J. Chem. Phys., 69, 380 (1972).

21. F. Wooten, "Optical Properties of Solids", Academic Press (New York) 1972.

22. T. A. Beckman and K. S. Pitzer, J. Phys. Chem., 65, 1527 (1961).

23. J. A. Vanderhoff, E. W. LeMaster, W. H. McKnight, J. C. Thompson and P. R. Antoniewicz, Phys. Rev. A4, 427 (1971).

24. R. Catterall, J. Chem. Phys. 43, 2262 (1965).

25. F. J. Dyson, Phys. Rev. 98, 349 (1955).

26. A. M. Stacy and M. J. Sienko, J. Chem. Phys, in press.

27. W. S. Glaunsinger and M. J. Sienko, J. Chem. Phys., 62, 1883 (1975).

28. P. P. Edwards, A. R. Lusis and M. J. Sienko, J. Chem. Phys., 72, 3103 (1980).

29. J. R. Buntaine, M. J. Sienko and P. P. Edwards, J. Phys. Chem., 84, 1230 (1980).

30. P. P. Edwards, J.R. Buntaine and M. J. Sienko, Phys. Rev., B19, 5835 (1979).

31. W. S. Glaunsinger, S. Zolotov and M. J. Sienko, J. Chem. Phys. 56, 4756 (1972).

32. W. S. Glaunsinger, T. R. White, R. B. VonDreele, D. A. Gordon, R. F. Marzke, A. L. Bowman, and J. L. Yarnell, Nature, 271, 414 (1978).

33. H. Oesterricher, N. Mammano and M. J. Sienko, J. Solid State Chem. 1, 10 (1969).

34. R. B. VonDreele, W. S. Glaunsinger, A. L. Bownman and J. L. Yarnell, J. Phys. Chem., 79, 2992 (1975).

35. J. E. Hart and W. J. Boag, J. Am. Chem. Soc., 84, 4090 (1962).

36. L. Kevan and B. C. Webser (eds.), "Electron-Solvent and Anion-Solvent Interactions", Elsevier, Amsterdam (1976).

37. L. Kevan, J. Phys. Chem., 56, 838 (1972).

38. J. H. Baxendale and P. H. G. Sharpe, Chem. Phys. Lett., 39, 401 (1976).

39. T. Shida, S. Iwata and T. Watanabe, J. Phys. Chem., 76, 3683 (1972).

40. L. Kevan, J. Phys. Chem., 84, 1232 (1980).

41. J. E. Willard, J. Phys. Chem., 79, 2966 (1975).

42. A. Ekstrom and J. E. Willard, J. Phys. Chem., 72, 4599 (1968).

43. L. Kevan, Acc. Chem. Res., 14, 138 (1981).

44. E. E. Budzinski, W. R. Potter, G. Potienko and H. C. Box, J. Chem. Phys., 70, 5040 (1979).

45. H. C. Box and H. G. Freund, Appl. Spectroscopy, 34, 293 (1980).

46. D. F. Feng and L. Kevan, Chem. Rev. 80, 1 (1980).

47. J. Jortner, Mol. Phys., 5, 257 (1962).

48. D. Copeland, N. R. Kestner and J. Jortner, J. Chem. Phys., 53, 1189 (1970).

49. K. Fueki, D. F. Feng and L. Kevan, J. Phys. Chem., 74, 1976 (1970); J. Am. Chem. Soc., 95, 1398 (1973).

50. T. Ichikawa and H. Yoshida, J. Chem. Phys., 73, 1540 (1980).

51. A. Banerjee and J. Simons, J. Chem. Phys., 68, 415 (1978).

52. J. J. Markham, "F-Centers in Alkali Halides", Academic Press (New York) (1966).

53. R. S. Alger, "Electron Paramagnetic Resonance; Techniques and Applications", John Wiley and Sons, Inc. (New York) (1968).

54. W. Schmitt and U. Schindewolf, Ber. Bunsenges, Phys. Chem., 81, 584 (1977).

55. N. F. Mott, Proc. Phys. Soc., A62, 416 (1949); Phil. Mag. 6, 287 (1961); Phil. Mag. 19, 835 (1969); and "Metal-Insulator Transitions", Taylor and Francis (London) (1974).

56. P. P. Edwards and M. J. Sienko, Phys. Rev. B17, 2575 (1978).

57. J. Hubbard, Proc. R. Soc., A276, 238 (1963); A277, 237 (1964); and A281, 401 (1964).

58. P. W. Anderson, Phys. Rev., 109, 1492 (1958) and Comments Sol. St. Phys. 1, 190 (1970).

59. R. R. DeWald and J. L. Dye, J. Phys. Chem., 68, 121 (1964).

60. S. Matalon, S. Golden and M. Ottolenghi, J. Phys. Chem., 73, 3098 (1969).

61. M. G. DeBacker and J. L. Dye, J. Phys. Chem., 75, 3092 (1971).

62. T. R. Tuttle, Jr., Chem. Phys. Lett., 20, 371 (1973).

63. J. L. Dye, M. G. DeBacker, J. A. Eyre and L. M. Dorfman, J. Phys. Chem., 76, 839 (1972).

64. J. M. Ceraso and J. L. Dye, J. Chem. Phys., 61, 1585 (1974).

65. J. L. Dye, C. W. Andrews and J. M. Ceraso, J. Phys. Chem., 79, 3076 (1975).

66. J. L. Dye, J. M. Ceraso, M. T. Lok, B. L. Barnett and F. J. Tehan, J. Am. Chem. Soc., 96, 608 (1974).

67. F. J. Tehan, B. L. Barnett and J. L. Dye, J. Am. Chem. Soc., 96, 7203 (1974).

68. C. J. Pedersen, J. Am. Chem. Soc., 89, 7017 (1967); 90, 3299 (1968).

69. B. Dietrich, J.-M. Lehn and J.-P. Sauvage, Tetrahedron Lett., 2885, 2889 (1969).

70. J. L. Dye, M. G. DeBacker and V. A. Nicely, J. Am. Chem. Soc., 92, 5226 (1970).

71. M. T. Lok, F. J. Tehan, and J. L. Dye, J. Phys. Chem., 76, 2975 (1972).

72. J. L. Dye, M.-T. Lok, F. J. Tehan, R. B. Coolen, N. Papadakis, J. M. Ceraso and M. G. DeBacker, Ber. Bunsengens. Phys. Chem., 75, 659 (1971).

73. J. L. Dye, C. W. Andrews and S. E. Matthews, J. Phys. Chem., 79, 3076 (1975).

74. J. M. Ceraso, Ph.D. Dissertation, Michigan State University, 1975.

75. J. L. Dye, M. R. Yemen, M. G. DaGue and J.-M. Lehn, J. Chem. Phys., 68, 1665 (1978).

76. M. G. DeGue, Ph.D.Dissertation, Michigan State University, 1979.

77. M. G. DaGue, J. S. Landers, H. L. Lewis and J. L. Dye, Chem. Phys. Lett., 66, 169 (1979).

78. J. L. Dye, M. G. DaGue, M. R. Yemen, J. S. Landers and H. L. Lewis, J. Phys. Chem., 84, 1096 (1980).

79. J. S. Landers, Ph.D. Dissertation, Michigan State University, 1981.

80. J. S. Landers, J. L. Dye, A. Stacy and M. J. Sienko, J. Phys. Chem., 85, 1096 (1981).

81. C. J. Pedersen and H. K. Frensdorff, Angew. Chem. Int. Ed. Engl., 2, 16 (1972).

82. R. M. Izatt, D. P. Nelson, J. H. Rytting, B. L. Haymore and J. J. Christensen, J. Am. Chem. Soc., 93, 1619 (1971).

83. J. J. Christensen, D. J. Eatough and R. M. Izatt, Chem. Rev., 74, 351 (1974).

84. R. M. Izatt, R. E. Terry, B. L. Haymore, L. D. Hansen, N. K. Dalley, A. G. Avonded and J. J. Christensen, J. Am. Chem. Soc., 98, 7620 (1976).

85. R. M. Izatt, R. E. Terry, D. P. Nelson, Y. Chan, D. J. Eatough, J. S. Bradshaw, L. D. Hansen and J. J. Christensen, J. Am. Chem. Soc., 98, 7626 (1976).

86. E. Mei, J. L. Dye and A. I. Popov, J. Am. Chem. Soc., 98, 1619 (1976).

87. E. Mei, J. L. Dye and A. I. Popov, J. Am. Chem. Soc., 99, 6532 (1977).

88. J. D. Lamb, R. M. Izatt, C. S. Swain and J. J. Christensen, J. Am. Chem. Soc., 102, 475 (1980).

89. C. J. Pedersen, Fed. Proc., 27, 1305 (1968).

90. H. K. Frensdorff, J. Am. Chem. Soc., 93, 600 (1971).

91. E. Mei, A. I. Popov and J. L. Dye, J. Phys. Chem., 81, 1677 (1977).

92. Sadegh Khazalei, Ph.D. Dissertation, Michigan State University, 1982.

93. G. W. Gokel, D. J. Cram, C. L. Liotta, H. P. Harris and F. L. Cook, J. Org. Chem., 39, 2445 (1974).

94. M. G. DeBacker and J. L. Dye, J. Phys. Chem., 75, 3092 (1971).

95. Bradley VanEck, Ph.D. Dissertation, Michigan State University, 1982.

96. L. H. Feldman, R. R. DeWald and J. L. Dye, Adv. Chem. Ser., 50, 163 (1965).

97. I. Hurley, T. R. Tuttle, Jr. and S. Golden, J. Chem. Phys. 48, 2818 (1968).

98. M. R. Yemen and J. L. Dye, private communication.

99. J. E. Wertz and J. R. Bolton "Electron Spin Resonance: Elementary Theory and Practical Applications", McGraw-Hill (New York) 1972.

100. T. Chang and A. H. Kahn, National Bureau of Standards Special Publication 260-59: Standard Reference Materials: Electron Paramagnetic Resonance Intensity Standard: SRM-2601; Description and Use," U.S. Department of Commerce (Washington, D.C.) 1978.

101. A. H. Morrish "The Physical Principles of Magnetism" John Wiley and Sons, Inc. (New York) 1965.

102. C. Kittle, "Introduction to Solid State Physics", 5th ed., John Wiley & Sons, Inc. (New York) 1976.

103. J. L. Dye and V. A. Nicely, J. Chem. Educ., 48, 443 (1971).

104. M. T. Lok, Ph.D. Dissertation, Michigan State University, 1973.

105. B. VanEck, L. D. Le, D. Issa and J. L. Dye, Inorg. Chem. to be published (1982).

106. L. N. Mulay, Ch. 7 in A. Weissberger and B. W. Rossiter, "Physical Methods of Chemistry", Vol. 1, John Wiley & Sons (New York) 1972.

107. Thin Wall Capillary Tubes, from "Charles Supper Co. Inc. (15 Tech. Circle, Natick, Mass. 01760).

108. L. D. Lee, D. Issa, B. VanEck and J. L. Dye, J. Phys. Chem., 86, 7 (1982).

109. R. Pyan, Ann. Phys. (Paris), 4, 543 (1969).

110. D. Issa and J. L. Dye, in press.

111. M. Cyrot, J. de physique (Paris), 33, 125 (1972).